Classical and Mixed Elements with Various Two-Dimensional Assumptions in Finite Element Analysis of Multilayered Plates (TBC)

cand. aer. Axel Büttner

Mai 2009

Abstract

The presented work deals with classical and mixed refined Finite Elements for multilayered plates based on Carrera Unified Formulation (CUF). In the first part, various two-dimensional axiomatic assumptions in the thickness direction theories are illustrated and discussed by considering: 1 - Taylor type expansion; 2 - combination of Legendre polynomials; 3 - Lagrange polynomials. Both cases of equivalent single layer description (the whole plate is seen as an equivalent single layer) and layer-wise description (each layer is seen as an independent plate) have been implemented. The order N of the thickness expansions is a free parameter of the present formulation. A large variety of plate theories are therefore obtained. FE matrices are written in a concise form by referring to the Carrera Unified Formulation and in terms of a few fundamental nuclei, whose form does not depend on the through-the-thickness polynomial assumption, order N, variables' description and element number of nodes. Advantages and disadvantages of the various FEs are discussed by encompassing static and dynamic problems related to significant multilayered plate problems.
The second part of this work employs mixed elements based on Reissner Mixed Variational Theorem to evaluate accurate stress fields and failure parameters in laminated composite structures. A priori fulfillment of interlaminar continuity of transverse shear and normal stress components is guaranteed by mixed assumptions. Comparison to corresponding classical formulation with only displacement variables is given. Complete three-dimensional stress field is evaluated and compared to three-dimensional elasticity solutions. Maximum stress criteria with evaluation of maximum loadings related to first ply failure are evaluated. The superiority of mixed method with respect to classical ones is concluded.
In the third part, the original Reissner Mixed Variational Theorem, RMVT, has been expanded to the electro-mechanical case. A mixed variational statement for the analysis of multilayered structures under the effect of mechanical and electrical fields is proposed. Beside displacements and transverse stresses it permits the direct evaluation of electric potetial ϕ and transverse electrical displacement D_z. The work has been organized in detail as follows: In the first Section, a short introduction of the Principle of Virtual Displacement (PVD) and Reissner's Mixed Variational Theorem (RMVT) is given. Classical models for multilayered plates are described. Section 2 introduces Carrera's Unified Formulation and discusses various two-dimensional plate theories based on different thickness functions $F_\tau(z)$ (Talyor, Legendre, Lagrange polynomials). Governing equations for the mechanical case are derived for PVD and RMVT theory, the Finite Element matrices are obtained. In Sec. 3, the derived models are applied to different test cases. Free vibration analyses as well as static analyses are performed, numerical results are discussed. The Maximum Stress Failure Criteria is introduced. In Sec. 4 an extension of RMVT model to electro-mechanical coupled fields in a condensed notation is performed. Results of electro-mechanical analysis for sensor and actuator configuration are discussed in Sec. 5.

Contents

Nomenclature

Abbreviations

CLT	Classical Lamination Theory
CUF	Carrera Unified Formulation
DOF	Degrees Of Freedom
ESL	Equivalent Single Layer
FE	Finite Element
FEM	Finite Element Method
FSDT	First Order Shear Deformation Theory
HOT	Higher Order Theories
HSDT	Higher Order Shear Deformation Theory
IC	Interlaminar Continuity
LGD	Legendre-Polynomials
LGR	Lagrange-Polynomials
LW	Layer-Wise
MUL2	FEM code for multilayered structures in multifield analysis using CUF
nDOFs	Number of Degrees Of Freedom
PVD	Principle of Virtual Displacement
RMVT	Reissners Mixed Variational Theorem
RMVT-σ_n-D_3	Extension of RMVT to electro-mechanical coupled case
TYL	Taylor-Polynomials
UF	Unified Formulation

Symbols

$\boldsymbol{u}$	Vector of displacements
$\boldsymbol{\sigma}_n$	Vector of transverse stresses $[N/m^2]$
$\boldsymbol{\sigma}_p$	Vector of in-plane stresses $[N/m^2]$
$\boldsymbol{V}_{\tau i}$	Vector containing primary unknowns
N_L	Number of layers
k	Index for the layer number
δW	Virtual work
F_τ	Set of thickness-functions
ζ	Dimensionless thickness-coordinate in z-direction

$\boldsymbol{D}_{n\Omega}$, $\boldsymbol{D}_{nz}$	Transverse and in-plane differential arrays
$\boldsymbol{\epsilon}_n$	Vector of normal strains
$\boldsymbol{\epsilon}_p$	Vector of in-plane strains
$\boldsymbol{q}_{\tau i}$	Vector containing nodal values of displacment
$\boldsymbol{g}_{\tau i}$	Vector containing nodal values of transverse stresses
$\boldsymbol{R}_{\tau i}$	Vector containing nodal values of all primary unknowns in the condensed notation
E	Young's modulus $[N/m^2]$
E_L	Young's modulus in fiber direction $[N/m^2]$
E_T	Young's modulus normal to the fiber direction $[N/m^2]$
G	Shear modulus $[N/m^2]$
ν	Poisson ratio
e_{ijn}	Piezoelectric coefficients $[C/m^2]$
ε_{ij}	permittivity coefficients $[J/(C \cdot m)]$
p	Pressure [Pa]
N_i	Shape functions
ER	Global scalar parameter for stress accuracy
X, Y, Z	Lamina normal strength $[N/m^2]$
R, S, T	Lamina shear strength in yz-, xz-, xy-direction respectively $[N/m^2]$
a, b	Dimension of the plate in x- and y-direction [m]
h	Thickness of the plate [m]
ϕ	Electric potential [V]
D_x, D_y, D_z	Electric displacement $[C/m^2]$
$\boldsymbol{\mathcal{S}}$	Vector of extensive variables in the condensed notation
$\boldsymbol{\mathcal{E}}$	Vector of intensive variables in the condensed notation

Indices

n	Normal direction
p	In-plane direction
M	Modeled quantity
G	Calculated by geometric relations
C	Calculated by constitutive relations
a	Not-modeled quantities in the condensed notaition
b	Modeled quantities in the condensed notation
k	Layer k
t	Top
b	Bottom

Chapter 1

Introduction

Laminated composites and sandwich structures combine light weight with high stiffness, high structural efficiency and durability, and are therefore increasingly used in aerospace, automotive and ship vehicles. Smart structures with piezoelectric layers or patches embedded inside represent a further example of multilayered structures [1]. Single-walled and multi-walled nanotubes can be considered as advanced present and future multilayered structures [2]. With respect to classical single-layered plates, the multilayered ones present some complicating effects due to their intrinsic transverse and in-plane strong anisotropy. The use of computational methods is mandatory to analyze anisotropic multilayered plates and shells. In case of thermal protection systems and smart structures, the complexity increases due to coupling interactions among mechanical, thermal and electric fields. Finite Element Method (FEM) represents a well established technique to solve structural problems in both linear and nonlinear cases. This work is focused on linear multilayered plate problems for pure mechanical and electro-mechanical coupled case.

1.1 Multilayered Structures

Ideal multilayered structures are made up by a certain number of layers N_L which can be of isotropic, orthotropic, as well as anisotropic material. The sequence of the various lamina orientations is indicated as the *stacking sequence*. All layers are supposed to be perfectly bonded together. Thus the displacement

$$\boldsymbol{u} = [u_x, u_y, u_z]^T \tag{1.1}$$

at the layer interfaces has to follow the condition

$$\boldsymbol{u}_t^k = \boldsymbol{u}_b^{k+1} \quad \text{for} \quad k = 1, \ldots, N_L - 1 \tag{1.2}$$

where k stands for the number of the layer between 1 and N_L. Subscript t describes the top surface of the layer while subscript b is related to the bottom surface. The notation can also be seen in Fig. 1.1. Bold letters denote arrays. For equilibrium reasons, i.e. the Cauchy theorem, also the transverse stresses

$$\boldsymbol{\sigma}_n = [\sigma_{xz}, \sigma_{yz}, \sigma_{zz}]^T \tag{1.3}$$

have to be continuous at the layer interfaces

$$\boldsymbol{\sigma}_{nt}^k = \boldsymbol{\sigma}_{nb}^{k+1} \quad \text{for} \quad k = 1, \ldots, N_L - 1 \tag{1.4}$$

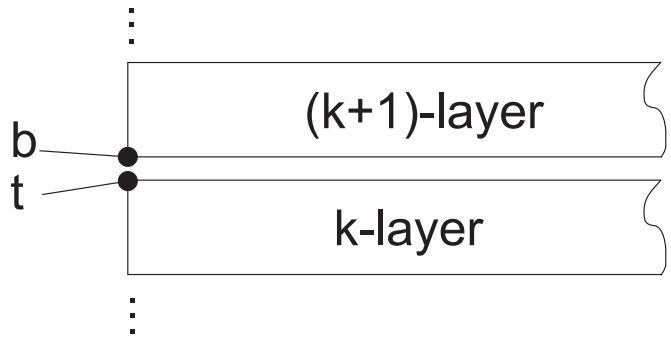

Figure 1.1: *Top and bottom of the neighboured layers*

The two conditions (1.2) and (1.4) follow the postulation of so called *interlaminar continuity* (IC). All layers shall have the same length a and width b but can be different in their thickness t_k. Also material properties can differ significantly in the z-direction for different layers. It is important to notice that due to this *transverse anisotropy* the gradients of displacement and transverse stresses can be discontinues in the layer interfaces. Typical thickness distributions for displacement and stresses are shown in Fig. 1.2.

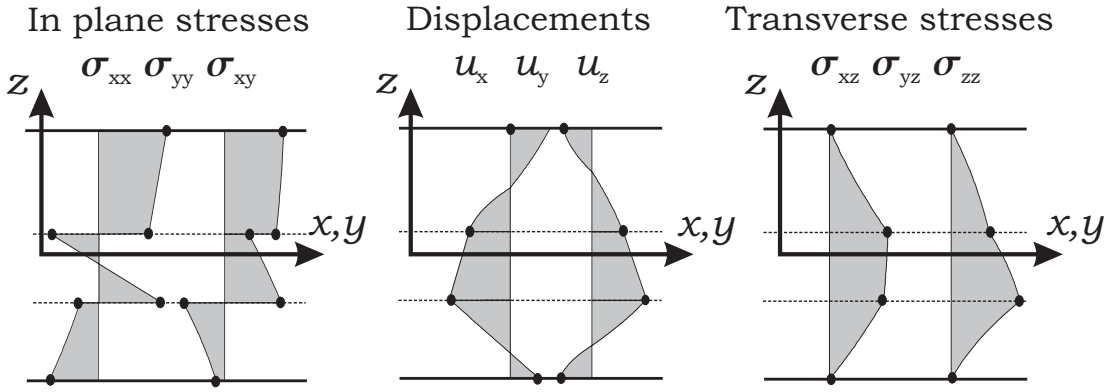

Figure 1.2: *Typical thickness distribution for displacement and stresses in a 3-layer-plate; Courtesy by [3]*

1.2 Principle Of Virtual Displacements

The Principle of Virtual Displacement (PVD) is a common theory to solve mechanical problems, i.e. plate problems, and is based on the Principle of Virtual Work. The virtual work is the work done by the virtual displacements. These displacements can be arbitrary, provided they are consistent with the constraints of the system. The primary results of models derived of PVD are the displacements. Related stresses have to be calculated afterwards, depending on the resulting displacement field. The virtual Work δW can be divided into two parts, the internal and external virtual work δW_i and δW_e

$$\delta W = \delta W_i + \delta W_e \tag{1.5}$$

If the body is situated at equilibrium, the summation of internal and external work gets zero so that

$$\delta W = 0 \tag{1.6}$$

External Virtual Work

The external virtual work is the work done by the virtual displacements on volume body forces f and surface frictions q on the boundary Γ_σ which describes the portion of the boundary part on which stresses are specified. The work is performed on the body so its sign has to be negative. It can be written as

$$\delta W_e = -\left(\int_\Omega \delta \boldsymbol{u}^T \ \boldsymbol{f} \ dv + \int_{\Gamma_\sigma} \delta \boldsymbol{u}^T \ \boldsymbol{q} \ ds \right) \tag{1.7}$$

where dv denotes the volume element in the material body and ds denotes a surface element.

Internal Virtual Work

When forces are applied on a deformable body, they cause a deformation and lead to internal stresses $\boldsymbol{\sigma}$ in the body. Thus the deformation performs work on these internal stresses. The deformation can be written in terms of strains $\boldsymbol{\epsilon}$, so that the internal virtual work takes the following form:

$$\delta W_i = \int_\Omega \ \delta \boldsymbol{\epsilon}^T \ \boldsymbol{\sigma} \ dv \tag{1.8}$$

Variational Statement

Combining these two parts, and separating stresses and strains to in-plane and normal components, denoted with p and n respectively, the variational statement with PVD reads

$$\int_\Omega \left(\delta \boldsymbol{\epsilon}_p^T \ \boldsymbol{\sigma}_p + \delta \boldsymbol{\epsilon}_n^T \ \boldsymbol{\sigma}_n - \delta \boldsymbol{u}^T \boldsymbol{f} \ \right) \ dv - \int_{\Gamma_\sigma} \delta \boldsymbol{u}^T \ \boldsymbol{q} \ ds = 0 \tag{1.9}$$

Classical PVD Models for Multilayered Plates

In many cases models derived for a homogenous plate with PVD are extended to multilayered structures. The basics of some of these classical theories shall be explained in the following part.

CLT The *Classical Laminate Theory* (CLT) is almost identical to the classical plate theory and bases on the Kirchhoff theory for plates. The following assumptions are made:

1. normals to the reference surface Ω remain normal after deformation
2. normals to the reference surface Ω remain straight after deformation
3. normals to the reference surface Ω remain unstrained after deformation

Thus the transverse strains ϵ_{xz}, ϵ_{yz} and ϵ_{zz} are discarded, what leads to the displacement assumptions

$$\begin{aligned} u_x(x,y,z) &= u_{x0}(x,y) - z \ u_{z,x}(x,y) \\ u_y(x,y,z) &= u_{y0}(x,y) - z \ u_{z,y}(x,y) \\ u_z(x,y,z) &= u_{z0}(x,y) \end{aligned} \tag{1.10}$$

Displacement components in correspondence to the reference plane are denoted via the subscript "0". The applicability of this very simple model is restricted to thin laminates with only slightly differing material properties of the layers.

FSDT Reissner and Mindlin postulated a kinematic field that accounts for constant transverse shear stress and strain components along the thickness. The normal deformation is still neglected but now shear effects are taken into account. The displacement assumptions read

$$\begin{aligned} u_x(x,y,z) &= u_{x0}(x,y) + z\ \phi_x(x,y) \\ u_y(x,y,z) &= u_{y0}(x,y) + z\ \phi_y(x,y) \\ u_z(x,y,z) &= u_{z0}(x,y) \end{aligned} \tag{1.11}$$

ϕ_x and ϕ_y can be interpreted as the rotation of the transverse normal about the $x-$ and $y-$ axes respectively. The model based on these kinematics assumption is named First Order Shear Deformation Theory (FSDT).

Both mentioned theories are the standard approaches to plate or laminated plate problems. More information can be found in literature, e.g. Reddy [4]. The assumption of linear displacement distributions over the whole plate is a significant restriction of the model. Some improvements in the description of multilayered plates can be made by introducing terms of higher order. Extensions of FSDT, only using higher order terms for the in plane displacements, are often referred to as *Higher Order Shear Deformation Theories* (HSDT). General extensions, including also the full description of the normal displacement u_z lead to the *Higher Order Theories* (HOT).

1.3 Reissner's Mixed Variational Theorem

The kinematics described above are not able to ensure the interlaminar continuity for transverse shear and normal stresses at the interfaces between the layers. Motivated by this inability Reissner developed an alternative concept in [5]. The Reissner Mixed Variational Theorem (RMVT) offers the possibility to fulfil a priori the interlaminar continuity by also assuming the normal stresses $\boldsymbol{\sigma}_n$ as primary variables. The resulting variational statement for the mixed case divided to in-plane and normal parts states:

$$\int_\Omega \delta\boldsymbol{\epsilon}_{p\,G}^T\ \boldsymbol{\sigma}_{p\,C} + \delta\boldsymbol{\epsilon}_{n\,G}^T \boldsymbol{\sigma}_{n\,M} + \delta\boldsymbol{\sigma}_{n\,M}^T\,(\boldsymbol{\epsilon}_{n\,G} - \boldsymbol{\epsilon}_{n\,C}) - \delta\boldsymbol{u}^T\boldsymbol{f}\ dv - \int_{\Gamma_\sigma} \delta\boldsymbol{u}^T\ \boldsymbol{q}\ ds = 0 \tag{1.12}$$

The index M now emphasizes that the normal stresses are assumed in the model. Strains which are calculated with geometrical relations are marked with the index G and the variables expressed in constitutive equations are denoted by C. Note that here the normal strains ϵ_n must be obtained from the constitutive equations. Therefore the normally used Hooke's law must be transformed. More details are given in Sec. 2.4.

Chapter 2

Unified Formulation

2.1 Main Idea of the Unified Formulation

The main idea of the Unified Formulation is using a generalized expansion for the unknowns in the thickness direction, based on a set of functions herein after called *thickness-functions*. In this way, the three-dimensional problem of multilayered plates can be reduced to a two-dimensional problem. As a first step, the assumption for the displacement field with the Unified Formulation shall be shown. In the most general case it can be written as follows:

$$\boldsymbol{u}(x,y,z) = F_t(z)\boldsymbol{u}_t(x,y) + F_r(z)\boldsymbol{u}_r(x,y) + F_b(z)\boldsymbol{u}_b(x,y) = F_\tau \boldsymbol{u}_\tau \qquad (2.1)$$
$$\text{where} \quad \tau = t,b,r \quad \text{and} \quad r = 2,\ldots,N$$

A cartesian reference system is considered, where z is the the out-of-plane axis. F_τ is the set of the thickness functions and N is the order of the expansion. With this formulation two different models along the thickness of the plate are possible, an equivalent single layer (ESL) and a layerwise (LW) description. The derivation of the governing equations according to the chosen variational statement becomes general, regardless the approximation approach (ESL or LW) and the polynomial expansion order.

2.2 Thickness-Functions

Different axiomatic assumptions in the thickness direction are discussed in the following section by considering Taylor type expansion, combination of Legendre polynomials and Lagrange polynomials. Bothe cases, layerwise and equivalent single layer, are considered.

2.2.1 Different Thickness Polynomials for Layerwise Description

In a layerwise (LW) model the thickness expansion is performed for each layer separately so that independent displacement variables are assumed for each layer k. The interlaminar continuity of the displacements must be imposed for each layer interface but the gradients at the layer interfaces can differ. The interlaminar continuity can be easily imposed when assembling the laminate array from the different layers; this is described in Sec. 2.5. Using this definitions, the generalized displacement assumptions

of the k-th layer can be stated as

$$\boldsymbol{u}^k = F_t\, u_t^k + F_b\, \boldsymbol{u}_b^k + F_r\, \boldsymbol{u}_r^k = F_\tau\, \boldsymbol{u}_\tau^k \tag{2.2}$$
$$\text{where} \quad \tau = t, b, r; \qquad r = 2, 3, \ldots, N \quad \text{and} \quad k = 1, 2, \ldots, N_L$$

The displacement variables $\boldsymbol{u}_t$ and $\boldsymbol{u}_b$ are the values related to the top and bottom surface of the layer. The interlaminar continuity condition can thus be stated as

$$\boldsymbol{u}_t^k = \boldsymbol{u}_b^{(k+1)}, \quad \text{with} \quad k = 1, \ldots, N_L - 1 \tag{2.3}$$

An assumption in this form exists for each layer.

Legendre Polynomials for LW

For the thickness functions F_τ, combinations of Legendre polynomials $P_j = P_j(\zeta_k)$ can be used, wherein ζ_k shall be the nondimensional thickness coordinate of the layer k defined in the domain $-1 \leq \zeta_k \leq 1$. The Legendre Polynomials up to 4th order are the following:

$$\begin{aligned} P_0 &= 1 \\ P_1 &= x \\ P_2 &= \frac{3}{2}(x^2 - 1) \\ P_3 &= \frac{5}{2}x^3 - \frac{3}{2}x \\ P_4 &= \frac{35}{8}x^4 - \frac{15}{4}x^2 + \frac{3}{8} \end{aligned} \tag{2.4}$$

Their graphical plot can be seen in Fig. 2.1. The following combinations of P_j are chosen for the thickness functions F_τ in order to use the top and bottom displacement values as variables $\boldsymbol{u}_\tau$:

$$F_t = (P_0 + P_1)/2; \qquad F_b = (P_0 - P_1)/2; \qquad F_r = P_r - P_{r-2} \tag{2.5}$$
$$\text{with} \quad r = 2, 3, \ldots, N$$

In this way the chosen thickness functions have the following properties:

$$\zeta_k = 1 \; : \qquad F_t = 1; \qquad F_r = 0; \qquad F_b = 0 \tag{2.6}$$
$$\zeta_k = -1 \; : \qquad F_t = 0; \qquad F_r = 0; \qquad F_b = 1 \tag{2.7}$$

The resulting distributions of F_t, F_b and F_r for $r = 2, 3, 4$ are depicted in Fig. 2.2.

Lagrange Polynomials for LW

Another possibility is the usage of Lagrange polynomials for the expansion in thickness direction. In this case the number and the formula for each F_τ depends on the order of the expansion. For the first 4 orders the Lagrange polynomials defined in the domain $-1 \leq \zeta \leq 1$ are presented in Tab. 2.1. For the first order, thickness functions based on Lagrange and Legendre polynomials are exactly the same. Unless otherwise noted,

1st order
$F_t = \frac{(1+\zeta)}{2}$
$F_b = \frac{(1-\zeta)}{2}$
2nd order
$F_t = \frac{-(1+\zeta)(\zeta-z_1)}{2\,(-1+z_1)}$
$F_2 = \frac{(-1+\zeta^2)}{(-1+z_1^2)}$
$F_b = \frac{(-1+\zeta)(\zeta-z_1)}{2\,(1+z_1)}$
3rd order
$F_t = \frac{(1+\zeta)(\zeta-z_1)(\zeta-z_2)}{2\,(-1+z_1)(-1+z_2)}$
$F_2 = \frac{-(-1+\zeta)(1+\zeta)(\zeta-z_1)}{(z_1-z_2)(-1+z_2^2)}$
$F_3 = \frac{(-1+\zeta)(1+\zeta)(\zeta-z_2)}{(-1+z_1^2)(z_1-z_2)}$
$F_b = \frac{-(-1+\zeta)(\zeta-z_1)(\zeta-z_2)}{2\,(1+z_1)(1+z_2)}$
4th order
$F_t = \frac{-(1+\zeta)(\zeta-z_1)(\zeta-z_2)(\zeta-z_3)}{2\,(-1+z_1)(-1+z_2)(-1+z_3)}$
$F_2 = \frac{(-1+\zeta)(1+\zeta)(\zeta-z_1)(\zeta-z_2)}{(z_1-z_3)(z_2-z_3)(-1+z_3^2)}$
$F_3 = \frac{-(-1+\zeta)(1+\zeta)(\zeta-z_1)(\zeta-z_3)}{(z_1-z_2)(-1+z_2^2)(z_2-z_3)}$
$F_4 = \frac{(-1+\zeta)(1+\zeta)(\zeta-z_2)(\zeta-z_3)}{(-1+z_1^2)(z_1-z_2)(z_1-z_3)}$
$F_b = \frac{(-1+\zeta)(\zeta-z_1)(\zeta-z_2)(\zeta-z_3)}{2\,(1+z_1)(1+z_2)(1+z_3)}$

Table 2.1: *Thickness functions $F_\tau(\zeta)$ with Lagrange Polynomials up to 4th order*

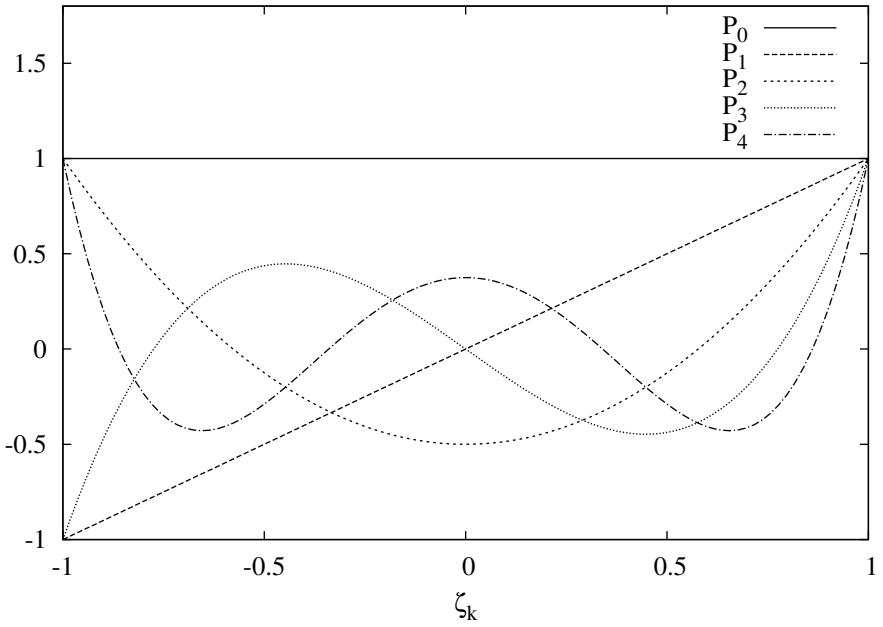

Figure 2.1: *Legendre Polynomials P_0 to P_4 over thickness ζ_k*

the parameters z_i for higher order Lagrange polynomials divide the domain $-1 \ldots 1$ in equal distances, i.e. for the 4th order case

$$z_1 = -0.5; \quad z_2 = 0; \quad z_3 = 0.5 \tag{2.8}$$

The graphical plots of the thickness functions from 2nd to 4th order are shown in Fig. 2.3 to 2.5. Analogously to the expansion based on Legendre polynomials, F_t and F_b for the thickness functions with Lagrange polynomials refer to the top and bottom surface of the layer with the same characteristics as in 2.6 and 2.7.

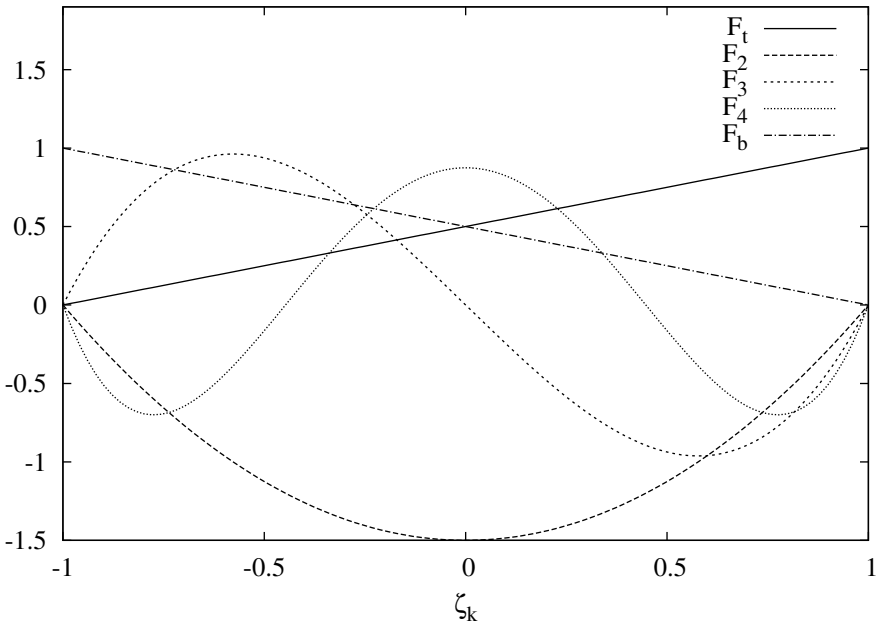

Figure 2.2: *Thickness functions F_τ over ζ_k for Legendre polynomials*

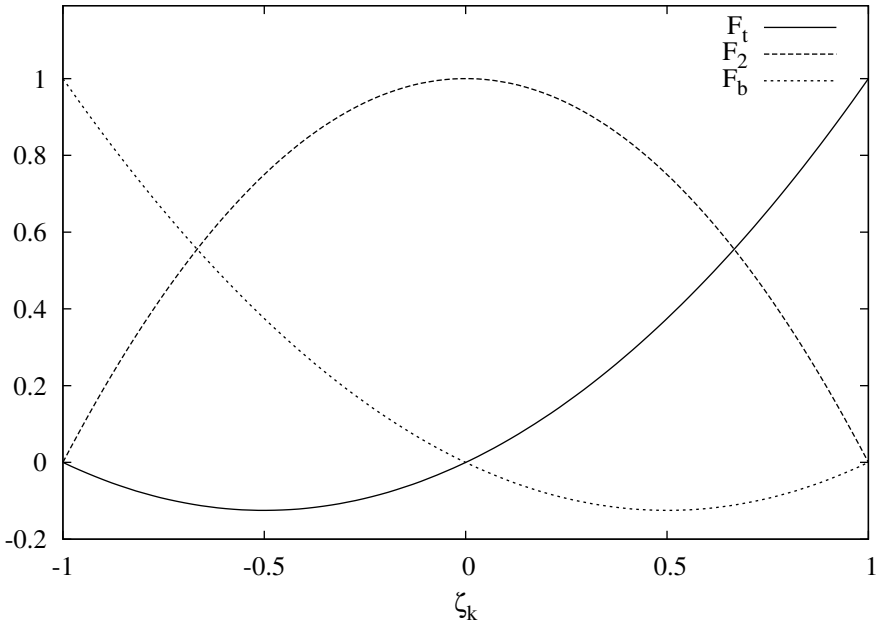

Figure 2.3: *Thickness functions F_τ over ζ_k for 2nd order Lagrange polynomials*

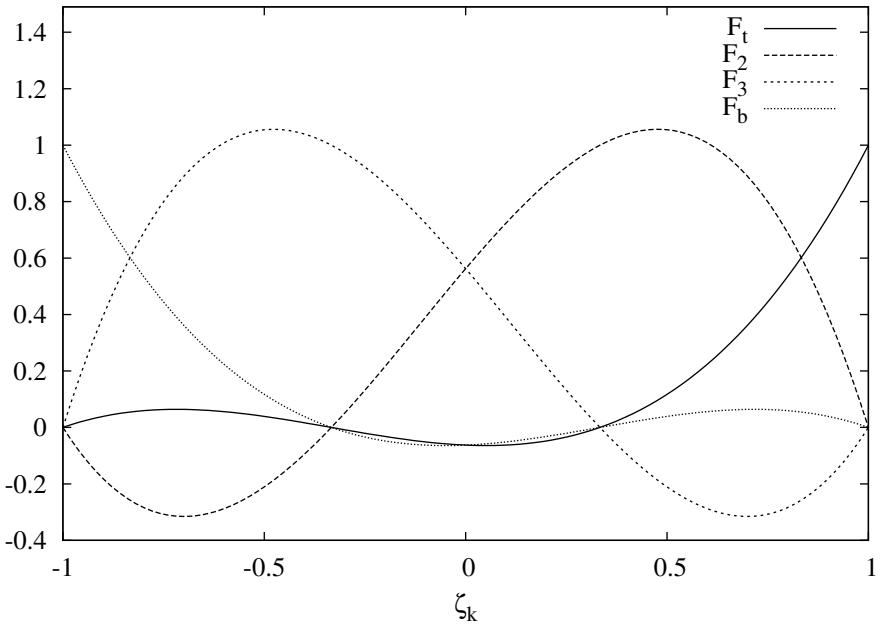

Figure 2.4: *Thickness functions F_τ over ζ_k for 3rd order Lagrange polynomials*

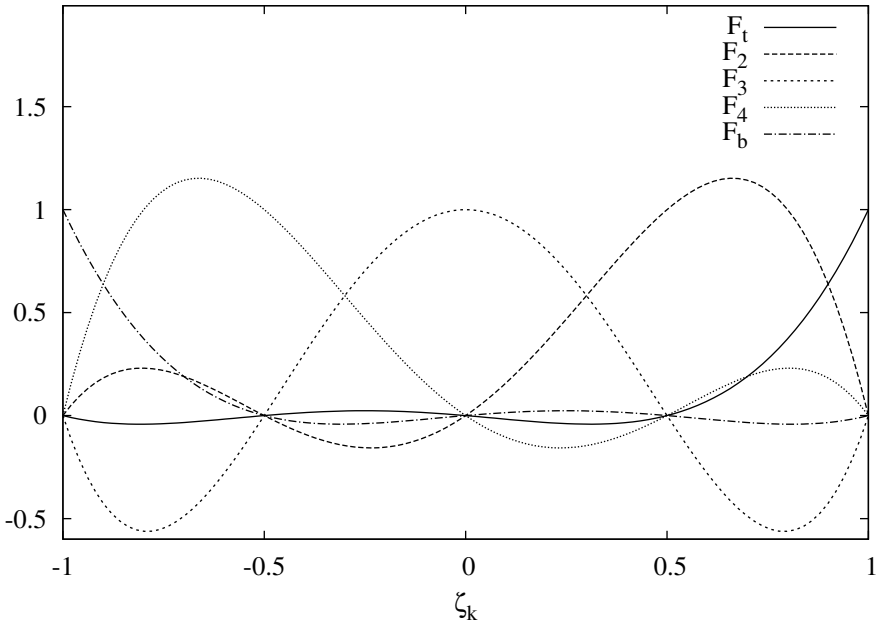

Figure 2.5: *Thickness functions F_τ over ζ_k for 4th order Lagrange polynomials*

2.2.2 Different Thickness Polynomials for ESL Description

With ESL models, a global assumption for the unknowns is considered along the thickness of the plate so that only one set of unknown variables exists. Also in ESL description it is possible to use Lagrange and Legendre polynomials as described in Sec. 2.2.1 considering the whole plate as only one layer. The assembly of the laminate array is shown in Sec. 2.5 again. Another way for ESL description is the usage of Taylor expansion in the thickness direction. Therefore the thickness-functions F_τ take the form

$$F_b = 1, \qquad F_r = z^r, \qquad F_t = z^N, \qquad r = 1, 2, \ldots, N-1 \tag{2.9}$$

In this case subscript b denotes values related to the plate reference mid-surface Ω, while subscript t is related to the highest order term. Depending on the used variational statement (PVD or RMVT), on the order of expansion N, and on the choice of the thickness function, different acronyms have been introduced in order to address them. Figure 2.6 shows how the acronyms are built: The first field can be "E"or "L" according to the ESL or LW description, respectively; the second field can be "D" or "M", according to the PVD or RMVT application, respectively; the third field can assume the numbers 1-4, according to the order of the adopted expansion in the thickness direction; the last field shows which type of polynomial has been chosen for the thickness expansion. For example LM2(LGR) means layerwise model based on mixed

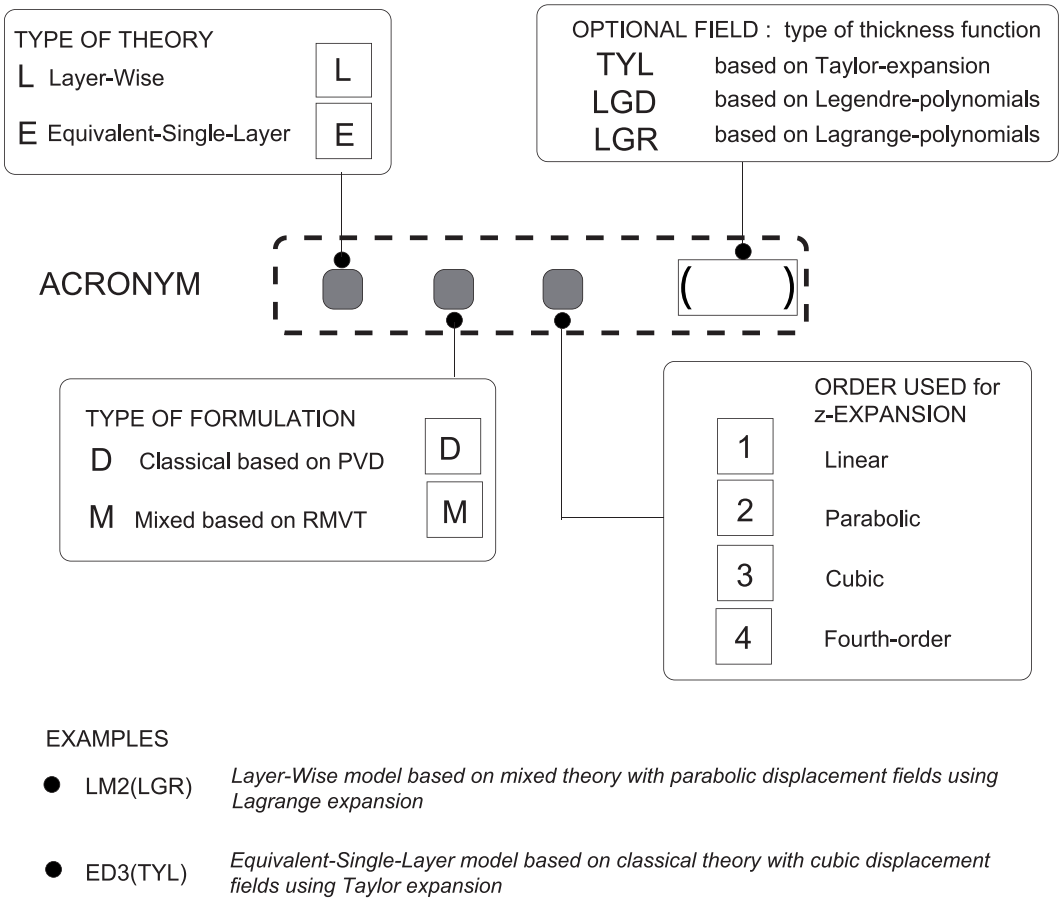

Figure 2.6: *System of the acronyms*

theory with parabolic displacement field using Lagrange expansion.

2.3 Governing Equations With PVD

Two basic assumptions in the description of the multilayered material are made. The first is the material law or the constitutive equations, represented by Hooke's law and the second is the geometric relation between the strains $\boldsymbol{\epsilon}$ and the displacements $\boldsymbol{u}$.

Constitutive Equations

The general material behavior is described by the Hooke's law, relating the stresses $\boldsymbol{\sigma}$ to the strains $\boldsymbol{\epsilon}$ via the elastic stiffness coefficients $\tilde{\boldsymbol{C}}$. As preparation for expanding the theory to the mixed case later on, stresses and strains are separated to in-plane and transverse components denoted with the subscript p and n respectively:

$$\begin{aligned} \boldsymbol{\sigma}_p &= [\sigma_{11}, \sigma_{22}, \sigma_{12}]^T \qquad \boldsymbol{\sigma}_n = [\sigma_{13}, \sigma_{23}, \sigma_{33}]^T \\ \boldsymbol{\epsilon}_p &= [\epsilon_{11}, \epsilon_{22}, \epsilon_{12}]^T \qquad \boldsymbol{\epsilon}_n = [\epsilon_{13}, \epsilon_{23}, \epsilon_{33}]^T \end{aligned} \tag{2.10}$$

wherein superscript T marks transposition. The Hooke's law in this separated form states

$$\begin{aligned} \boldsymbol{\sigma}_p &= \tilde{\boldsymbol{C}}_{pp}\,\boldsymbol{\epsilon}_p + \tilde{\boldsymbol{C}}_{pn}\,\boldsymbol{\epsilon}_n \\ \boldsymbol{\sigma}_n &= \tilde{\boldsymbol{C}}_{np}\,\boldsymbol{\epsilon}_p + \tilde{\boldsymbol{C}}_{nn}\,\boldsymbol{\epsilon}_n \end{aligned} \tag{2.11}$$

By substituting the index couples 11, 22, 33, 23, 13, 12 with new indices ranging from 1 to 6 respectively, the arrays of the elastic material properties for monoclinic behavior explicitly read

$$\tilde{\boldsymbol{C}}_{pp} = \begin{bmatrix} \tilde{C}_{11} & \tilde{C}_{12} & \tilde{C}_{16} \\ \tilde{C}_{12} & \tilde{C}_{22} & \tilde{C}_{26} \\ \tilde{C}_{16} & \tilde{C}_{26} & \tilde{C}_{66} \end{bmatrix} \qquad \tilde{\boldsymbol{C}}_{pn} = \begin{bmatrix} 0 & 0 & \tilde{C}_{13} \\ 0 & 0 & \tilde{C}_{23} \\ 0 & 0 & \tilde{C}_{36} \end{bmatrix}$$

$$\tilde{\boldsymbol{C}}_{np} = \begin{bmatrix} 0 & 0 & 0 \\ 0 & 0 & 0 \\ \tilde{C}_{13} & \tilde{C}_{23} & \tilde{C}_{36} \end{bmatrix} \qquad \tilde{\boldsymbol{C}}_{nn} = \begin{bmatrix} \tilde{C}_{55} & \tilde{C}_{45} & 0 \\ \tilde{C}_{45} & \tilde{C}_{44} & 0 \\ 0 & 0 & \tilde{C}_{33} \end{bmatrix}$$

Geometrical Relation

To express the strains $\boldsymbol{\epsilon}_p$ and $\boldsymbol{\epsilon}_n$ in terms of the displacements $\boldsymbol{u}$ the geometric relations are used in linearized form, only considering first derivatives. They can be written in the following tensor notation:

$$\boldsymbol{\epsilon}_p = \boldsymbol{D}_p \boldsymbol{u} \qquad \boldsymbol{\epsilon}_n = \boldsymbol{D}_n \boldsymbol{u} \tag{2.12}$$

The arrays $\boldsymbol{D_p}$ and $\boldsymbol{D_n}$ contain the differential operators. Their explicit form reads

$$\boldsymbol{D}_p = \begin{bmatrix} \partial_x & 0 & 0 \\ 0 & \partial_y & 0 \\ \partial_y & \partial_x & 0 \end{bmatrix} \qquad \boldsymbol{D}_n = \begin{bmatrix} \partial_z & 0 & \partial_x \\ 0 & \partial_z & \partial_y \\ 0 & 0 & \partial_z \end{bmatrix}$$

In order to use the fundamental lemma of virtual calculus later on, the differential operator array $\boldsymbol{D}_n$ can be separated into an in-plane and a transverse differential operator array

$$\boldsymbol{D}_n = \boldsymbol{D}_{n\Omega} + \boldsymbol{D}_{nz} \tag{2.13}$$

with

$$\boldsymbol{D}_{n\Omega} = \begin{bmatrix} 0 & 0 & \partial_x \\ 0 & 0 & \partial_y \\ 0 & 0 & 0 \end{bmatrix} \qquad \boldsymbol{D}_{nz} = \begin{bmatrix} \partial_z & 0 & 0 \\ 0 & \partial_z & 0 \\ 0 & 0 & \partial_z \end{bmatrix}$$

Finite Element Discretization

When the finite element method is applied, the unknowns can be expressed in terms of their nodal values, by using the shape functions N_i.

$$\boldsymbol{u}_\tau^k(x,y) = N_i(x,y)\,\boldsymbol{q}_{\tau i}^k \qquad i = 1,2,...,N_n \tag{2.14}$$

where N_n denotes the number of nodes concerning the considered finite element and $\boldsymbol{q}_{\tau i}^k$ is the vector containing nodal values of the displacement.

$$\boldsymbol{q}_{\tau i}^k = [q_{u_x\tau i},\, q_{u_y\tau i},\, q_{u_z\tau i}]^T \tag{2.15}$$

Substituting Eq. (2.14) in Eq. (2.2), the final expression for the displacements can be obtained:

$$\boldsymbol{u}^k(x,y,z) = F_\tau(z)\,N_i(x,y)\,\boldsymbol{q}_{\tau i}^k \tag{2.16}$$

Derivation of Finite Element Matrices

The internal virtual work of the PVD (1.8) formulated for a multilayered plate can be written as:

$$\sum_{k=1}^{N_L} \int_{\Omega_k} \int_{h_k} \left\{ \delta\boldsymbol{\epsilon}_p^{k\,T}\boldsymbol{\sigma}_p^k + \delta\boldsymbol{\epsilon}_n^{k\,T}\boldsymbol{\sigma}_n^k \right\} d\Omega_k\, dz = \delta W_i \tag{2.17}$$

where k identifies the layer and N_L is the number of layers in the laminate. Ω_k and h_k are the planar surface and the thickness of the k-th layer. Restricting Eq. (2.17) to the layer k and introducing Hooke's law (2.11), it becomes:

$$\int_{\Omega_k} \int_{h_k} \left[\delta\boldsymbol{\epsilon}_p^{k\,T} \left(\tilde{\boldsymbol{C}}_{pp}^k\,\boldsymbol{\epsilon}_p^k + \tilde{\boldsymbol{C}}_{pn}^k\,\boldsymbol{\epsilon}_n^k \right) + \delta\boldsymbol{\epsilon}_n^{k\,T} \left(\tilde{\boldsymbol{C}}_{np}^k\,\boldsymbol{\epsilon}_p^k + \tilde{\boldsymbol{C}}_{nn}^k\,\boldsymbol{\epsilon}_n^k \right) \right] d\Omega_k\, dz = \delta W_i^k \tag{2.18}$$

Due to the fact that the base function F_τ is independent of x and y and considering the separated differential operator (2.13) as well as the finite element discretization (2.14), the strains $\boldsymbol{\epsilon}_p$ and $\boldsymbol{\epsilon}_n$ can be written in the following way:

$$\boldsymbol{\epsilon}_p^k = F_\tau \boldsymbol{D}_p (N_i\,\boldsymbol{I})\,\boldsymbol{q}_{\tau i}^k \tag{2.19}$$

$$\boldsymbol{\epsilon}_n^k = F_\tau \boldsymbol{D}_{n\Omega}\,(N_i\,\boldsymbol{I})\,\boldsymbol{q}_{\tau i}^k + F_{\tau,z} N_i\,\boldsymbol{q}_{\tau i}^k \tag{2.20}$$

where $\boldsymbol{I} = \begin{bmatrix} 1 & 0 & 0 \\ 0 & 1 & 0 \\ 0 & 0 & 1 \end{bmatrix}$ and $F_{\tau,z} = \frac{\partial F_\tau}{\partial z}$.

Including these strain-displacement relations (2.19) and (2.20) in Eq. (2.18), the following statement of the internal virtual work can be obtained (subscripts τ and i are

related to virtual variations while subscript s and j concern the real values):

$$\begin{aligned}
&\int_{\Omega_k} \delta \boldsymbol{q}_{\tau i}^{kT}\, \boldsymbol{D}_p^T\,(N_i \boldsymbol{I})\, \tilde{\boldsymbol{C}}_{pp}^k \left[\int_{h_k} (F_\tau F_s)\, dz\right] \boldsymbol{D}_p\,(N_j \boldsymbol{I})\, \boldsymbol{q}_{sj}^k\, d\Omega_k + \\
&+ \int_{\Omega_k} \delta \boldsymbol{q}_{\tau i}^{kT}\, \boldsymbol{D}_p^T\,(N_i \boldsymbol{I})\, \tilde{\boldsymbol{C}}_{pn}^k \left[\int_{h_k} (F_\tau F_s)\, dz\right] \boldsymbol{D}_{n\Omega}\,(N_j \boldsymbol{I})\, \boldsymbol{q}_{sj}^k\, d\Omega_k + \\
&+ \int_{\Omega_k} \delta \boldsymbol{q}_{\tau i}^{kT}\, \boldsymbol{D}_p^T\,(N_i \boldsymbol{I})\, \tilde{\boldsymbol{C}}_{pn}^k \left[\int_{h_k} \left(F_\tau F_{s_{,z}}\right) dz\right] N_j\, \boldsymbol{q}_{sj}^k\, d\Omega_k + \\
&+ \int_{\Omega_k} \delta \boldsymbol{q}_{\tau i}^{kT}\, \boldsymbol{D}_{n\Omega}^T\,(N_i \boldsymbol{I})\, \tilde{\boldsymbol{C}}_{np}^k \left[\int_{h_k} (F_\tau F_s)\, dz\right] \boldsymbol{D}_p\,(N_j \boldsymbol{I})\, \boldsymbol{q}_{sj}^k\, d\Omega_k + \\
&+ \int_{\Omega_k} \delta \boldsymbol{q}_{\tau i}^{kT}\, \boldsymbol{D}_{n\Omega}^T\,(N_i \boldsymbol{I})\, \tilde{\boldsymbol{C}}_{nn}^k \left[\int_{h_k} (F_\tau F_s)\, dz\right] \boldsymbol{D}_{n\Omega}\,(N_j \boldsymbol{I})\, \boldsymbol{q}_{sj}^k\, d\Omega_k + \\
&+ \int_{\Omega_k} \delta \boldsymbol{q}_{\tau i}^{kT}\, \boldsymbol{D}_{n\Omega}^T\,(N_i \boldsymbol{I})\, \tilde{\boldsymbol{C}}_{nn}^k \left[\int_{h_k} \left(F_\tau F_{s_{,z}}\right) dz\right] N_j\, \boldsymbol{q}_{sj}^k\, d\Omega_k + \\
&+ \int_{\Omega_k} \delta \boldsymbol{q}_{\tau i}^{kT}\, N_i\, \tilde{\boldsymbol{C}}_{np}^k \left[\int_{h_k} \left(F_{\tau_{,z}} F_s\right) dz\right] \boldsymbol{D}_p\,(N_j \boldsymbol{I})\, \boldsymbol{q}_{sj}^k\, d\Omega_k + \\
&+ \int_{\Omega_k} \delta \boldsymbol{q}_{\tau i}^{kT}\, N_i\, \tilde{\boldsymbol{C}}_{nn}^k \left[\int_{h_k} \left(F_{\tau_{,z}} F_s\right) dz\right] \boldsymbol{D}_{n\Omega}\,(N_j \boldsymbol{I})\, \boldsymbol{q}_{sj}^k\, d\Omega_k + \\
&+ \int_{\Omega_k} \delta \boldsymbol{q}_{\tau i}^{kT}\, N_i\, \tilde{\boldsymbol{C}}_{nn}^k \left[\int_{h_k} \left(F_{\tau_{,z}} F_{s_{,z}}\right) dz\right] N_j \boldsymbol{q}_{sj}^k\, d\Omega_k = \delta W_i^k
\end{aligned} \tag{2.21}$$

As usual in two-dimensional modellings, the integration in the thickness-direction can be made a priori. Therfore the following layer-integrals are introduced:

$$\left(E_{\tau s},\ E_{\tau s_{,z}},\ E_{\tau_{,z} s},\ E_{\tau_{,z} s_{,z}}\right) = \int_{h_k} \left(F_\tau F_s,\ F_\tau F_{s_{,z}},\ F_{\tau_{,z}} F_s,\ F_{\tau_{,z}} F_{s_{,z}}\right) dz \tag{2.22}$$

The layer stiffnesses can be written as

$$\left(\tilde{\boldsymbol{Z}}_{pp}^{k\tau s},\ \tilde{\boldsymbol{Z}}_{pn}^{k\tau s},\ \tilde{\boldsymbol{Z}}_{np}^{k\tau s},\ \tilde{\boldsymbol{Z}}_{nn}^{k\tau s}\right) = \left(\tilde{\boldsymbol{C}}_{pp}^k,\ \tilde{\boldsymbol{C}}_{pn}^k,\ \tilde{\boldsymbol{C}}_{np}^k,\ \tilde{\boldsymbol{C}}_{nn}^k E_{\tau s}\right) \tag{2.23}$$

$$\begin{aligned}
&\left(\tilde{\boldsymbol{Z}}_{pn}^{k\tau s_{,z}},\ \tilde{\boldsymbol{Z}}_{nn}^{k\tau s_{,z}},\ \tilde{\boldsymbol{Z}}_{np}^{k\tau_{,z} s},\ \tilde{\boldsymbol{Z}}_{nn}^{k\tau_{,z} s},\ \tilde{\boldsymbol{Z}}_{nn}^{k\tau_{,z} s_{,z}}\right) = \\
&= \left(\tilde{\boldsymbol{C}}_{pn}^k\, E_{\tau s_{,z}},\ \tilde{\boldsymbol{C}}_{nn}^k\, E_{\tau s_{,z}},\ \tilde{\boldsymbol{C}}_{np}^k\, E_{\tau_{,z} s},\ \tilde{\boldsymbol{C}}_{nn}^k\, E_{\tau_{,z} s}^k,\ \tilde{\boldsymbol{C}}_{nn}^k\, E_{\tau_{,z} s_{,z}}\right)
\end{aligned} \tag{2.24}$$

Now Eq. (2.21) can be written in the following compact form

$$\delta \mathbf{q}_{\tau i}^{kT}\, \mathbf{K}^{k\tau s ij}\, \mathbf{q}_{sj}^k = \delta W_i^k \tag{2.25}$$

with the finite element matrix

$$\begin{aligned}
\boldsymbol{K}^{k\tau s ij} = {} & \triangleleft \boldsymbol{D}_p^T\,(N_i \boldsymbol{I}) \left[\tilde{\boldsymbol{Z}}_{pp}^{k\tau s}\, \boldsymbol{D}_p\,(N_j \boldsymbol{I}) + \tilde{\boldsymbol{Z}}_{pn}^{k\tau s}\, \boldsymbol{D}_{n\Omega}\,(N_j \boldsymbol{I}) + \tilde{\boldsymbol{Z}}_{pn}^{k\tau s_{,z}} N_j\right] + \\
& + \boldsymbol{D}_{n\Omega}^T\,(N_i \boldsymbol{I}) \left[\tilde{\boldsymbol{Z}}_{np}^{k\tau s}\, \boldsymbol{D}_p\,(N_j \boldsymbol{I}) + \tilde{\boldsymbol{Z}}_{nn}^{k\tau s}\, \boldsymbol{D}_{n\Omega}\,(N_j \boldsymbol{I}) + \tilde{\boldsymbol{Z}}_{nn}^{k\tau s_{,z}} N_j\right] + \\
& + N_i \left[\tilde{\boldsymbol{Z}}_{np}^{k\tau_{,z} s}\, \boldsymbol{D}_p\,(N_j \boldsymbol{I}) + \tilde{\boldsymbol{Z}}_{nn}^{k\tau_{,z} s}\, \boldsymbol{D}_{n\Omega}\,(N_j \boldsymbol{I}) + \tilde{\boldsymbol{Z}}_{nn}^{k\tau_{,z} s_{,z}} N_j\right] \triangleright_\Omega
\end{aligned} \tag{2.26}$$

where the symbol $\lhd \ldots \rhd_\Omega$ denotes the integral on Ω. The matrix (2.26) itself is a 3×3 array and consists of the fundamental nucleus of finite element matrices related to PVD applications. Explicitly it reads:

$$
\begin{aligned}
K_{11}^{k\tau sij} &= \tilde{Z}_{pp11}^{k\tau s} \lhd N_{i,x} N_{j,x} \rhd_\Omega + \tilde{Z}_{pp16}^{k\tau s} \lhd N_{i,y} N_{j,x} \rhd_\Omega + \tilde{Z}_{pp16}^{k\tau s} \lhd N_{i,x} N_{j,y} \rhd_\Omega + \\
&+ \tilde{Z}_{pp66}^{k\tau s} \lhd N_{i,y} N_{j,y} \rhd_\Omega + \tilde{Z}_{nn55}^{k\tau,zs,z} \lhd N_i N_j \rhd_\Omega \\
K_{12}^{k\tau sij} &= \tilde{Z}_{pp12}^{k\tau s} \lhd N_{i,x} N_{j,y} \rhd_\Omega + \tilde{Z}_{pp26}^{k\tau s} \lhd N_{i,y} N_{j,y} \rhd_\Omega + \tilde{Z}_{pp16}^{k\tau s} \lhd N_{i,x} N_{j,x} \rhd_\Omega + \\
&+ \tilde{Z}_{pp66}^{k\tau s} \lhd N_{i,y} N_{j,x} \rhd_\Omega + \tilde{Z}_{nn45}^{k\tau,zs,z} \lhd N_i N_j \rhd_\Omega \\
K_{13}^{k\tau sij} &= \tilde{Z}_{pn13}^{k\tau s,z} \lhd N_{i,x} N_j \rhd_\Omega + \tilde{Z}_{pn36}^{k\tau s,z} \lhd N_{i,y} N_j \rhd_\Omega + \tilde{Z}_{nn55}^{k\tau,zs} \lhd N_i N_{j,x} \rhd_\Omega + \\
&+ \tilde{Z}_{nn45}^{k\tau,zs} \lhd N_i N_{j,y} \rhd_\Omega \\
K_{21}^{k\tau sij} &= \tilde{Z}_{pp12}^{k\tau s} \lhd N_{i,y} N_{j,x} \rhd_\Omega + \tilde{Z}_{pp16}^{k\tau s} \lhd N_{i,x} N_{j,x} \rhd_\Omega + \tilde{Z}_{pp26}^{k\tau s} \lhd N_{i,y} N_{j,y} \rhd_\Omega + \\
&+ \tilde{Z}_{pp66}^{k\tau s} \lhd N_{i,x} N_{j,y} \rhd_\Omega + \tilde{Z}_{nn45}^{k\tau,zs,z} \lhd N_i N_j \rhd_\Omega \\
K_{22}^{k\tau sij} &= \tilde{Z}_{pp22}^{k\tau s} \lhd N_{i,y} N_{j,y} \rhd_\Omega + \tilde{Z}_{pp26}^{k\tau s} \lhd N_{i,x} N_{j,y} \rhd_\Omega + \tilde{Z}_{pp26}^{k\tau s} \lhd N_{i,y} N_{j,x} \rhd_\Omega + \\
&+ \tilde{Z}_{pp66}^{k\tau s} \lhd N_{i,x} N_{j,x} \rhd_\Omega + \tilde{Z}_{nn44}^{k\tau,zs,z} \lhd N_i N_j \rhd_\Omega \\
K_{23}^{k\tau sij} &= \tilde{Z}_{pn23}^{k\tau s,z} \lhd N_{i,y} N_j \rhd_\Omega + \tilde{Z}_{pn36}^{k\tau s,z} \lhd N_{i,x} N_j \rhd_\Omega + \tilde{Z}_{nn45}^{k\tau,zs} \lhd N_i N_{j,x} \rhd_\Omega + \\
&+ \tilde{Z}_{nn44}^{k\tau,zs} \lhd N_i N_{j,y} \rhd_\Omega \\
K_{31}^{k\tau sij} &= \tilde{Z}_{nn55}^{k\tau s,zk} \lhd N_{i,x} N_j \rhd_\Omega + \tilde{Z}_{nn45}^{k\tau s,zk} \lhd N_{i,y} N_j \rhd_\Omega + \tilde{Z}_{np13}^{k\tau,zs} \lhd N_i N_{j,x} \rhd_\Omega + \\
&+ \tilde{Z}_{np36}^{k\tau,zs} \lhd N_i N_{j,y} \rhd_\Omega \\
K_{32}^{k\tau sij} &= \tilde{Z}_{nn45}^{k\tau s,zk} \lhd N_{i,x} N_j \rhd_\Omega + \tilde{Z}_{nn44}^{k\tau s,zk} \lhd N_{i,y} N_j \rhd_\Omega + \tilde{Z}_{np23}^{k\tau,zs} \lhd N_i N_{j,y} \rhd_\Omega + \\
&+ \tilde{Z}_{np36}^{k\tau,zs} \lhd N_i N_{j,x} \rhd_\Omega \\
K_{33}^{k\tau sij} &= \tilde{Z}_{nn55}^{k\tau sk} \lhd N_{i,x} N_{j,x} \rhd_\Omega + \tilde{Z}_{nn45}^{k\tau sk} \lhd N_{i,y} N_{j,x} \rhd_\Omega + \tilde{Z}_{nn45}^{k\tau sk} \lhd N_{i,x} N_{j,y} \rhd_\Omega + \\
&+ \tilde{Z}_{nn44}^{k\tau sk} \lhd N_{i,y} N_{j,y} \rhd_\Omega + \tilde{Z}_{nn33}^{k\tau,zs,z} \lhd N_i N_j \rhd_\Omega
\end{aligned}
\tag{2.27}
$$

Introducing the external work of applied loadings provides

$$
\delta \boldsymbol{q}_{\tau i}^{kT} \, \boldsymbol{K}^{k\tau sij} \, \boldsymbol{q}_{sj}^{k} = \delta \boldsymbol{q}_{\tau i}^{kT} \, \boldsymbol{P}_{\tau i}^{k} \tag{2.28}
$$

and leads by imposing the definition of the virtual variations for each layer k to the following equilibrium conditions:

$$
\delta \boldsymbol{q}_{\tau i}^{kT} : \qquad \boldsymbol{K}^{k\tau sij} \, \boldsymbol{q}_{sj}^{k} = \boldsymbol{P}_{\tau i}^{k} \tag{2.29}
$$

In order to write the finite element matrix for the whole multilayered plate, the coupling of indices (τ, s) and (i, j) of the fundamental nucleus of $\boldsymbol{K}^{k\tau sij}$ have to be expanded, see also Sec. 2.5

2.4 Governing Equations with RMVT

For the RMVT case, the governing equations and thus the fundamental nuclei shall be derived. In addition to the displacement formulation, an assumption also on the

transverse stresses $\boldsymbol{\sigma}_n$ has to be made. The general approach is exactly the same as for the PVD-model. The variational statement is the adapted one of the mixed formulation (1.12).

Stress Assumption

Additionally to the displacement assumption (2.1) the mixed formulation also requires an assumption of the transverse stress field which is done in accordance to (2.1). Again, subscript M is used to underline the fact that the transverse stresses are now assumed by the model.

$$\begin{aligned} &\boldsymbol{\sigma}^k_{nM} = F_t\boldsymbol{\sigma}^k_{nt} + F_r\boldsymbol{\sigma}^k_{nr} + F_b\boldsymbol{\sigma}^k_{nb} = F_\tau\boldsymbol{\sigma}^k_{n\tau} \\ &\text{where} \quad \tau = t, b, r \quad \text{and} \quad r = 2, 3, \ldots, N \end{aligned} \tag{2.30}$$

Constitutive Equations

In order to use the mixed formulation, the conventional Hooke's law has to be modified. Transverse stresses are assumed and can not any more be expressed in terms of the strains $\boldsymbol{\epsilon}_p$ and $\boldsymbol{\epsilon}_n$. The mixed formulation of the constitutive equations now expresses $\boldsymbol{\sigma}_p$ and $\boldsymbol{\epsilon}_n$ in terms of $\boldsymbol{\sigma}_{nM}$ and $\boldsymbol{\epsilon}_p$ and can be therefore written as:

$$\begin{aligned} \boldsymbol{\sigma}^k_{pC} &= \boldsymbol{C}^k_{pp}\,\boldsymbol{\epsilon}^k_{pG} + \boldsymbol{C}^k_{pn}\boldsymbol{\sigma}^k_{nM} \\ \boldsymbol{\epsilon}^k_{nC} &= \boldsymbol{C}^k_{np}\boldsymbol{\epsilon}^k_{pG} + \boldsymbol{C}^k_{nn}\boldsymbol{\sigma}^k_{nM} \end{aligned} \tag{2.31}$$

Subscript C denotes that these quantities are calculated by the constitutive equations while subscript G indicates the calculation of the variables by geometric relations. Equations (2.31) are formally derived by transformation of the conventional Hooke's law (2.11). The elasticity arrays of the mixed equations are thus obtained by

$$\boldsymbol{C}_{pp} = \tilde{\boldsymbol{C}}_{pp} - \tilde{\boldsymbol{C}}_{pn}\tilde{\boldsymbol{C}}^{-1}_{nn}\tilde{\boldsymbol{C}}_{np}; \qquad \boldsymbol{C}_{pn} = \tilde{\boldsymbol{C}}_{pn}\tilde{\boldsymbol{C}}^{-1}_{nn} \tag{2.32}$$

$$\boldsymbol{C}_{np} = -\tilde{\boldsymbol{C}}^{-1}_{nn}\tilde{\boldsymbol{C}}_{np}; \qquad \boldsymbol{C}_{nn} = \tilde{\boldsymbol{C}}^{-1}_{nn} \tag{2.33}$$

Geometric Relations

The geometric relations are the same as used for the displacement formulation, see Eq. (2.12).

Finite Element Discretization

In addition to the displacements $\boldsymbol{u}^k$ also the transverse stresses $\boldsymbol{\sigma}^k_n$ are expressed in terms of their nodal values via the same shape functions N_i.

$$\boldsymbol{\sigma}^k_{n\tau} = N_i\,\boldsymbol{g}^k_{\tau i}\,; \qquad i = 1, 2, \ldots, N_n \tag{2.34}$$

where

$$\boldsymbol{g}^k_{\tau i} = [g^k_{13\tau i}\,,\ g^k_{23\tau i},\ g^k_{33\tau i}]^T \tag{2.35}$$

Substituting Eq. (2.34) in Eq. (2.30) one gets

$$\boldsymbol{\sigma}^k_{nM} = F_\tau\,N_i\,\boldsymbol{g}^k_{\tau i} \tag{2.36}$$

Derivation of Finite Element Matrices

The internal virtual work formulated for a multilayered plate for the RMVT case can be written as:

$$\sum_{k=1}^{N_L} \int_{\Omega_k} \int_{h_k} [\, \delta \boldsymbol{\epsilon}_{pG}^{kT} \, \boldsymbol{\sigma}_{pC}^{k} + \delta \boldsymbol{\epsilon}_{nG}^{kT} \, \boldsymbol{\sigma}_{nM}^{k} + \delta \boldsymbol{\sigma}_{nM}^{kT} \, (\boldsymbol{\epsilon}_{nG}^{k} - \boldsymbol{\epsilon}_{nC}^{k}) \,] d\Omega_k \; dz = \delta W_i \tag{2.37}$$

Restricting Eq. (2.37) to layer k and introducing Hooke's law (2.11), one gets:

$$\begin{aligned} \delta W_i^k = \int_{\Omega_k} \int_{h_k} [& \delta \boldsymbol{\epsilon}_{pG}^{kT} \, \mathbf{C}_{pp}^{k} \, \boldsymbol{\epsilon}_{pG}^{k} + \delta \boldsymbol{\epsilon}_{pG}^{kT} \, \mathbf{C}_{pn}^{k} \, \boldsymbol{\sigma}_{nM}^{k} + \delta \boldsymbol{\epsilon}_{nG}^{kT} \, \boldsymbol{\sigma}_{nM}^{k} + \\ & + \delta \boldsymbol{\sigma}_{nM}^{kT} \, \boldsymbol{\epsilon}_{nG}^{k} - \delta \boldsymbol{\sigma}_{nM}^{kT} \, \mathbf{C}_{np}^{k} \, \boldsymbol{\epsilon}_{pG}^{k} - \delta \boldsymbol{\sigma}_{nM}^{kT} \, \mathbf{C}_{nn}^{k} \, \boldsymbol{\sigma}_{nM}^{k}] d\Omega_k \; dz \end{aligned} \tag{2.38}$$

Now substituting Eqs. (2.19), (2.20) and (2.36) in Eq. 2.38one has

$$\begin{aligned} \delta W_i^k = & \lhd \{ \delta \boldsymbol{q}_{\tau i}^{kT} \, [\boldsymbol{D}_p^T \, (N_i \boldsymbol{I}) \, \boldsymbol{Z}_{pp}^{k\tau s} \, \boldsymbol{D}_p \, (N_j \boldsymbol{I})] \, \boldsymbol{q}_{sj}^{k} \} \rhd_\Omega + \\ & + \lhd \{ \delta \boldsymbol{q}_{\tau i}^{kT} \, [\boldsymbol{D}_p^T \, (N_i \boldsymbol{I}) \, \boldsymbol{Z}_{pn}^{k\tau s} N_j] \, \boldsymbol{g}_{sj}^{k} \} \rhd_\Omega + \\ & + \lhd \{ \delta \boldsymbol{q}_{\tau i}^{kT} \, [\boldsymbol{D}_{n\Omega}^T \, (N_i \boldsymbol{I}) \, E_{\tau s} N_j + E_{\tau, z s} N_i N_j \boldsymbol{I}] \, \boldsymbol{g}_{sj}^{k} \} \rhd_\Omega + \\ & + \lhd \{ \delta \boldsymbol{g}_{\tau i}^{kT} \, [N_i E_{\tau s} \boldsymbol{D}_{n\Omega} \, (N_j \boldsymbol{I}) + E_{\tau s, z} N_i N_j \boldsymbol{I}] \, \boldsymbol{q}_{sj}^{k} \} \rhd_\Omega + \\ & - \lhd \{ \delta \boldsymbol{g}_{\tau i}^{kT} \, [N_i \boldsymbol{Z}_{np}^{k\tau s} \boldsymbol{D}_p \, (N_j \boldsymbol{I})] \, \boldsymbol{q}_{sj}^{k} \} \rhd_\Omega + \\ & - \lhd \{ \delta \boldsymbol{g}_{\tau i}^{kT} \, [N_i \boldsymbol{Z}_{nn}^{k\tau s} N_j] \, \boldsymbol{g}_{sj}^{k} \} \rhd_\Omega \end{aligned}$$

with the following layer stiffness

$$\left(\boldsymbol{Z}_{pp}^{k\tau s}, \boldsymbol{Z}_{pn}^{k\tau s}, \boldsymbol{Z}_{np}^{k\tau s}, \boldsymbol{Z}_{nn}^{k\tau s} \right) = \left(\boldsymbol{C}_{pp}^{k}, \boldsymbol{C}_{pn}^{k}, \boldsymbol{C}_{np}^{k}, \boldsymbol{C}_{nn}^{k} \right) E_{\tau s}$$

which leads to

$$\delta W_i^k = \delta \boldsymbol{q}_{\tau i}^{kT} \left[\boldsymbol{K}_{uu}^{k\tau sij} \boldsymbol{q}_{sj}^{k} + \boldsymbol{K}_{u\sigma}^{k\tau sij} \boldsymbol{g}_{sj}^{k} \right] + \delta \boldsymbol{g}_{\tau i}^{kT} \left[\boldsymbol{K}_{\sigma u}^{k\tau sij} \boldsymbol{q}_{sj}^{k} + \boldsymbol{K}_{\sigma\sigma}^{k\tau sij} \boldsymbol{g}_{sj}^{k} \right] \tag{2.39}$$

where

$$\begin{aligned} \boldsymbol{K}_{uu}^{k\tau sij} &= \lhd \left[\boldsymbol{D}_p^T \, (N_i \boldsymbol{I}) \, \boldsymbol{Z}_{pp}^{k\tau s} \, \boldsymbol{D}_p \, (N_j \boldsymbol{I}) \right] \rhd_\Omega \\ \boldsymbol{K}_{u\sigma}^{k\tau sij} &= \lhd \left[\boldsymbol{D}_p^T \, (N_i \boldsymbol{I}) \, \boldsymbol{Z}_{pn}^{k\tau s} N_j + \boldsymbol{D}_{n\Omega}^T \, (N_i \boldsymbol{I}) \, E_{\tau s} N_j + E_{\tau, z s} N_i N_j \boldsymbol{I} \right] \rhd_\Omega \\ \boldsymbol{K}_{\sigma u}^{k\tau sij} &= \lhd \left[N_i E_{\tau s} \boldsymbol{D}_{n\Omega} \, (N_j \boldsymbol{I}) + E_{\tau s, z} N_i N_j \, \boldsymbol{I} - N_i \boldsymbol{Z}_{np}^{k\tau s} \boldsymbol{D}_p \, (N_j \boldsymbol{I}) \right] \rhd_\Omega \\ \boldsymbol{K}_{\sigma\sigma}^{k\tau sij} &= \lhd \left[-N_i \boldsymbol{Z}_{nn}^{k\tau s} N_j \right] \rhd_\Omega \end{aligned} \tag{2.40}$$

Analogously to the PVD case, introducing the external work of applied forces and imposing the definition of virtual variations leads to the following equilibrium equations for the mixed case:

$$\begin{aligned} \boldsymbol{K}_{uu}^{k\tau sij} \boldsymbol{q}_{sj}^{k} + \boldsymbol{K}_{u\sigma}^{k\tau sij} \boldsymbol{g}_{sj}^{k} &= \boldsymbol{P}_{\tau i}^{k} \\ \boldsymbol{K}_{\sigma u}^{k\tau sij} \boldsymbol{q}_{sj}^{k} + \boldsymbol{K}_{\sigma\sigma}^{k\tau sij} \boldsymbol{g}_{sj}^{k} &= \mathbf{0} \end{aligned} \tag{2.41}$$

As can be seen, for RMVT four 3×3 nuclei are be obtained, which explicitly read:

$$
\begin{aligned}
K^{k\tau sij}_{uu11} &= Z^{k\tau s}_{pp11} \lhd N_{i,x} N_{j,x} \rhd_\Omega + Z^{k\tau s}_{pp16} \lhd N_{i,y} N_{j,x} \rhd_\Omega + Z^{k\tau s}_{pp16} \lhd N_{i,x} N_{j,y} \rhd_\Omega + \\
&\quad + Z^{k\tau s}_{pp\,66} \lhd N_{i,y} N_{j,y} \rhd_\Omega \\
K^{k\tau sij}_{uu12} &= Z^{k\tau s}_{pp12} \lhd N_{i,x} N_{j,y} \rhd_\Omega + Z^{k\tau s}_{pp26} \lhd N_{i,y} N_{j,y} \rhd_\Omega + Z^{k\tau s}_{pp16} \lhd N_{i,x} N_{j,x} \rhd_\Omega + \\
&\quad + Z^{k\tau s}_{pp\,66} \lhd N_{i,y} N_{j,x} \rhd_\Omega \\
K^{k\tau sij}_{uu13} &= 0 \\
K^{k\tau sij}_{uu21} &= Z^{k\tau s}_{pp12} \lhd N_{i,y} N_{j,x} \rhd_\Omega + Z^{k\tau s}_{pp16} \lhd N_{i,x} N_{j,x} \rhd_\Omega + Z^{k\tau s}_{pp26} \lhd N_{i,y} N_{j,y} \rhd_\Omega + \\
&\quad + Z^{k\tau s}_{pp\,66} \lhd N_{i,x} N_{j,y} \rhd_\Omega \\
K^{k\tau sij}_{uu22} &= Z^{k\tau s}_{pp22} \lhd N_{i,y} N_{j,y} \rhd_\Omega + Z^{k\tau s}_{pp26} \lhd N_{i,x} N_{j,y} \rhd_\Omega + Z^{k\tau s}_{pp26} \lhd N_{i,y} N_{j,x} \rhd_\Omega + \\
&\quad + Z^{k\tau s}_{pp\,66} \lhd N_{i,x} N_{j,x} \rhd_\Omega \\
K^{k\tau sij}_{uu23} &= 0 \\
K^{k\tau sij}_{uu31} &= 0 \\
K^{k\tau sij}_{uu32} &= 0 \\
K^{k\tau sij}_{uu33} &= 0
\end{aligned}
\tag{2.42}
$$

$$
\begin{aligned}
K^{k\tau sij}_{u\sigma 11} &= E_{\tau,_z s} \lhd N_i N_j \rhd_\Omega \\
K^{k\tau sij}_{u\sigma 12} &= 0 \\
K^{k\tau sij}_{u\sigma 13} &= Z^{k\tau s}_{pn13} \lhd N_{i,x} N_j \rhd_\Omega + Z^{k\tau s}_{pn36} \lhd N_{i,y} N_j \rhd_\Omega \\
K^{k\tau sij}_{u\sigma 21} &= 0 \\
K^{k\tau sij}_{u\sigma 22} &= E_{\tau,_z s} \lhd N_i N_j \rhd_\Omega \\
K^{k\tau sij}_{u\sigma 23} &= Z^{k\tau s}_{pn23} \lhd N_{i,y} N_j \rhd_\Omega + Z^{k\tau s}_{pn36} \lhd N_{i,x} N_j \rhd_\Omega \\
K^{k\tau sij}_{u\sigma 31} &= E_{\tau s} \lhd N_{i,x} N_j \rhd_\Omega \\
K^{k\tau sij}_{u\sigma 32} &= E_{\tau s} \lhd N_{i,y} N_j \rhd_\Omega \\
K^{k\tau sij}_{u\sigma 33} &= E_{\tau,_z s} \lhd N_i N_j \rhd_\Omega
\end{aligned}
\tag{2.43}
$$

$$
\begin{aligned}
K^{k\tau sij}_{\sigma u11} &= E_{\tau s,_z} \triangleleft N_i N_j \triangleright_\Omega \\
K^{k\tau sij}_{\sigma u12} &= 0 \\
K^{k\tau sij}_{\sigma u13} &= E_{\tau s} \triangleleft N_i N_{j,x} \triangleright_\Omega \\
K^{k\tau sij}_{\sigma u21} &= 0 \\
K^{k\tau sij}_{\sigma u22} &= E_{\tau s,_z} \triangleleft N_i N_j \triangleright_\Omega \\
K^{k\tau sij}_{\sigma u23} &= E_{\tau s} \triangleleft N_i N_{j,y} \triangleright_\Omega \\
K^{k\tau sij}_{\sigma u31} &= -Z^{k\tau s}_{np13} \triangleleft N_i N_{j,x} \triangleright_\Omega - Z^{k\tau s}_{np36} \triangleleft N_i N_{j,y} \triangleright_\Omega \\
K^{k\tau sij}_{\sigma u32} &= -Z^{k\tau s}_{np23} \triangleleft N_i N_{j,y} \triangleright_\Omega - Z^{k\tau s}_{np36} \triangleleft N_i N_{j,x} \triangleright_\Omega \\
K^{k\tau sij}_{\sigma u33} &= E_{\tau s,_z} \triangleleft N_i N_j \triangleright_\Omega
\end{aligned}
\tag{2.44}
$$

$$
\boldsymbol{K}^{k\tau sij}_{\sigma\sigma} = \begin{bmatrix}
-Z^{k\tau s}_{nn55} \triangleleft N_i N_j \triangleright_\Omega & -Z^{k\tau s}_{nn45} \triangleleft N_i N_j \triangleright_\Omega & 0 \\
-Z^{k\tau s}_{nn45} \triangleleft N_i N_j \triangleright_\Omega & -Z^{k\tau s}_{nn44} \triangleleft N_i N_j \triangleright_\Omega & 0 \\
0 & 0 & -Z^{k\tau s}_{nn33} \triangleleft N_i N_j \triangleright_\Omega
\end{bmatrix} \tag{2.45}
$$

The complete fundamental nucleus for RMVT, denoted by the subscript M, is the following 6×6 nucleus:

$$
\boldsymbol{K}^{k\tau sij}_{M} = \begin{bmatrix}
\boldsymbol{K}^{k\tau sij}_{uu} & \boldsymbol{K}^{k\tau sij}_{u\sigma} \\
\boldsymbol{K}^{k\tau sij}_{\sigma u} & \boldsymbol{K}^{k\tau sij}_{\sigma\sigma}
\end{bmatrix} \tag{2.46}
$$

2.5 Assembling from Layer to Multilayer

Starting point for the assembling procedure of each matrix is the related fundamental nucleus. Three main steps are necessary to carry out the final matrices:

1. Assembling of the matrices at element and layer level for each layer
2. Assembling of the matrices at multilayer level, depending on the used variables description
3. Assembling of the matrices at structure level

The assembly shall be shown in detail for the PVD case. In order to obtain multilayer matrices for the mixed case, the procedure is exactly the same as for the PVD case, while using the fundamental nuclei (2.46) for the mixed case. By expanding the indices

(τ, s) of the fundamental nucleus for PVD, see (2.26), the nucleus can be written as

$$\boldsymbol{K}^{kij} = \begin{bmatrix} \boldsymbol{K}^{kttij} & \boldsymbol{K}^{kt2ij} & \dots & \boldsymbol{K}^{ktNij} & \boldsymbol{K}^{ktbij} \\ \boldsymbol{K}^{k2tij} & \boldsymbol{K}^{k22ij} & \dots & \boldsymbol{K}^{k2Nij} & \boldsymbol{K}^{k2bij} \\ \dots & & & & \\ \dots & & & & \\ \dots & & & & \\ \boldsymbol{K}^{kNtij} & \boldsymbol{K}^{kN2ij} & \dots & \boldsymbol{K}^{kNNij} & \boldsymbol{K}^{kNbij} \\ \boldsymbol{K}^{kbtij} & \boldsymbol{K}^{kb2ij} & \dots & \boldsymbol{K}^{kbNij} & \boldsymbol{K}^{kbbij} \end{bmatrix} \tag{2.47}$$

with $i, j = 1, 2, \dots, N_n$. Now also expanding the indices (i, j) one gets:

$$\boldsymbol{K}^{k} = \begin{bmatrix} \boldsymbol{K}^{k11} & \boldsymbol{K}^{k12} & \dots & \boldsymbol{K}^{k1N_n} \\ \boldsymbol{K}^{k21} & \boldsymbol{K}^{k22} & \dots & \boldsymbol{K}^{k2N_n} \\ \dots & & & \\ \dots & & & \\ \dots & & & \\ \boldsymbol{K}^{kN_n1} & \boldsymbol{K}^{kN_n2} & \dots & \boldsymbol{K}^{kN_nN_n} \end{bmatrix} \tag{2.48}$$

This procedure has to be done for every layer. The scheme for the assembly at element and layer level is shown in Fig. 2.7 for a 4-node element with 3rd order expansion in $z-$direction.

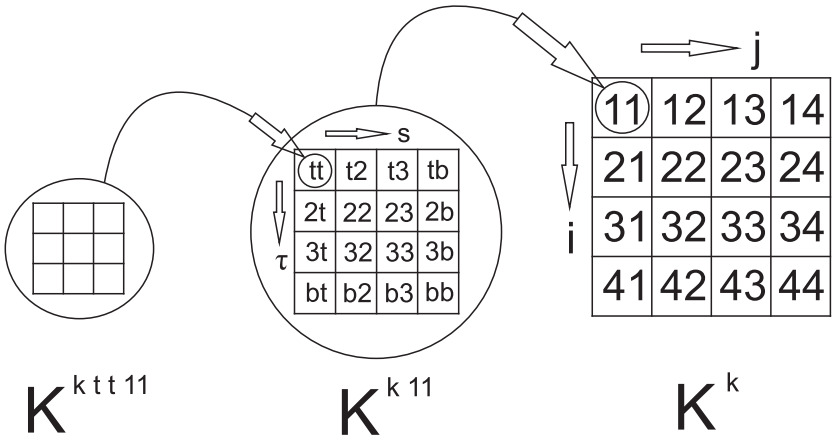

Figure 2.7: *Assembly of the stiffness-matrix at element and layer-level; 4-node element with 3rd order expansion in $z-$direction*

The assembly of the matrices at multilayer level depends on the used variables description. For ESL case this can be done very easily. The layer matrices $\boldsymbol{K}^k$ have to be simply summed to get the final matrix at multilayer level (see Fig. 2.8). In layerwise description, primary variables are independent in each layer. Continuity is only required at the interfaces. Assembly procedure is shown in Fig. 2.9.

Finally the assembling of the matrices at structure level has to be done applying the usual methodologies of the finite element method. Further information of these procedures can be found in many books, i.e. [6]. In order to obtain multilayer matrices for the mixed case, the procedure is the same as written for the PVD case, but now using the fundamental nuclei (2.46) for the mixed case.

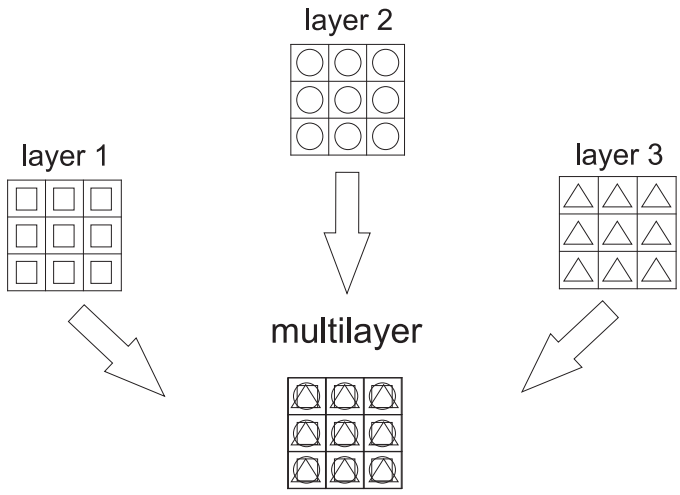

Figure 2.8: *Assembly of the stiffness-matrix at multilayer-level for ESL case; 3 layers*

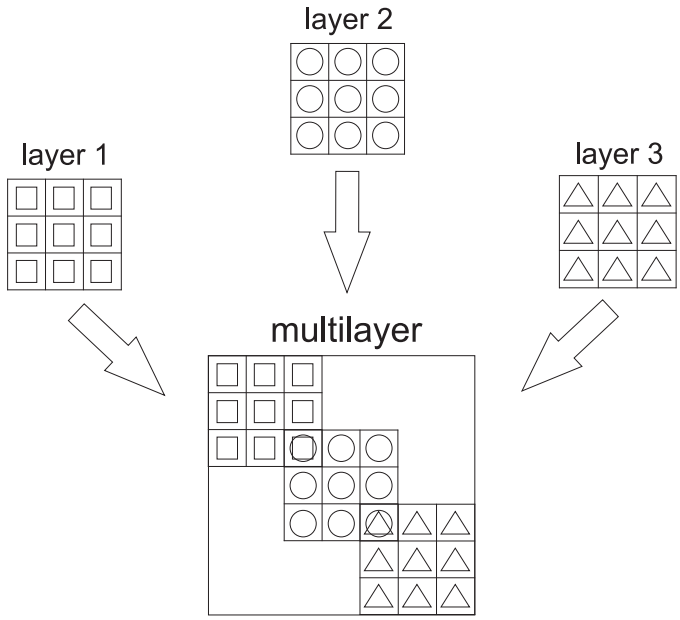

Figure 2.9: *Assembly of the stiffness-matrix at multilayer-level for LW case; 3 layers*

Chapter 3

Numerical Results for Pure Mechanical Case

3.1 PVD Analysis

Static and dynamic analysis have been performed with different polynomials choices and various order of expansion for the thickness functions. The aim is to try to provide an answer to the question: which is the most reliable and computational efficient FE model?

3.1.1 Free Vibration Analysis

Free vibration analysis is performed by using the governing equation (2.29). The undamped dynamic problem can be written in terms of the following ordinary differential equations system:

$$\boldsymbol{M}\ddot{\boldsymbol{q}} + \boldsymbol{K}\boldsymbol{q} = \boldsymbol{P} \tag{3.1}$$

where $\boldsymbol{M}$ is the mass-matrix, $\boldsymbol{K}$ is the stiffness-matrix, $\boldsymbol{q}$ is the vector of nodal displacement unknowns, $\ddot{\boldsymbol{q}}$ is the vector of accelerations and $\boldsymbol{P}$ is the vector of nodal loads. Moreover, the i-th natural frequency ω_i of the system can be calculated by solving the generalized eigenvector-eigenvalue problem, where $\boldsymbol{a}_i$ is the i-th eigenvector:

$$(-\omega_i^2\,\boldsymbol{M} + \boldsymbol{K})\,\boldsymbol{a}_i = 0 \tag{3.2}$$

The circular frequency as a global parameter of various single and multilayered plates has been analysed and compared with analyical values. For both cases, ESL and LW, results with the different kinds of polyinomials above described have been obtained. The following three cases have been investigated:

(1) Single layer square plate, isotropic material, simply supported
$a = b = 0.5\,\mathrm{m}$, $a/h = 250$, $E = 73\,\mathrm{GPa}$, $\nu = 0.34$, $\rho = 2800\,\mathrm{kg/m^3}$,

(2) Single layer square plate, orthotropic material, fully clamped
$a = b = 0.3\,\mathrm{m}$, $a/h = 93.75$, $E_1 = 14.17\,\mathrm{GPa}$, $E_2 = E_3 = 8.88\,\mathrm{GPa}$, $G = 2.93\,\mathrm{GPa}$, $\nu_{12} = 0.295$; $\rho = 1771.5\,\mathrm{kg/m^3}$

(3) Multilayered orthotropic square plate, cross-ply skew symmetric (0°/90°) and symmetric (0°/90°/0°) laminates (the total thickness of layers 90° and 0° oriented is the same)
$a/h = 5$, $G_{LT}/E_T = G_{LZ}/E_T = 0.50$, $G_{TT}/E_T = 0.35$, $\nu_{LT} = \nu_{LZ} = 0.3$, $\nu_{TT} = 0.49$; various E_L/E_T ratios

Single Layer Plates

To confirm the correctness of the formulations of both models, LW and ESL, the circular frequencies of case (1) have been analyzed and compared to the exact analytical values. As it is only one single layer, the results for LW and ESL description should be exactly the same. Table 3.1 shows the perfect accordance of both models. As case (1) is a very thin plate there are no significant differences also for the different orders of the expansion. It is noticeable that for higher frequecy modes in this case, the results of first order expansion are even a bit closer to the exact solution than for higher order expansion. This is an effect of the correction of the constitutive coefficients embedded in the first order to withstand the thickness locking. Convergence to the exact solution by refining the mesh can be seen in Tab. 3.2 for both models.
The second single layer plate, described as case (2) above, has been investigated with two different elements (*Q4* and *Q9*). The convergence for refining the mesh is confirmed in Tab. 3.3 and 3.4. You can see in the results for the $Q9$-element that also a slight oscillation around the exact value can appear.

frequency modes $\omega_{(m,n)}$	$(1,1)$	$(2,1)$	$(1,2)$	$(2,2)$
Analytical values				
3D closed form solution[7]	39.7	98.2	98.2	157.2
MUL2, Q4, 8x8				
LD4(LGR)	40.1	105.6	105.6	169.7
LD3(LGR)	40.1	105.6	105.6	169.7
LD2(LGR)	40.1	105.6	105.6	169.7
LD1(LGR)	40.1	104.9	104.9	168.9
LD4(LGD)	40.1	105.6	105.6	169.7
LD3(LGD)	40.1	105.6	105.6	169.7
LD2(LGD)	40.1	105.6	105.6	169.7
LD1(LGD)	40.1	104.9	104.9	168.9
ED4(TYL)	40.1	105.6	105.6	169.7
ED3(TYL)	40.1	105.6	105.6	169.7
ED2(TYL)	40.1	105.6	105.6	169.7
ED1(TYL)	40.1	104.9	104.9	168.9
ED4(LGR)	40.1	105.6	105.6	169.7
ED3(LGR)	40.1	105.6	105.6	169.7
ED2(LGR)	40.1	105.6	105.6	169.7
ED1(LGR)	40.1	104.9	104.9	168.9
ED4(LGD)	40.1	105.6	105.6	169.7
ED3(LGD)	40.1	105.6	105.6	169.7
ED2(LGD)	40.1	105.6	105.6	169.7
ED1(LGD)	40.1	104.9	104.9	168.9

Table 3.1: *Case (1): Frequency modes $\omega_{(m,n)}$ with m, n = number of half-waves in x- and y-direction*

frequency modes $\omega_{(m,n)}$	$(1,1)$	$(2,1)$	$(1,2)$	$(2,2)$
Analytical values				
3D closed form solution[7]	39.7	98.2	98.2	157.2
MUL2, Q4, 8×8				
ED1(TYL)	40.1	104.9	104.9	168.9
ED1(LGR)	40.1	104.9	104.9	168.9
ED1(LGD)	40.1	104.9	104.9	168.9
LD1(LGR)	40.1	104.9	104.9	168.9
LD1(LGD)	40.1	104.9	104.9	168.9
MUL2, Q4, 10×10				
ED1(TYL)	39.8	102.5	102.5	164.7
ED1(LGR)	39.8	102.5	102.5	164.7
ED1(LGD)	39.8	102.5	102.5	164.7
LD1(LGR)	39.8	102.5	102.5	164.7
LD1(LGD)	39.8	102.5	102.5	164.7
MUL2, Q4, 12×12				
ED1(TYL)	39.7	101.3	101.3	162.4
ED1(LGR)	39.7	101.3	101.3	162.4
ED1(LGD)	39.7	101.3	101.3	162.4
LD1(LGR)	39.7	101.3	101.3	162.4
LD1(LGD)	39.7	101.3	101.3	162.4

Table 3.2: *Case (1): Convergence for frequency modes $\omega_{(m,n)}$ with m, n = number of half-waves in x- and y-direction*

frequency number ω_i	1	2	3	4	5	6	7
Analytical values*							
	150.39	284.49	330.18	444.91	502.75	610.52	646.42
MUL2, Q4, 8×8							
ED1(TYL)	155.42	313.62	367.92	493.60	635.72	779.95	781.21
ED1(LGR)	155.42	313.62	367.92	493.60	635.72	779.95	781.21
ED1(LGD)	155.42	313.62	367.92	493.60	635.72	779.95	781.21
MUL2, Q4, 12×12							
ED1(TYL)	151.70	294.59	343.52	461.26	550.08	670.97	692.85
ED1(LGR)	151.70	294.59	343.52	461.26	550.08	670.97	692.85
ED1(LGD)	151.70	294.59	343.52	461.26	550.08	670.97	692.85
MUL2, Q4, 16×16							
ED1(TYL)	150.45	288.52	335.74	450.88	525.27	639.34	666.70
ED1(LGR)	150.45	288.52	335.74	450.88	525.27	639.34	666.70
ED1(LGD)	150.45	288.52	335.74	450.88	525.27	639.34	666.70

Table 3.3: *Case (2): Convergence studies for the first 7 frequencies ω_i with Q4 elements; (*)The free vibration frequencies of the pultruded GRP, square plates are computed on the basis of the homogeneous orthotropic and anisotropic thin plate theory. Approximate closed-form expressions are referred to, see [8]*

frequency number ω_i	1	2	3	4	5	6	7
Analytical values*							
	150.39	284.49	330.18	444.91	502.75	610.52	646.42
MUL2, Q9, 3×3							
ED1(TYL)	150.43	303.21	355.17	479.04	616.02	752.31	756.65
ED1(LGR)	150.43	303.21	355.17	479.04	616.02	752.31	756.65
ED1(LGD)	150.43	303.21	355.17	479.04	616.02	752.31	756.65
MUL2, Q9, 6×6							
ED1(TYL)	148.96	282.29	327.84	440.30	505.81	614.60	645.08
ED1(LGR)	148.96	282.29	327.84	440.30	505.81	614.60	645.08
ED1(LGD)	148.96	282.29	327.84	440.30	505.81	614.60	645.08
MUL2, Q9, 9×9							
ED1(TYL)	148.89	281.34	326.57	438.59	498.33	604.98	637.73
ED1(LGR)	148.89	281.34	326.57	438.59	498.33	604.98	637.73
ED1(LGD)	148.89	281.34	326.57	438.59	498.33	604.98	637.73

Table 3.4: *Case (2): Convergence studies for the first 7 frequencies ω_i with Q9 elements; (*)The free vibration frequencies of the pultruded GRP, square plates are computed on the basis of the homogeneous orthotropic and anisotropic thin plate theory. Approximate closed-form expressions are referred to, see [8]*

Multilayered Plates

In the next step, circular frequencies for the more complex and intersting case of multilayered plates have been investigated with different polynomials for the thickness-functions. Therefore the results of free vibration analysis of case (3) are compared with the exact 3D-solution and different availiable analytical results, see [9]. Frequencies are presented in dimensionless form ($\bar{\omega} = \omega h\sqrt{\rho/E_T}$) in Tab. 3.5 and Tab. 3.6. The tables show that even for a 3×3 mesh with a Q9 element, the results are very close to the analogous analytical LD and ED values. LW analyses lead to better results than ESL ones; with a 6×6 mesh even the exact analytical value can be obtained in layerwise case. The results for thickness-functions based on Legendre and Lagrange polynomials are in both cases, LW and ESL, the same for the first 6 significant digits. In contrast, for the equivalent single layer case it is now obvious that the choice of Taylor or Lagrange/Legendre expansion leads to different results. With Taylor expansion, results converge faster to the analytical value and are closer to the exact $3D$ result. Furthermore the results of ESL anylysis with Lagrange and Legendre expansion show no difference between $N_L = 2$ and $N_L = 3$ as the total thickness of the multilayered plate and the total thickness of layers oriented 90° and 0° remains the same.

N_l	2		3
E_L/E_T	3	30	3
Analytical values [9]			
3D Exact	0.2392	0.3117	0.2516
ED4	0.2394	0.3133	0.2518
ED3	0.2394	0.3167	0.2519
ED2	0.2418	0.3198	0.2569
ED1	0.2662	0.3367	0.2778
MUL2, Q9, 3×3			
ED4(TYL)	0.2398	0.3138	0.2523
ED3(TYL)	0.2399	0.3172	0.2523
ED2(TYL)	0.2423	0.3203	0.2573
ED1(TYL)	0.2459	0.3272	0.2587
ED4(LGR)	0.2551	0.4141	0.2551
ED3(LGR)	0.2551	0.4143	0.2551
ED2(LGR)	0.2587	0.4335	0.2587
ED1(LGR)	0.2640	0.4343	0.2640
ED4(LGD)	0.2551	0.4141	0.2551
ED3(LGD)	0.2551	0.4143	0.2551
ED2(LGD)	0.2587	0.4335	0.2587
ED1(LGD)	0.2640	0.4343	0.2640
MUL2, Q9, 6×6			
ED3(TYL)	0.2395	0.3168	0.2519
ED3(LGR)	0.2547	0.4139	0.2547
ED3(LGD)	0.2547	0.4139	0.2547

Table 3.5: *Case (3): Frequency parameter* $\bar{\omega} = \omega h\sqrt{\rho/E_T}$ *with ESL model*

N_l	2		3
E_L/E_T	3	30	3
Analytical values[9]			
3D Exact	0.2392	0.3117	0.2516
LD4	0.2392	0.3117	0.2516
LD3	0.2392	0.3117	0.2516
LD2	0.2395	0.3168	0.2517
LD1	0.2478	0.3210	0.2556
MUL2, Q9, 3×3			
LD4(LGR)	0.2396	0.3121	0.2520
LD3(LGR)	0.2396	0.3122	0.2520
LD2(LGR)	0.2399	0.3172	0.2521
LD1(LGR)	0.2482	0.3214	0.2560
LD4(LGD)	0.2396	0.3121	0.2520
LD3(LGD)	0.2396	0.3122	0.2520
LD2(LGD)	0.2399	0.3172	0.2521
LD1(LGD)	0.2482	0.3214	0.2560
MUL2, Q9, 6×6			
LD3(LGR)	0.2392	0.3118	0.2516
LD3(LGD)	0.2392	0.3118	0.2516

Table 3.6: *Case (3): Frequency parameter* $\bar{\omega} = \omega h\sqrt{\rho/E_T}$ *with layerwise model*

3.1.2 Pagano Problem - Cylindrical Bending

Also a mechanical analysis for composite laminates in cylindrical bending has been performed with different kind of polynomials for ESL and LW theories. The results are compared to the exact solutions by Pagano [10]. Therefore the following material data have been used:

symmetric 3-ply laminate (0°/90°/0°) with layers of equal thickness; $a/h = 4$
$E_L = 25 \times 10^6$ psi[1], $E_T = 10^6$ psi, $G_{LT} = 0.5 \times 10^6$ psi, $G_{TT} = 0.2 \times 10^6$ psi, $\nu_{LT} = \nu_{TT} = 0.25$
simply supported at the tips $x = 0$ and $x = a$
sinusoidal load in x-direction (see also Fig. 3.1): $p = p_0 sin(\frac{\pi x}{a})$

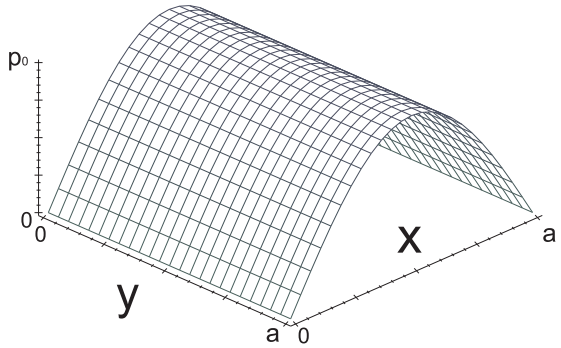

Figure 3.1: *Sinusoidal load in x-direction:* $p = p_0 sin(\frac{\pi x}{a})$

The results for the displacement u_1 and stresses σ_{11}, σ_{13} and σ_{33} are presented in the following normalized form:

$$\widetilde{u}_1 = \frac{E_T u_1(0,z)}{h p_0}, \quad \widetilde{\sigma}_{11} = \frac{\sigma_{11}(a/2,z)}{p_0}, \quad \widetilde{\sigma}_{33} = \frac{\sigma_{33}(a/2,z)}{p_0}, \quad \widetilde{\sigma}_{13} = \frac{\sigma_{13}(0,z)}{p_0}$$

At first, the convergence for different meshes has been determined to choose an adequate solution for the problem. Therefore the displacement $\widetilde{u}_3$ in the middle of the plate and the in-plane stress $\widetilde{\sigma}_{11}$ have been calculated, each with a 10×1, 30×1 and 50×1 mesh, see Tab. 3.7; the 50×1 mesh has been applied for any further investigations.

Equivalent Single Layer Results

Different approaches lead to different distribution of variables through the thickness of the plate. This justifies the fact that a single-point comparison between results obtained by various approaches is not sufficient to asses the corresponding level of accuracy. A more complete picture can be obtained by looking at the distribution of stresses and displacement variables through the thickness-plate direction which is done in the Figs. 3.2 - 3.6. For the ESL case, the choice of Taylor-polynomials leads to different results than Lagrange and Legendre expansions. Figure 3.2 shows a very good behavior for Taylor expansion at the top, bottom and center of the plate for the inplane displacement u_1; only at the interfaces 3D solution cannot be fully obtained. Using Lagrange and Legendre polynomials, results close to the exact solution mainly appear

[1] 1 psi = 6894.7573 Pa

$\widetilde{u}_3$		*top*	*middle*	*bottom*
	3D Pagano	7.738	7.391	7.269
10×1	LD3(LGD)	7.795	7.426	7.303
30×1	LD3(LGD)	7.763	7.399	7.278
50×1	LD3(LGD)	7.760	7.397	7.276
$\widetilde{\sigma}_{11}$		*top*	*middle*	*bottom*
	3D Pagano	18.81	0.09762	-18.10
10×1	LD3(LGD)	18.62	0.09904	-17.90
30×1	LD3(LGD)	18.79	0.09723	-18.08
50×1	LD3(LGD)	18.80	0.09708	-18.09

Table 3.7: *Pagano cylindrical bending: Convergence for $\widetilde{u}_3$ and $\widetilde{\sigma}_{11}$ in the center of the plate*

at the top or the bottom area of the plate. Also in Fig. 3.6 results for the transverse shear stress σ_{13} with Taylor expansion are slightly closer to the exact solution than the ones obtained with Lagrange and Legendre polynomials. Ont the other hand, you can see in Figs. 3.3, 3.5 and 3.6 that the error related to different polynomials assumptions is very much depending on the z-position. A general conclusion on the fairness of a given approach can hardly be made.

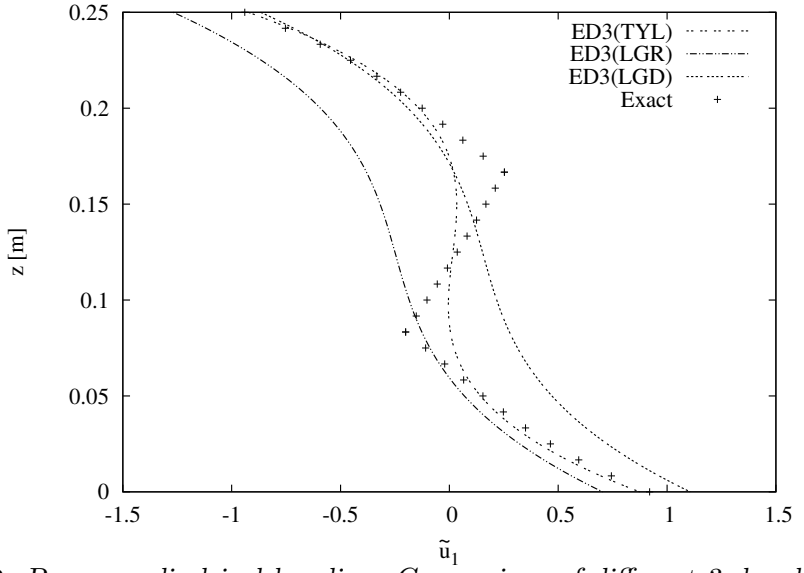

Figure 3.2: *Pagano cylindrical bending: Comparison of different 3rd order ED polynomials for $\widetilde{u}_1$*

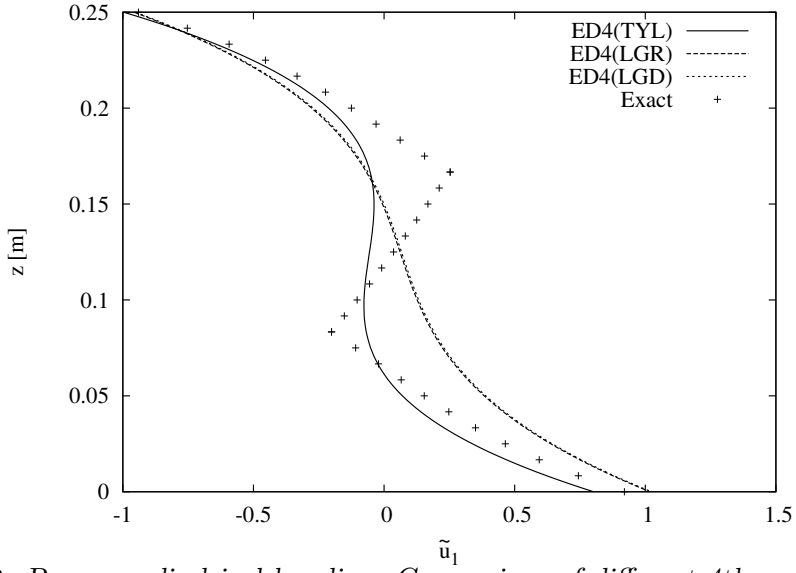

Figure 3.3: *Pagano cylindrical bending: Comparison of different 4th order ED polynomials for* $\widetilde{u}_1$

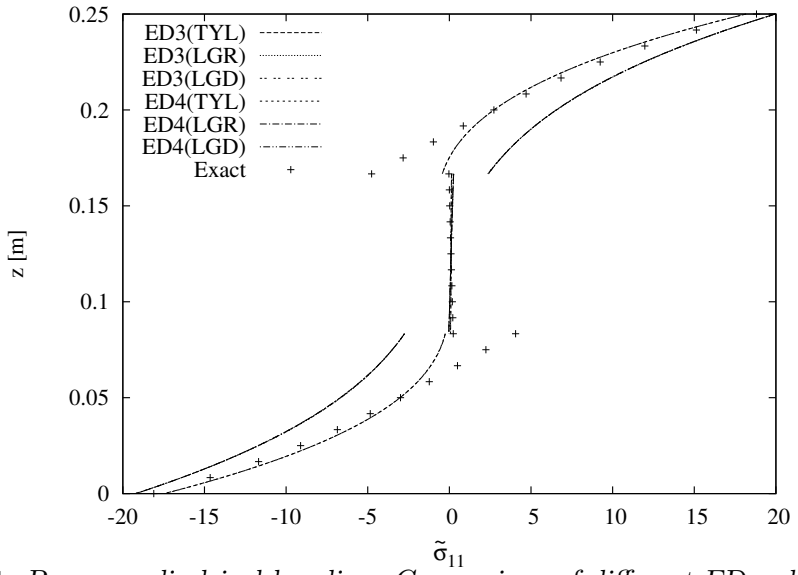

Figure 3.4: *Pagano cylindrical bending: Comparison of different ED polynomials for* $\widetilde{\sigma}_{11}$

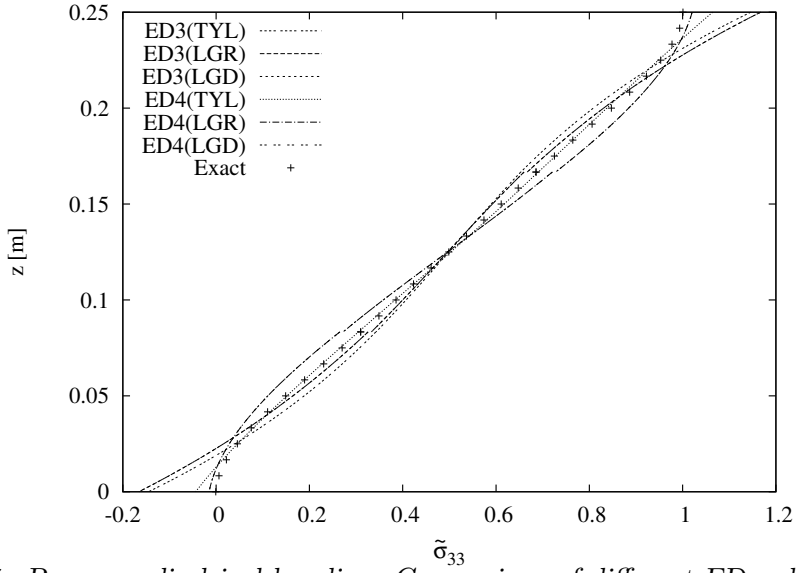

Figure 3.5: *Pagano cylindrical bending: Comparison of different ED polynomials for* $\widetilde{\sigma}_{33}$

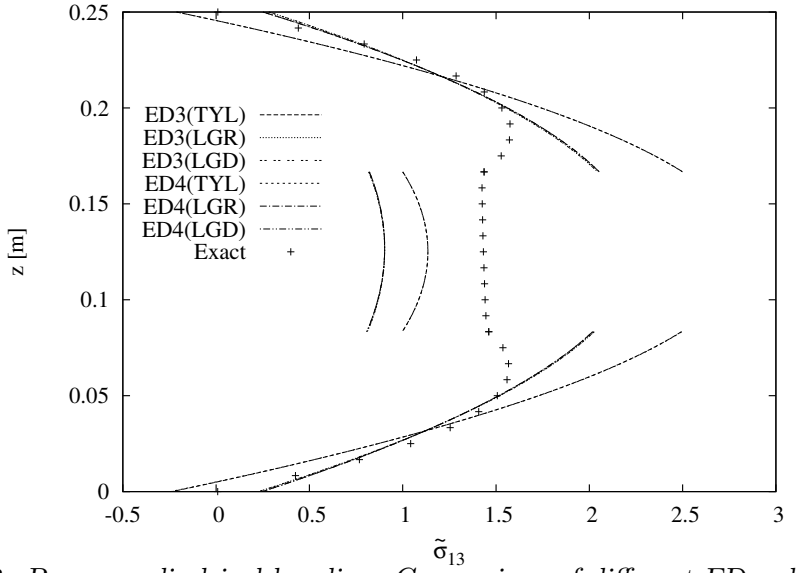

Figure 3.6: *Pagano cylindrical bending: Comparison of different ED polynomials for* $\widetilde{\sigma}_{13}$

Layerwise Results

For the LW case there are very little differences in the corresponding results for Lagrange and Legendre polynomials, see Figs. 3.7 to 3.11. Almost the same accuracy is obtained with both expansion for a fixed order. Only for the in-plane displacement u_1, the result for Legendre Polynomials of 2nd-order expansion shows a slight irregularity, see Fig. 3.7 and 3.8. This could be caused by the fact that u_1 is calculated directly in the simply supported boundary of the plate which is a very sensitive point in FEM modeling. You can see that layerwise models are able to reproduce 3D through-the-thickness distribution of displacements (Fig. 3.8), shear stress (Fig. 3.10) and transverse stress variables (Fig. 3.11 to 3.13) for higher order analysis.

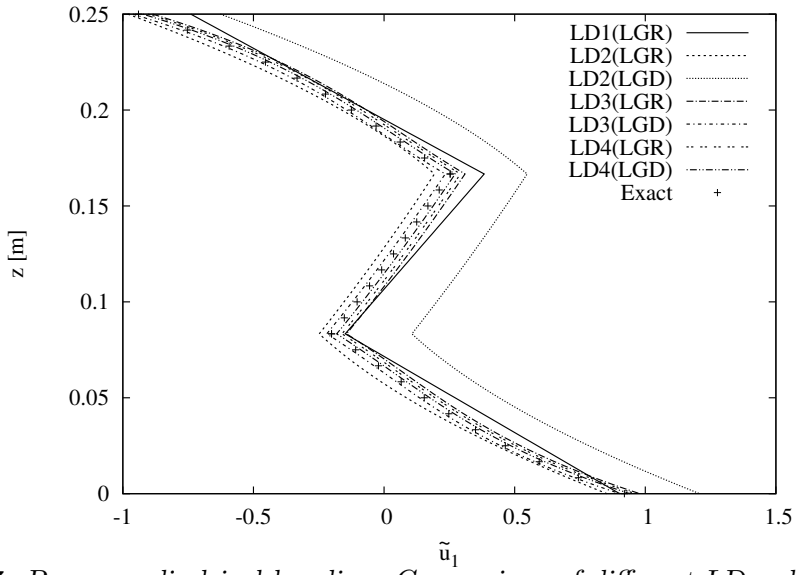

Figure 3.7: *Pagano cylindrical bending: Comparison of different LD polynomials for* $\widetilde{u}_1$

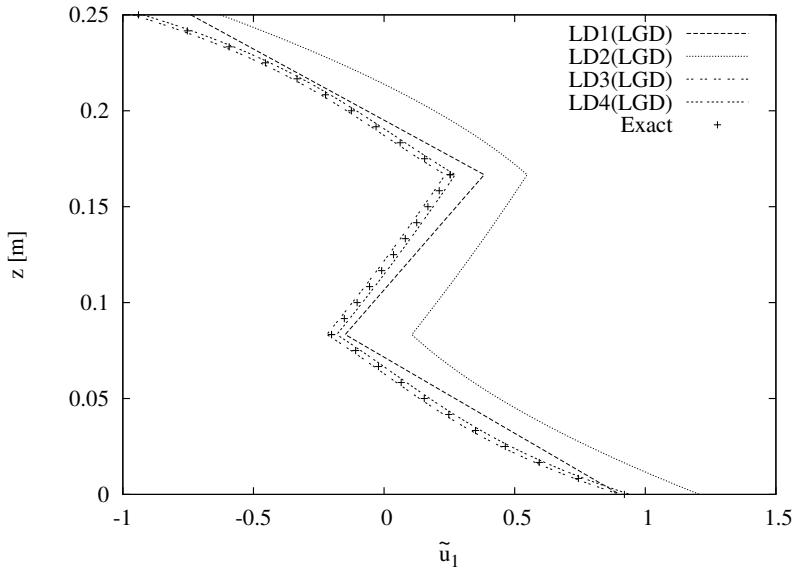

Figure 3.8: *Pagano cylindrical bending: LGD polynomials for* $\widetilde{u}_1$

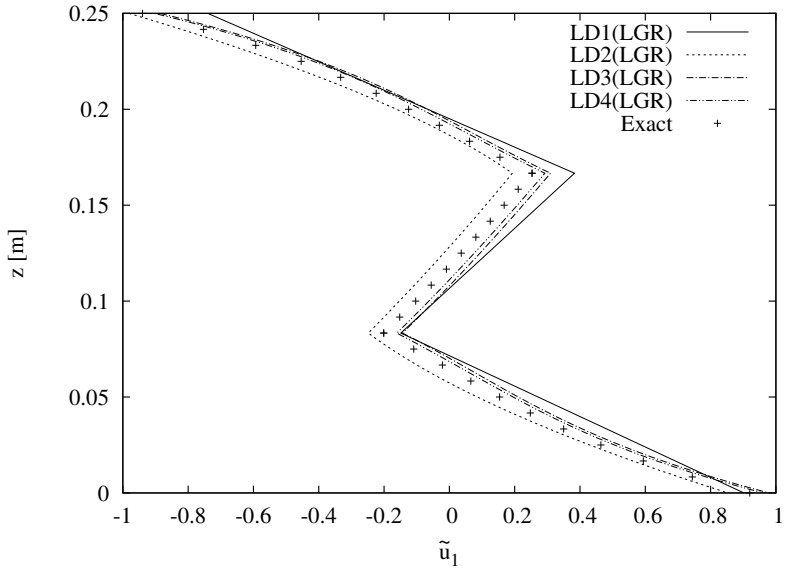

Figure 3.9: *Pagano cylindrical bending: LGR polynomials for* $\widetilde{u}_1$

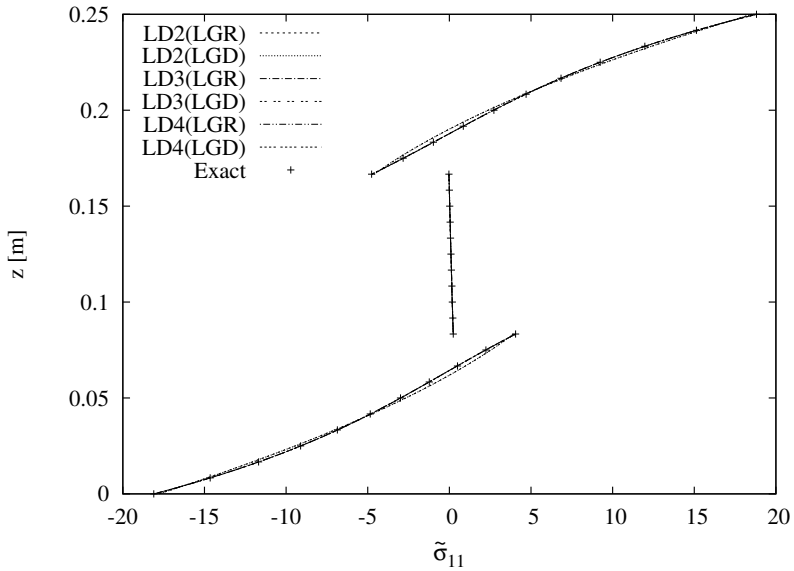

Figure 3.10: *Pagano cylindrical bending: Comparison of different LD theories for* $\widetilde{\sigma}_{11}$

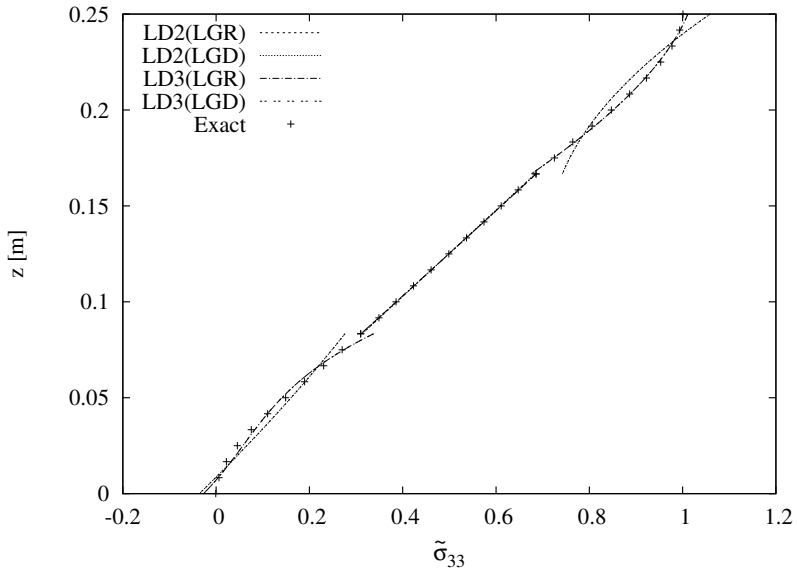

Figure 3.11: *Pagano cylindrical bending: Comparison of different LD theories for* $\widetilde{\sigma}_{33}$

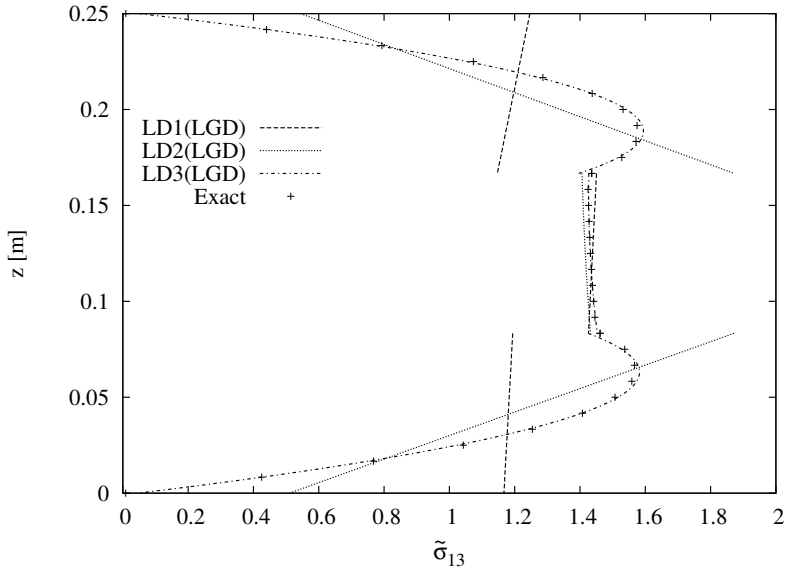

Figure 3.12: *Pagano cylindrical bending: Comparison of different LD theories for* $\widetilde{\sigma}_{13}$

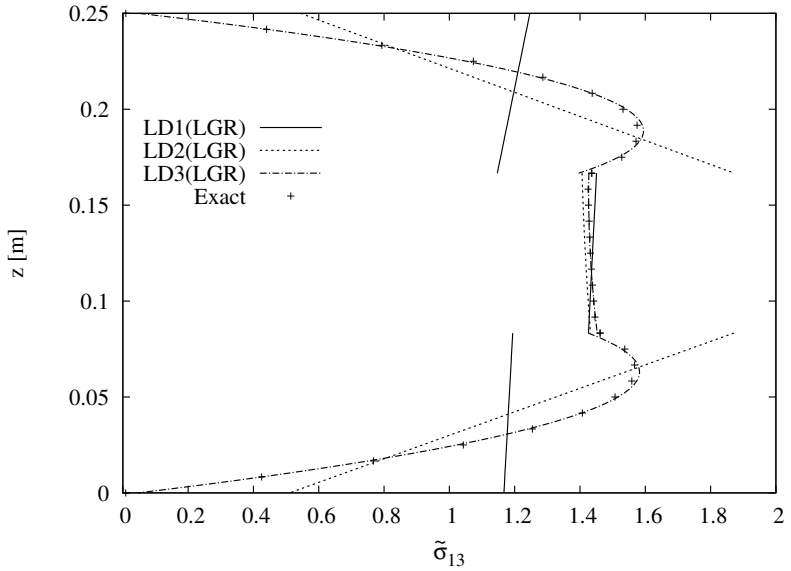

Figure 3.13: *Pagano cylindrical bending: Comparison of different LD theories for* $\widetilde{\sigma}_{13}$

3.1.3 FE models accuracy versus Degrees of Freedom

Another interesting point is the consideration of the degrees of freedom for ESL and LW results. Further comparisons among ESL and LW theories, different polynomials choices and various order of expansion for the thickness functions are provided in this section to answer the question: which is the most reliable and computational efficient FE model?
Table 3.8 shows the number of degrees of freedom (nDOFs) related to various theories when they are employed to model the cylindrical bending of the Pagano problem with a 50×1 mesh of Q4 FEs. ED1 cases correspond to the most available plate/shell element available in commercial codes. The LD4 analysis requires more than 6 time the nDOFs considered in the ED1 analysis. It is significant to notice that the third order ESL analysis (ED3) requires the same nDOFs as the first order LW analysis (LD1) (see Tab. 3.8). Of course, such an equivalence is due to the considered lay-out, which consists of a three-layered plate. LD1 would result more expensive or more convenient by incerasing/decreasing the number of constituent layers, respectively. An extensive

Order	1	2	3	4
DOF LD	**1224**	2142	3060	3978
DOF ED	612	918	**1224**	1530

Table 3.8: *Degrees of freedom (DOF) for 3 layers with a Q4* 50×1 *mesh*

comparison between LD1 and ED3 results is proposed in the following.
In-plane displacement results are compared in Tab. 3.9 while in-plane normal stresses are compared in Tab. 3.10. The comparison for $\widetilde{u}_1$ and for $\widetilde{\sigma}_{11}$ quantities is also given in Figs. 3.14 and 3.15. It is obvious that only the layerwise analyses are able to show the particular effects at the layer interfaces. Only for transverse stresses, results are still not fully satisfying. Transverse normal stress $\widetilde{\sigma}_{33}$ and transverse shear stress $\widetilde{\sigma}_{13}$ are shown in Figs. 3.16 and 3.17. You can see that even with layerwise model LD1 there are problems calculating accurate transverse stresses at the top, the bottom and especially the layer interfaces. Results show discontinuities at the interfaces which should be continuous due to physical reasons. The following conclusion can be made: As far as computational effort is concerned, linear LW description should be preferred to higher order ESL theories. If also accurate results for transverse stresses are needed, the usage of mixed models based on Reissner's Mixed Variational Theorem (RMVT) is recommended. Advantages and results on RMVT model are discussed in the following section.

	top	1st interface	2nd interface	bottom
Pagano Exact	-0.940	0.253	-0.201	0.920
LD1(LGR)	-0.740	0.383	-0.149	0.902
ED3(TYL)	-0.924	0.0190	0.00475	0.874
ED3(LGR)	-1.269	-0.381	-0.127	0.704
ED3(LGD)	-0.867	0.0212	0.276	1.107

Table 3.9: *Pagano cylindrical bending: Comparison of different FE models with same DOF for* $\widetilde{u}_1$

	top	1st interface top/bottom	2nd interface top/bottom	bottom
Pagano Exact	18.81	-4.762 / -0.026	0.237 / 4.058	-18.10
LD1(LGR)	16.50	-5.547 / -0.121	0.325 / 4.767	-15.92
ED3(TYL)	18.17	-0.432 / 0.133	0.0708 / -0.2438	-17.47
ED3(LGR)	19.97	2.357 / 0.248	-0.0315 / -2.752	-19.24
ED3(LGD)	19.97	2.357 / 0.248	-0.0315 / -2.752	-19.24

Table 3.10: *Pagano cylindrical bending: Comparison of different FE models with same DOF for* $\widetilde{\sigma}_{11}$

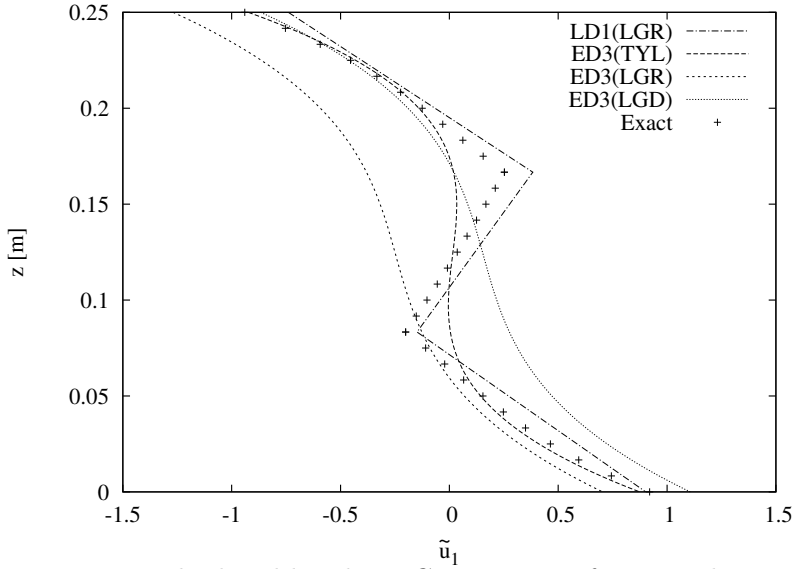

Figure 3.14: *Pagano cylindrical bending: Comparison of ED3 and LD1 theories with same DOF for* $\widetilde{u}_1$

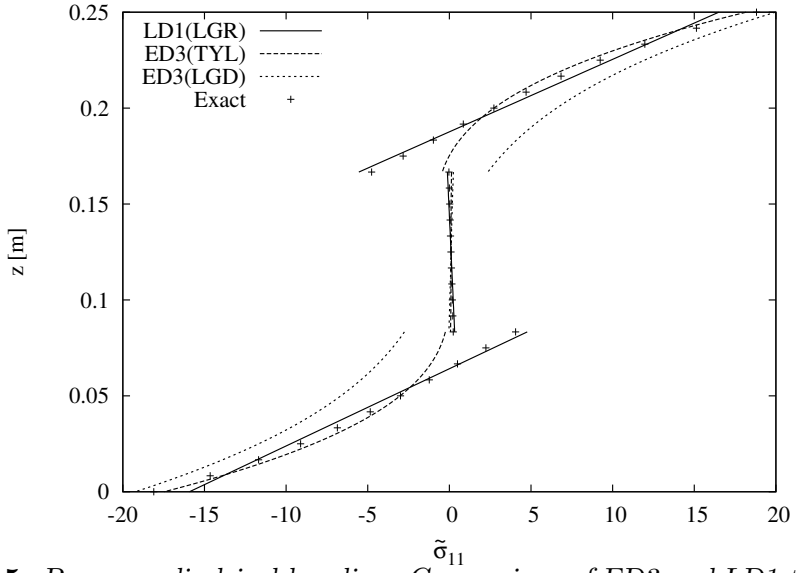

Figure 3.15: *Pagano cylindrical bending: Comparison of ED3 and LD1 theories with same DOF for* $\widetilde{\sigma}_{11}$

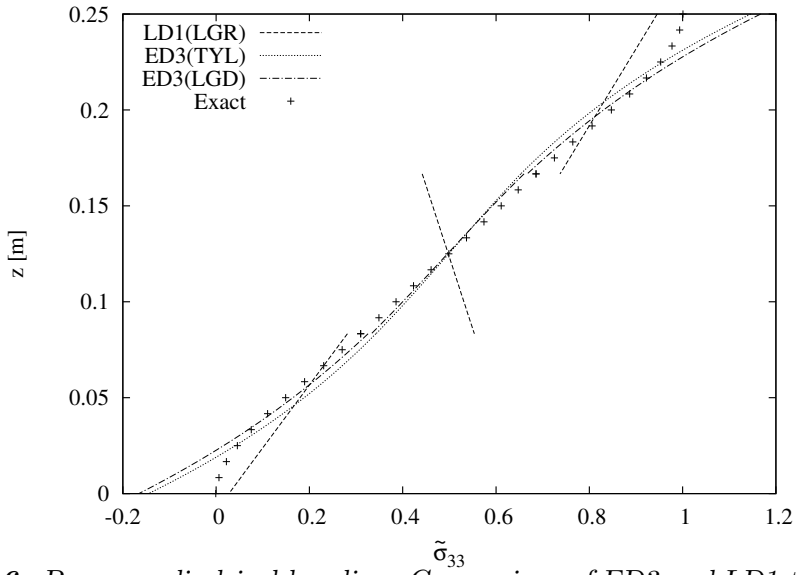

Figure 3.16: *Pagano cylindrical bending: Comparison of ED3 and LD1 theories with same DOF for* $\widetilde{\sigma}_{33}$

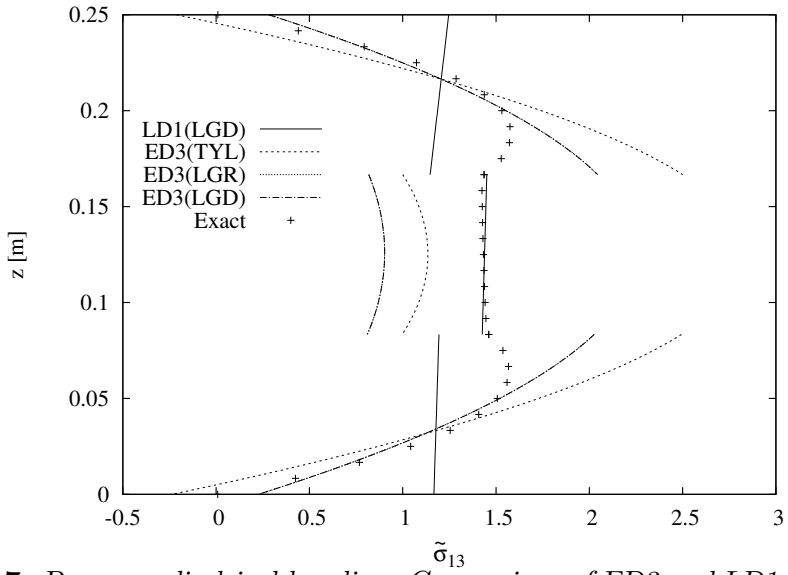

Figure 3.17: *Pagano cylindrical bending: Comparison of ED3 and LD1 theories with same DOF for* $\widetilde{\sigma}_{13}$

3.2 RMVT Analysis

The results obtained above using PVD are already very accurate for higher order expansions, especially for layerwise analysis. But there are still some problems with modelling transverse stresses with PVD. As seen in the previous section, discontinuities can appear at the layer interfaces. An extension of PVD with the aim of an improved description of the transverse stresses is the use of *Reissner's Mixed Variational Theorem*. RMVT offers the possibility to fulfil "a priori" the interlaminar continuity by also assuming the transverse stresses $\boldsymbol{\sigma}_n$ as primary variables.

3.2.1 Pagano Problem - Cylindrical Bending

Mechanical analysis again for the Pagano-problem have been performed with RMVT-model. Results have been compared to PVD results and 3D exact solution. Figures 3.18 to 3.22 clearly show the advantage of the mixed model: Transverse stresses are continuous at the layer interfaces. With higher order models the 3D solution is fully obtained also for transverse stresses. For inplane stresses results are very similar to those obtained with PVD. Also in this case, higher order analyses lead to 3D solution, see Figs. 3.23 and 3.24. The same applies for displacement results which is not shown here for sake of brevity.

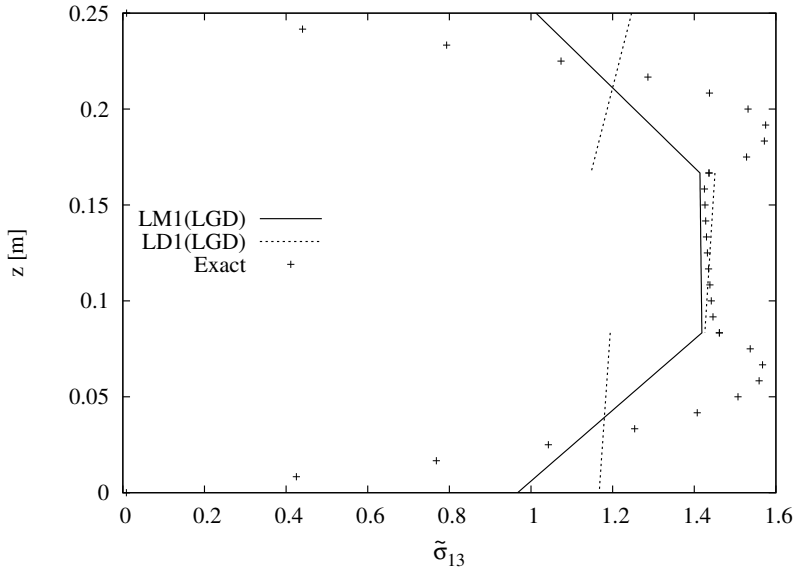

Figure 3.18: *Comparison of 1st order LM and LD for* σ_{13}

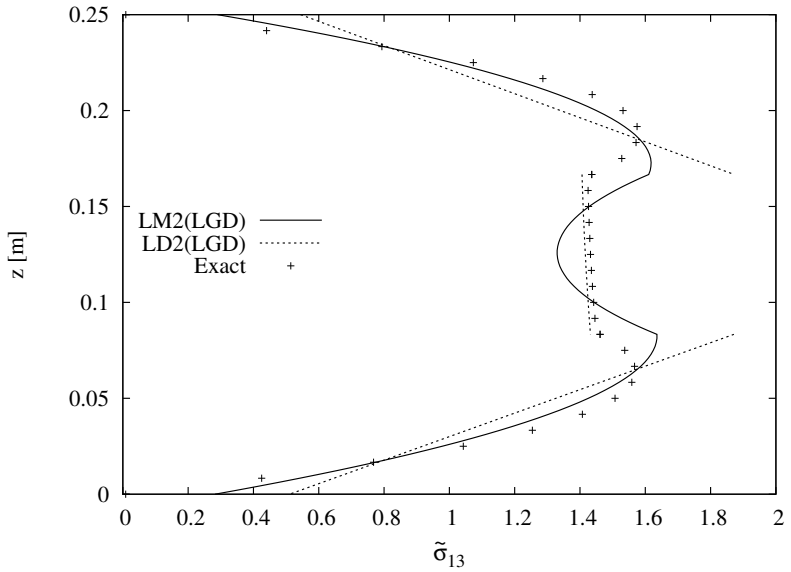

Figure 3.19: *Comparison of 2nd order LM and LD for* σ_{13}

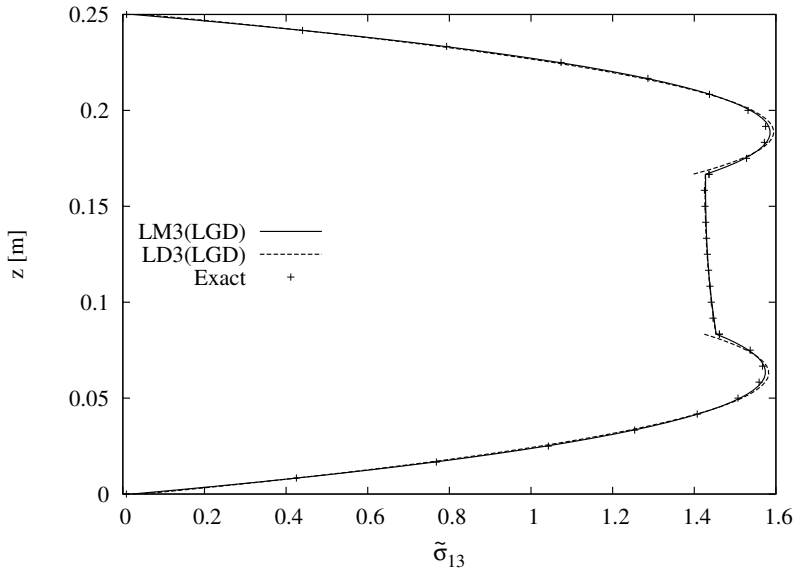

Figure 3.20: *Comparison of 3rd order LM and LD for* σ_{13}

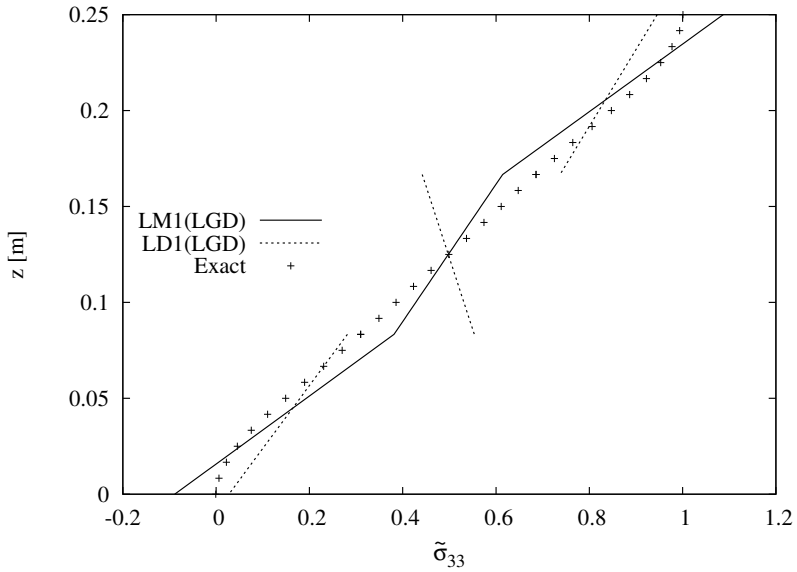

Figure 3.21: *Comparison of 1st order LM and LD for* σ_{33}

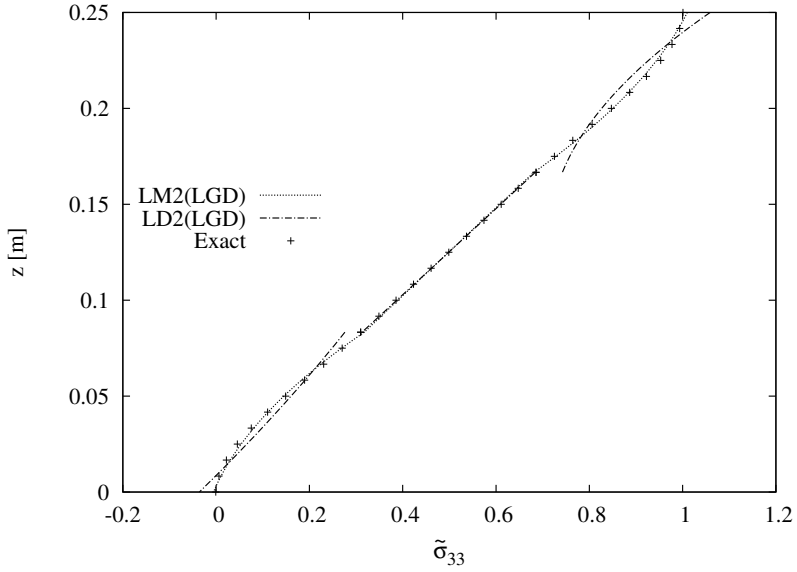

Figure 3.22: *Comparison of 2nd order LM and LD for* σ_{33}

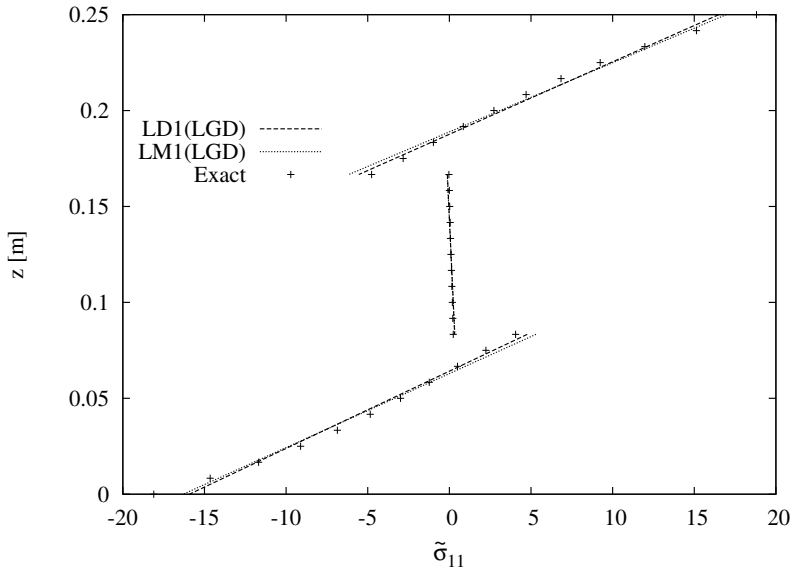

Figure 3.23: *Comparison of 1st order LM and LD for* σ_{11}

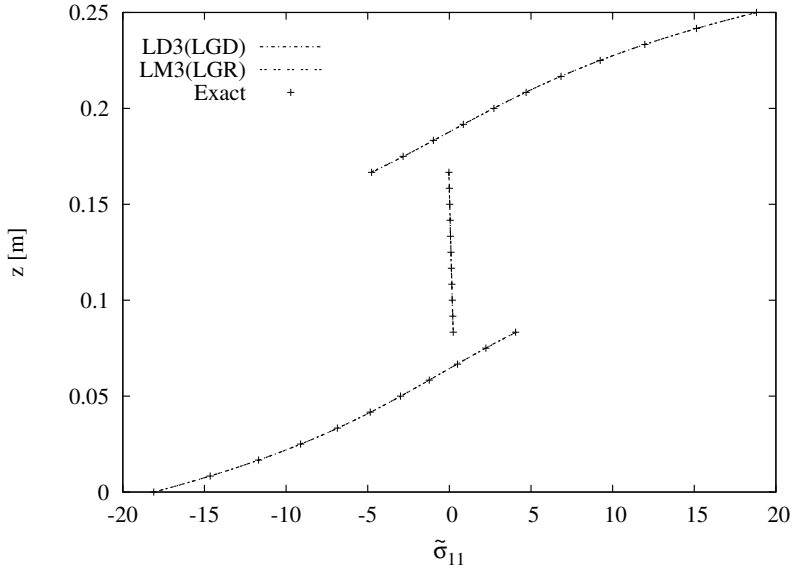

Figure 3.24: *Comparison of 3rd order LM and LD for* σ_{11}

3.2.2 A Global Scalar Parameter for Stress Accuracy Evaluation

To describe the performance of modeling stresses with a FEM model, it is necessary to consider all 6 stresses σ_{11}, σ_{22}, σ_{12}, σ_{13}, σ_{23}, σ_{33} and their distribution along z. Only looking at particular stresses or particular locations in the thickness-direction cannot describe the quality of a model satisfactorily. Therefore a simple global parameter for the accuracy of stresses of different FEM models has been adopted. The idea is to consider all 6 stresses and give their accuracy in comparison to a reference solution by

- numerically integrating the area between FEM and reference solution along z

- dividing the result through the total area of the reference solution along z

for each of the 6 stress-components. To obtain as final value a kind of normalized error ***ER*** in % it is multiplied with factor 100%. Results for all stresses can be summed afterwards. Following this criteria, results close to zero confirm a very accurate modeling (low error), high values identify problems with accurate modeling.

Two stacking sequences have been considered, the symmetric [0/90/0] and the anti-symmetric [90/0] case (stacking-sequence starts form the top). In addition, the dependency of the error on the lamination angle is shown for the anti-symmetric case.

Material properties of the considered plates are:
$E_L = 132.5\,\text{MPa}$, $E_T = 10.8\,\text{MPa}$, $G_{LT} = 5.7\,\text{MPa}$, $G_{TT} = 3.4\,\text{MPa}$, $\nu_{LT} = 0.24$, $\nu_{TT} = 0.49$.

Tables 3.11 and 3.12 show the results for ***ER*** for all 6 stresses. For plane stresses, results are very accurate, nearly all models provide an error of only around 1% or even less. With transverse stresses the error rises for PVD models, especially ED1 solution is totally out of range. RMVT-based models are able to describe also transverse stresses very accurate, especially higher orders provide nearly the exact solution for all 6 stresses. ED1 results are the worst, other theories all lie in-between. The necessity of using mixed theories for getting accurate results in all stresses is confirmed. In Fig. 3.25 also the dependency of ER on the lamination angle for different theories is shown. For different theories, different behaviors can be found.

	$ER(\sigma_{11})$ $(a/2, a/2)$	$ER(\sigma_{22})$ $(a/2, a/2)$	$ER(\sigma_{12})$ $(0, 0)$	$ER(\sigma_{13})$ $(0, a/2)$	$ER(\sigma_{23})$ $(a/2, 0)$	$ER(\sigma_{33})$ $(a/2, a/2)$	sum
Classical ESL							
ED1	1.85	1.95	1.65	37.74	37.38	873.07	953.6
ED2	1.33	1.31	0.61	34.22	34.19	46.07	117.7
ED3	0.72	0.73	0.35	18.78	19.20	38.69	78.5
ED4	0.62	0.63	0.22	17.75	18.07	33.43	70.7
Classical LW							
LD1	3.73	3.79	2.38	34.56	34.54	371.59	450.6
LD2	0.79	0.80	0.43	22.74	23.17	8.19	56.1
LD3	0.13	0.13	0.02	13.08	13.33	4.55	31.2
LD4	0.12	0.12	0.02	13.08	13.33	3.63	30.3
Mixed LW							
LM1	5.82	5.94	1.11	30.71	30.44	8.59	82.6
LM2	0.88	0.89	0.49	14.15	14.41	2.51	33.3
LM3	0.46	0.46	0.39	0.92	0.92	0.36	3.5

Table 3.11: *ER in % for all 6 stresses; stacking sequence* [90/0] *(top-to-bottom); mesh* 15×15*; Pagano 3D solution as reference*

	$ER(\sigma_{11})$ $(a/2, a/2)$	$ER(\sigma_{22})$ $(a/2, a/2)$	$ER(\sigma_{12})$ $(0, 0)$	$ER(\sigma_{13})$ $(0, a/2)$	$ER(\sigma_{23})$ $(a/2, 0)$	$ER(\sigma_{33})$ $(a/2, a/2)$	sum
Classical ESL							
ED1	4.76	4.98	2.77	49.51	40.35	403.17	505.5
ED2	4.46	4.25	2.89	48.41	36.34	13.01	109.4
ED3	0.83	0.93	0.71	20.55	21.70	17.18	61.9
ED4	0.91	0.43	0.71	20.57	21.75	4.63	49.0
Classical LW							
LD1	1.37	4.80	0.95	23.47	30.13	140.56	201.3
LD2	0.19	0.55	0.15	5.68	21.16	4.03	31.8
LD3	0.05	0.24	0.09	4.79	19.52	2.02	26.7
LD4	0.05	0.24	0.09	4.79	19.52	1.97	26.7
Mixed LW							
LM1	2.46	5.93	1.38	4.92	22.06	71.29	108.0
LM2	0.41	0.63	0.44	3.01	7.53	0.52	12.5
LM3	0.21	0.33	0.35	0.42	0.63	0.31	2.3

Table 3.12: *ER in % for all 6 stresses; stacking sequence* [0/90/0]*; mesh* 15×15*; Pagano 3D solution as reference*

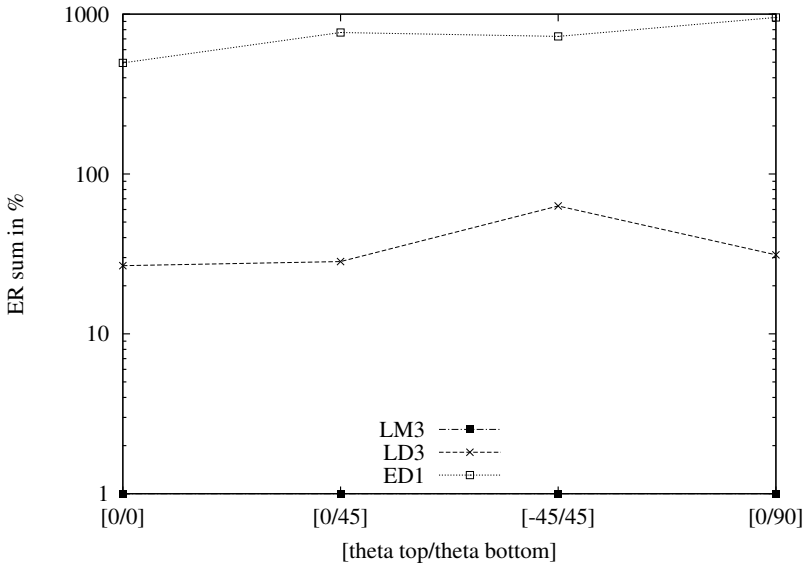

Figure 3.25: *Dependency of ER on the lamination angle for the [90/0] stacking sequence; LM3 results as reference; mesh* 15×15

3.3 Failure Analysis

Composite materials are characterized by a mechanics and a failure mechanics which are more complicate than those of conventional materials. A correct design requires an accurate and effective prediction of failure parameters, such as failure loadings, failure locations and failure indices. Highly accurate mechanical models are therefore needed to effectively describe the mechanics of composites and predict their failure. The RMVT model presented in this work is able to model all stresses with very high accuracy, and therefore particularly suitable for failure forecast. In this work, the Maximum Stress failure criteria has been adopted and shall be introduced in short form in the following part. Further investigations could be part of future works, including also other failure criteria, i.e. the criteria for composite laminates of Puck.

3.3.1 Maximum Stress Failure Criteria

The idea of Maximum Stress criteria is to compare the lamina stress status with the lamina normal and shear strength. Failure occurs when the ratio is greater or equal to 1.

$$\begin{aligned} \frac{|\sigma_{11}|}{X} \geq 1; \qquad & \frac{|\sigma_{23}|}{R} \geq 1 \\ \frac{|\sigma_{22}|}{Y} \geq 1; \qquad & \frac{|\sigma_{13}|}{S} \geq 1 \\ \frac{|\sigma_{33}|}{Z} \geq 1; \qquad & \frac{|\sigma_{12}|}{T} \geq 1 \end{aligned} \tag{3.3}$$

X, Y, and Z represent the lamina normal strengths while R, S, and T are the lamina shear strengths (23, 13, 12) in the layers. Normal strengths depend on the sign of the corresponding stress component. In the case of tensile stresses, the tensile strengths X_T, Y_T and Z_T must be used in Eq. (3.3). For negative values of the normal stress components the compressive strengths X_C, Y_C and Z_C have to be used. Due to the linearity of the problem, a relation of proportionality holds between the applied loading $p_{zz}^{(0)}$ and every stress component. This means for every equation in (3.3) a failure loading $p_{zz}^{(F)}$ can be calculated with the following formula:

$$\begin{aligned} p_{zz,11}^{(F)} &= p_{zz}^{(0)} \frac{X}{|\sigma_{11}|} \qquad & p_{zz,23}(F) &= p_{zz}^{(0)} \frac{R}{|\sigma_{23}|} \\ p_{zz,22}^{(F)} &= p_{zz}^{(0)} \frac{Y}{|\sigma_{22}|} \qquad & p_{zz,13}(F) &= p_{zz}^{(0)} \frac{S}{|\sigma_{13}|} \\ p_{zz,33}^{(F)} &= p_{zz}^{(0)} \frac{Z}{|\sigma_{33}|} \qquad & p_{zz,12}(F) &= p_{zz}^{(0)} \frac{T}{|\sigma_{12}|} \end{aligned} \tag{3.4}$$

The minimum failure load is the minimum value of Eq. (3.4). Failure indices can be computed along the thickness z considering the minimum failure load as reference.

3.3.2 Results with Maximum Stress Criteria

Two different stacking sequences, the symmetric [0/90/0] and [0/45/0] as well as the antisymmetric [0/90/0/90] configurations have been investigated. Stacking sequence starts from plate top. Ply angles are measured with respect to the $x-$axis. All of the plies are made of the $T300/5208$ graphite/epoxy material. Its mechanical properties are:

$E_L = 132.5\,\text{MPa}$, $E_T = 10.8\,\text{MPa}$, $G_{LT} = 5.7\,\text{MPa}$, $G_{TT} = 3.4\,\text{MPa}$, $\nu_{LT} = 0.24$, $\nu_{TT} = 0.49$.

Material strengths are:
$X_t = 1515\,\text{MPa}$, $X_c = 1697\,\text{MPa}$, $Y_t = 43.8\,\text{MPa}$, $Y_c = 43.8\,\text{MPa}$, $Z_t = 43.8\,\text{MPa}$, $Z_c = 43.8\,\text{MPa}$, $R = 86.9\,\text{MPa}$, $S = 67.6\,\text{MPa}$, $T = 86.9\,\text{MPa}$

All layers have the same thickness, the plate sides are of equal length. Three different thickness ratios are considered $a/h = 100$, 50, 10 in order to deal with thin and moderately thick plates. A bi-sinusoidal loading with a half wave for each side is addressed.

First results presented in this work point out the necessity to use mixed formulation for failure analysis. With PVD model, wrong transverse shear stresses σ_{13} and σ_{23} appear in the center of the plate which should be zero, see Fig. 3.33 and 3.34. For thin plates these wrong stresses can be so high that they cause the minimum failure load and lead to wrong results. For thicker plates the minimum failure load is not affected, but in the distribution of the failure index along the z-direction, you can see that information get lost in some areas where these wrong transverse stresses are too high. Therefore only mixed models should be used for running failure analysis. Results for minimum first-ply failure loading values are presented in Tab. 3.13. LM models achieve very accurate results already with 2*nd*-order expansion. For all the addressed cases, minimum failure load occurs in the center point of the plate but in different locations along the z-direction for the different stacking-sequences. For the [0/45/0] case, critical points are found in the layer interfaces which can be seen in Fig. 3.30 and Fig. 3.31, while for [0/90/0] and [0/90/0/90] failure occurs on the top of the plate (see Fig. 3.26 to 3.29). Results for the [0/90/0] and [0/90/0/90] are compared with Pagano 3D exact solution. Convergence is shown in Tab. 3.14. Furthermore analysis have been done for the 3-layer case with step wise changing the orientation of the middle layer in steps of 15 deg. Results are shown in Fig. 3.32 It can be seen that the most critical point for failure in the z-direction depends a lot on the ply angles of the laminate and can change from the top to the interfaces of the lamination.

a/h [MPa]	100 $\times 10^{-2}$	50 $\times 10^{-1}$	10 $\times 1$
Analytical			
3D Pagano	9.1838	3.6434	7.2858
MUL2, Q4, 8×8			
ED1	3.6496*	2.6682*	5.9578
ED2	3.4410*	2.7355*	7.7215
ED3	3.4386*	2.7280*	7.1818
ED4	3.4386*	2.7280*	7.3307
LD1	3.4620*	2.7470*	6.5592
LD2	3.4382*	2.7268*	7.2457
LD3	3.4382*	2.7267*	7.2847
LD4	3.4382*	2.7267*	7.2901
LM1	8.2752	3.2824	6.5338
LM2	9.2822	3.6798	7.2344
LM3	9.2829	3.6805	7.2579
LM4	9.2829	3.6807	7.2613

(*)Minimum failure loading due to wrong transverse shear stresses

Table 3.13: *Minimum first-ply failure loading values; [0/90/0] stacking sequence*

[MPa]	$a/h = 100$ $\times 10^{-2}$	$a/h = 50$ $\times 10^{-1}$	$a/h = 10$ $\times 1$
3D Pagano	9.1838	3.6434	7.2858
LM2, $Q4, 6 \times 6$	9.3656	3.7106	7.2115
LM2, $Q4, 8 \times 8$	9.2822	3.6798	7.2344
LM2, $Q4, 10 \times 10$	9.2455	3.6660	7.2432

Table 3.14: *Convergence for first-ply failure loading values with Maximum Stress Criterion; [0/90/0] stacking sequence*

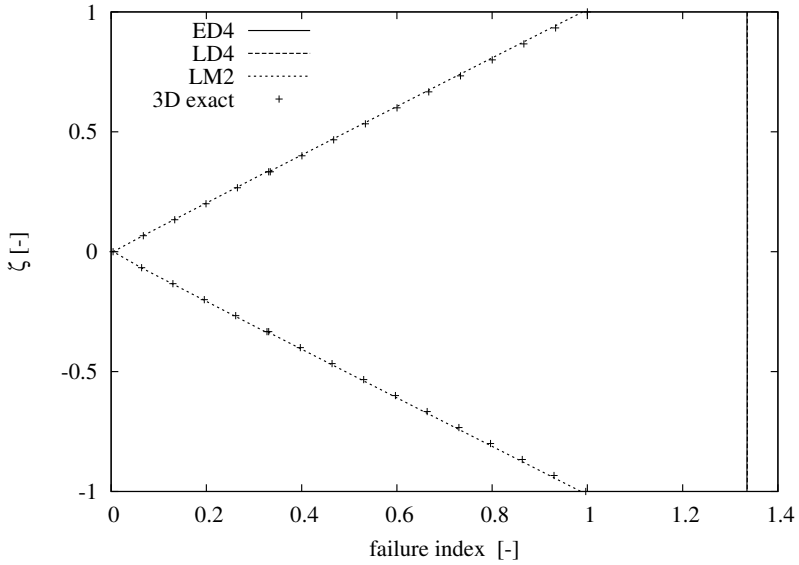

Figure 3.26: *Failure index via max stress criterion along thickness* ζ*;* $a/h = 50$*,* $[0/90/0]$

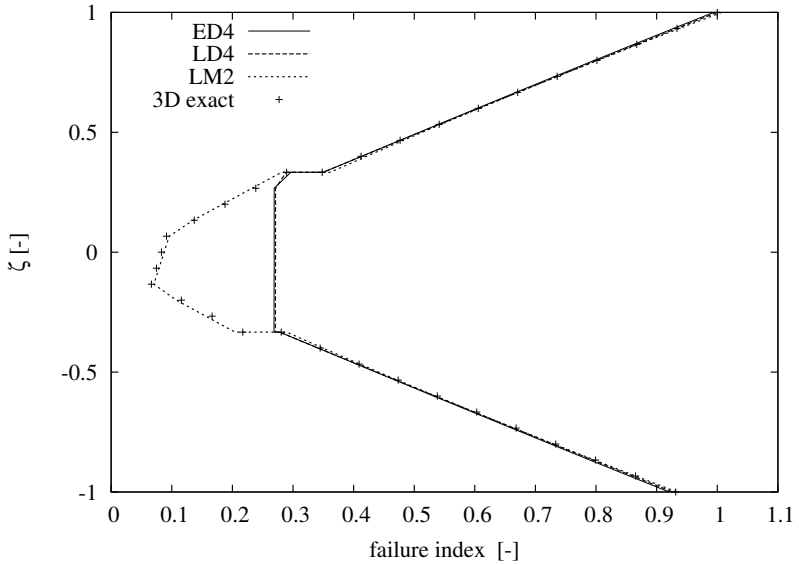

Figure 3.27: *Failure index via max stress criterion along thickness* ζ*;* $a/h = 10$*,* $[0/90/0]$

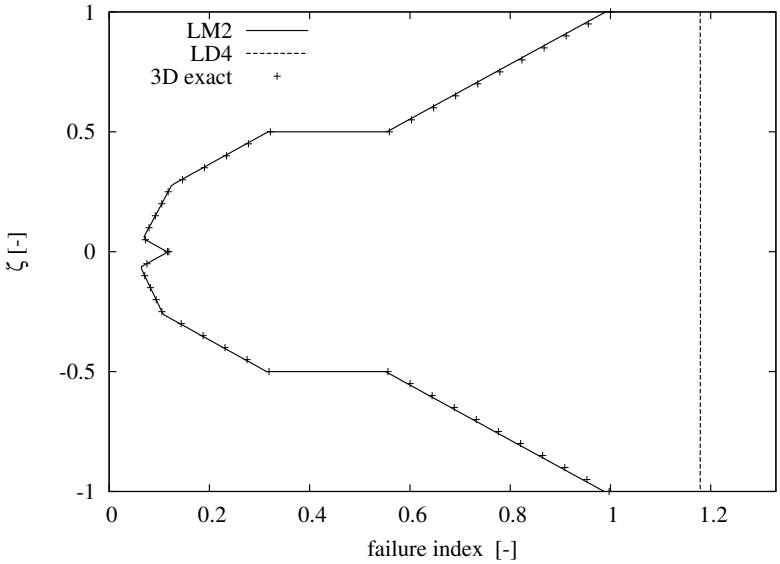

Figure 3.28: *Failure index via max stress criterion along thickness* ζ*;* $a/h = 50$*,* $[0/90/0/90]$

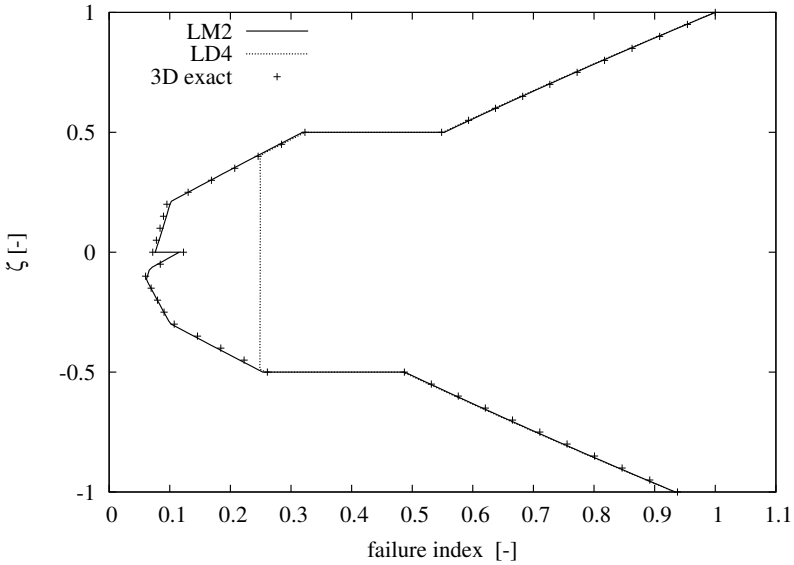

Figure 3.29: *Failure index via max stress criterion along thickness* ζ*;* $a/h = 10$*,* $[0/90/0/90]$

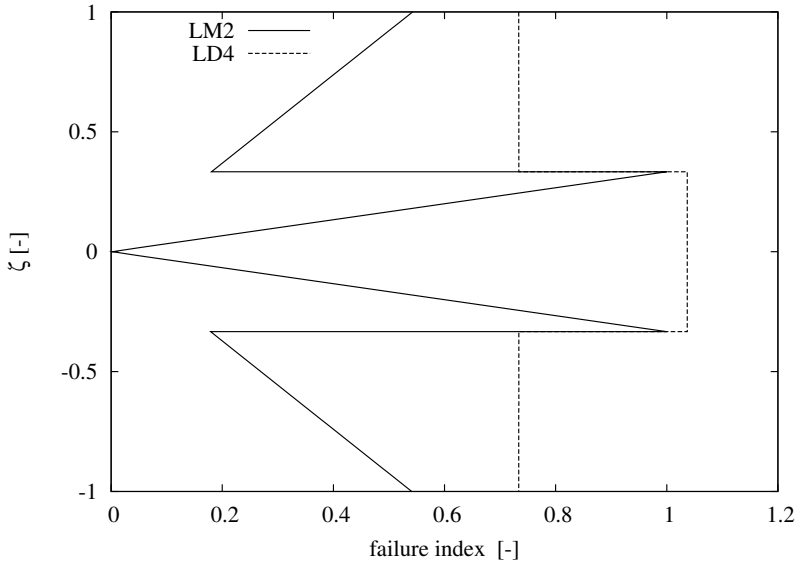

Figure 3.30: *Failure index via max stress criterion along thickness* ζ*;* $a/h = 50$*,* $[0/45/0]$

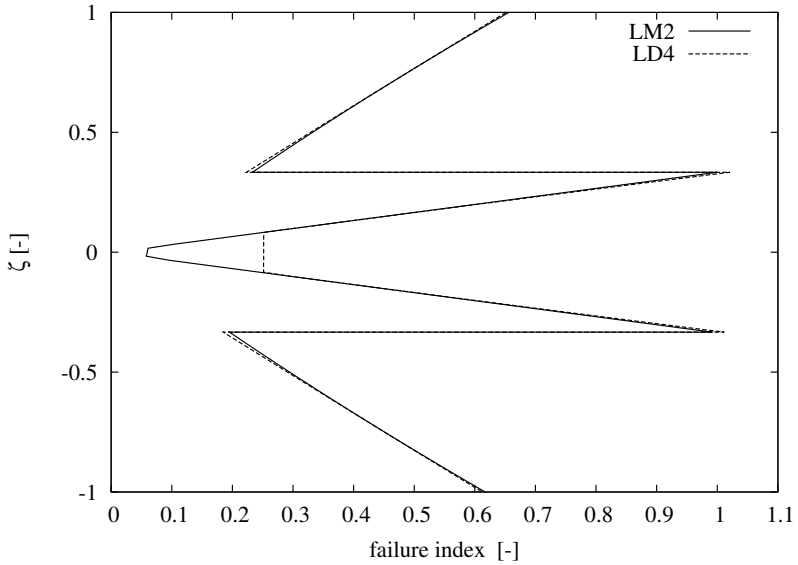

Figure 3.31: *Failure index via max stress criterion along thickness* ζ*;* $a/h = 10$*,* $[0/45/0]$

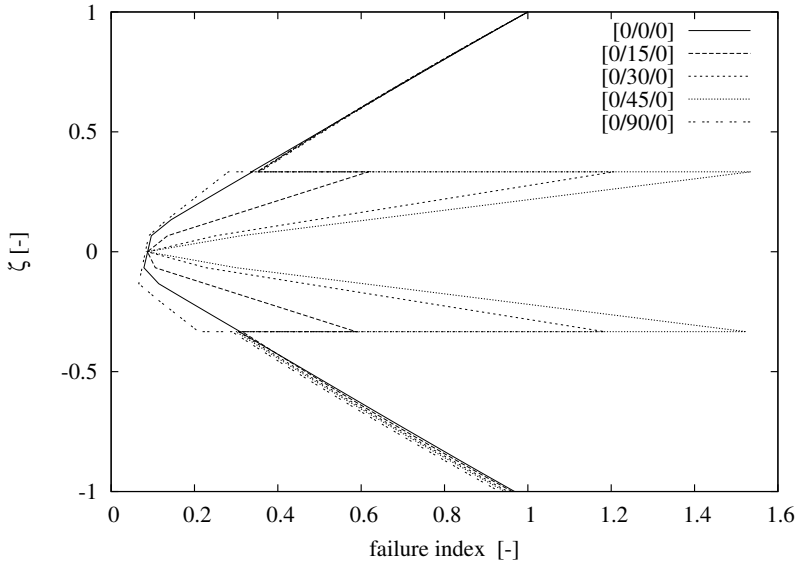

Figure 3.32: *Failure index via max stress criterion along ζ for various lamination angles; $a/h = 10$, load is minimum failure load at the top; LM2 model*

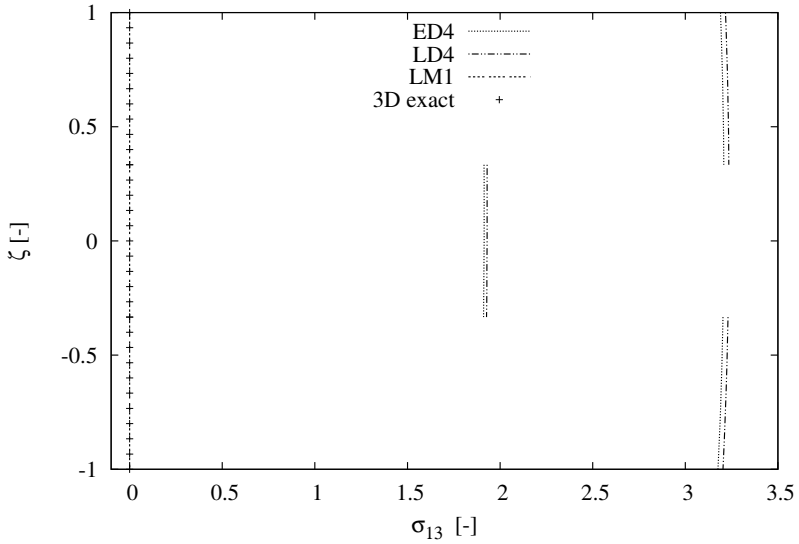

Figure 3.33: *σ_{13} in the center of the plate along thickness ζ; $a/h = 10$, $[0/90/0]$*

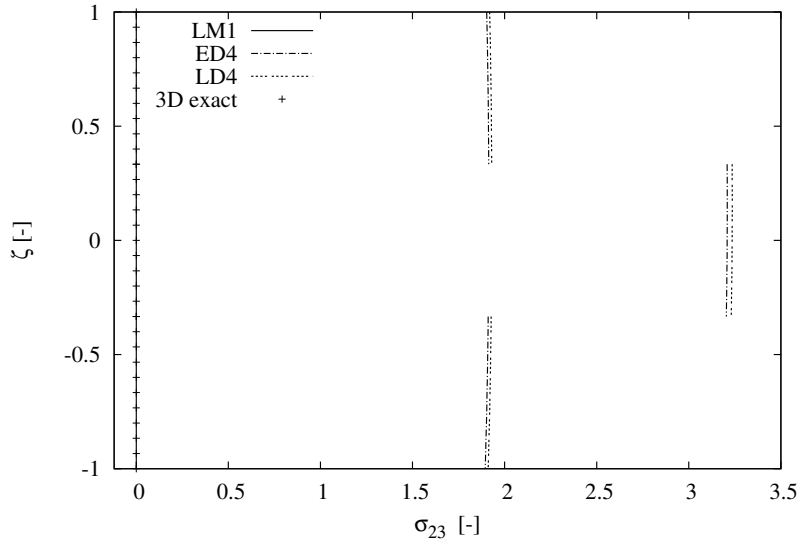

Figure 3.34: *σ_{23} in the center of the plate along thickness ζ; $a/h = 10$, [0/90/0]*

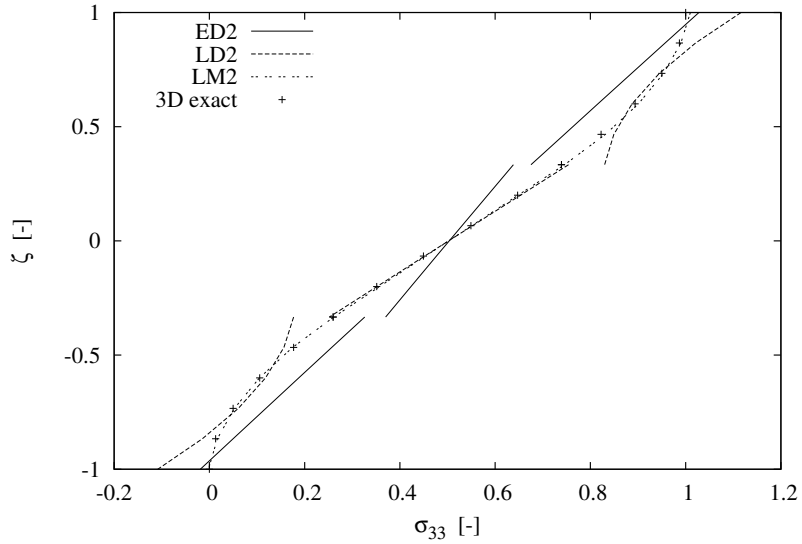

Figure 3.35: *σ_{33} in the center of the plate along thickness ζ; $a/h = 10$, [0/90/0]*

Chapter 4

Electro-Mechanical RMVT

Smart structures such as piezoelectric materials can be considered the candidates for next generation structures in aerospace vehicles as well as for advanced products in the automotive and ship industries. Piezoelectric materials can be simple integrated in composite structures. Very often, piezoelectric layers are embedded in laminated structures made of anisotropic composite materials. Thus they offer the possibility to combine the low density, superior mechanical and thermal properties of composite materials with the capacity to act as senors, actuators and for controlling. The advantage of using RMVT consists in the possibility of assuming two independent set of variables: A set of primary unknowns and a set of extensive variables which are modeled in the thickness plate z-direction. This leads to the "a-priori" and complete fulfillment of the interlaminar continuity for the modeled extensive variables, with consequent satisfaction of the C_z^0 requirements. In Sec. 4.10, the RMVT has be used to obtain accurate results for transverse stresses in pure mechanical problems. The idea is to expand the RMVT to other variables of the multifield case. In the electro-mechanical coupled case, an additional assumption for the transverse electric displacement D_z is made.

4.1 Considered variational statements

For sake of completeness the PVD statement for the electromechanical case is introduced at first. Main focus shall be put on the expansion of RMVT to the electromechanical coupling, the so called RMVT-σ_n-D_z, which is described in Sec. 4.1.2.

4.1.1 The PVD for the electro-mechanical case

Dividing stresses and strains into in-plane and out-of-plane components the mechanical PVD statement reads (see also Sec. 1.2):

$$\int_V (\delta\boldsymbol{\epsilon}_{pG}^T\,\boldsymbol{\sigma}_{pC} + \delta\boldsymbol{\epsilon}_{nG}^T\,\boldsymbol{\sigma}_{nC})\,dV \;=\; \delta W_e, \tag{4.1}$$

with:

$$\boldsymbol{\epsilon}_p^T = \left\{ \begin{array}{ccc} \epsilon_{xx} & \epsilon_{yy} & \epsilon_{xy} \end{array} \right\}; \qquad \boldsymbol{\sigma}_p^T = \left\{ \begin{array}{ccc} \sigma_{xx} & \sigma_{yy} & \sigma_{xy} \end{array} \right\};$$
$$\boldsymbol{\epsilon}_n^T = \left\{ \begin{array}{ccc} \epsilon_{zz} & \epsilon_{xz} & \epsilon_{yz} \end{array} \right\}; \qquad \boldsymbol{\sigma}_n^T = \left\{ \begin{array}{ccc} \sigma_{zz} & \sigma_{xz} & \sigma_{yz} \end{array} \right\}.$$

Cartesian x, y, z reference system is considered and notation already used in previous sections is referred to: subscript "p" denotes in-plane unknowns and subscript "n"

denotes out-of-plane unknowns; subscript "z" indicates the through-the-thickness z-direction, while subscripts "x" and "y" are for the two in-plane directions.
In the case of applied electro-mechanical loading on a surface Ω the virtual variation of the external work, employing Einstein's summation convention over repeated indices, can be expressed as:

$$\delta W_e = \int_\Omega \left(\bar{t}_i \, \delta u_i - \bar{Q} \, \delta \phi \right) \, d\Omega, \tag{4.2}$$

where:
$\bar{t}_i$ is the mechanical loading in i-direction (pressure);
u_i is the displacement component in i-direction;
$\bar{Q}$ is the charge density on the plate surface;
ϕ is the electric potential.
Including electrical contributions, the PVD in Eq. (4.1) becomes:

$$\int_V (\delta \boldsymbol{\epsilon}_{pG}^T \, \boldsymbol{\sigma}_{pC} + \delta \boldsymbol{\epsilon}_{nG}^T \, \boldsymbol{\sigma}_{nC} \delta - \delta \boldsymbol{E}_{pG}^T \, \boldsymbol{D}_{pC} - \delta E_{nG} \, D_{nC}) \, dV \; = \; \delta W_e, \tag{4.3}$$

with:

$$\boldsymbol{E}_p^T = \left\{ \; E_x \quad E_y \; \right\}; \qquad \boldsymbol{D}_p^T = \left\{ \; D_x \quad D_y \; \right\}; \tag{4.4}$$

$$E_n = \left\{ \; E_z \; \right\}; \qquad D_n = \left\{ \; D_z \; \right\}. \tag{4.5}$$

D and E indicate the electric displacement and the electric field, respectively. The condensed vectorial notation discussed in [11] is employed in the follwing part. The two multifield variables are introduced:

$$\boldsymbol{\mathcal{S}}^T = \left\{ \; \sigma_{xx} \quad \sigma_{yy} \quad \sigma_{xy} \quad -D_x \quad -D_y \quad \sigma_{zz} \quad \sigma_{xz} \quad \sigma_{yz} \quad -D_z \; \right\}, \tag{4.6}$$

$$\boldsymbol{\mathcal{E}}^T = \left\{ \; \epsilon_{xx} \quad \epsilon_{yy} \quad \epsilon_{xy} \quad E_x \quad E_y \quad \epsilon_{zz} \quad \epsilon_{xz} \quad \epsilon_{yz} \quad E_z \quad \right\}, \tag{4.7}$$

where $\boldsymbol{\mathcal{S}}$ is the vector of extensive variables and $\boldsymbol{\mathcal{E}}$ is the vector of intensive ones. Applying the condensed notation, it is possible to rewrite Eq. (4.3) for multifield problems in the following simple form:

$$\int_V \left(\delta \boldsymbol{\mathcal{E}}_G^T \, \boldsymbol{\mathcal{S}}_C \right) dV \; = \; \delta W_e. \tag{4.8}$$

4.1.2 The RMVT-σ_n-D_z

The RMVT statement with "a-priori" modeling of the transverse stresses $\boldsymbol{\sigma}_n$ and transverse electric displacement D_z (or D_n) is here called RMVT-σ_n-D_z The expansion of the classical RMVT to the electro-mechanical case leads to the following equation [12]:

$$\begin{aligned} \int_V (&\delta \boldsymbol{\epsilon}_{pG}^T \, \boldsymbol{\sigma}_{pC} + \delta \boldsymbol{\epsilon}_{nG}^T \, \boldsymbol{\sigma}_{nC} - \delta \boldsymbol{E}_{pG}^T \, \boldsymbol{D}_{pC} - \delta E_{nG} \, D_n + \delta \boldsymbol{\sigma}_{nM}^T (\epsilon_{nG} - \epsilon_{nC}) + \\ &- \delta D_n (E_{nG} - E_{nC})) \, dV \; = \; \delta W_e. \end{aligned} \tag{4.9}$$

By referring to the condensed notation and considering that subscript "a" indicates "not modeled quantities", while subscripts "b" is related to "modeled quantities", the following vectors can be introduced:

$$\boldsymbol{\mathcal{S}}_{aC} = \left\{ \; \sigma_{xx} \quad \sigma_{yy} \quad \sigma_{xy} \quad -D_x \quad -D_y \; \right\}_C^T$$

is the vector of not-modeled extensive variables, which are calculated by constitutive relations;

$$\boldsymbol{\mathcal{S}}_b = \left\{ \begin{array}{cccc} \sigma_{zz} & \sigma_{xz} & \sigma_{yz} & -D_z \end{array} \right\}^T$$

is the vector of modeled extensive variables;

$$\boldsymbol{\mathcal{E}}_{aG} = \left\{ \begin{array}{ccccc} \epsilon_{xx} & \epsilon_{yy} & \epsilon_{xy} & E_x & E_y \end{array} \right\}_G^T$$

is the vector of intensive variables associated to $\boldsymbol{\mathcal{S}}_{aC}$ and calculated by geometrical relations;

$$\boldsymbol{\mathcal{E}}_{bG} = \left\{ \begin{array}{cccc} \epsilon_{zz} & \epsilon_{xz} & \epsilon_{yz} & E_z \end{array} \right\}_G^T$$

is the vector of intensive variables associated to $\boldsymbol{\mathcal{S}}_b$ and calculated by geometrical relations;

$$\boldsymbol{\mathcal{E}}_{bC} = \left\{ \begin{array}{cccc} \epsilon_{zz} & \epsilon_{xz} & \epsilon_{yz} & E_z \end{array} \right\}_C^T$$

is the vector of intensive variables associated to $\boldsymbol{\mathcal{S}}_b$ and calculated by constitutive relations.

In so doing, the RMVT statement with "a-priori" modeling of the transverse electric displacement D_z and transverse stresses $\boldsymbol{\sigma}_n$ takes the following form:

$$\int_V \left(\delta \boldsymbol{\mathcal{E}}_{aG}^T \boldsymbol{\mathcal{S}}_{aC} + \delta \boldsymbol{\mathcal{E}}_{bG}^T \boldsymbol{\mathcal{S}}_b + \delta \boldsymbol{\mathcal{S}}_b^T \left(\boldsymbol{\mathcal{E}}_{bG} - \boldsymbol{\mathcal{E}}_{bC} \right) \right) dV = \delta W_e. \tag{4.10}$$

Equation (4.10) has the same topology as the RMVT statement for pure mechanical case, see Eq. (2.37) In the following section, the constitutive relations are obtained for the RMVT-σ_n-D_z variational statement in the condensed notation, according to Eq. (4.10).

4.2 Constitutive relations

Physical constitutive equations for PVD applications can be written for the electro-mechanical case:

$$\begin{aligned} \sigma_{ij} &= C_{ij\,lm} \epsilon_{lm} - e_{ij\,l} E_l, \\ D_l &= e_{lij}\, \epsilon_{ij} + \varepsilon_{lm} E_m, \end{aligned} \tag{4.11}$$

where standard tensor notation is used and Einstein's summation convention is implied over repeated indices. $C_{ij\,lm}$ are the elastic coefficients (Hooke's law); e_{lij} are the piezoelectric coefficients and ε_{ij} stand for the permittivity coefficients. To be noted that $2\epsilon_{ij}$ components in tensorial notation correspond to ϵ_{ij} components in vectorial notation, when $i \neq j$). More detailed information on the constitutive equations for the electromechanical case can be found in [3]
The constitutive relations for the RMVT variational statement in the condensed form of Eq. (4.10) are obtained in the following:

In a first step, primary unknowns variables are specified and collected in the vector $\boldsymbol{V}^{kT}$:

$$\boldsymbol{V}^{kT} = \left\{ \begin{array}{cccccccc} u_x^k & u_y^k & u_z^k & \phi^k & \sigma_{zz}^k & \sigma_{xz}^k & \sigma_{yz}^k & D_z^k \end{array} \right\},$$

It is useful to rewrite vectors introduced in Sec.4.1.2:

$$\boldsymbol{\mathcal{E}}_a^{kT} = \left\{ \begin{array}{ccccc} \epsilon_{xx}^k & \epsilon_{yy}^k & \epsilon_{xy}^k & E_x^k & E_y^k \end{array} \right\}; \qquad \boldsymbol{\mathcal{E}}_b^{kT} = \left\{ \begin{array}{cccc} \epsilon_{zz}^k & \epsilon_{xz}^k & \epsilon_{yz}^k & E_z^k \end{array} \right\};$$
$$\boldsymbol{\mathcal{S}}_a^{kT} = \left\{ \begin{array}{ccccc} \sigma_{xx}^k & \sigma_{yy}^k & \sigma_{xy}^k & -D_x^k & -D_y^k \end{array} \right\}; \qquad \boldsymbol{\mathcal{S}}_b^{kT} = \left\{ \begin{array}{cccc} \sigma_{zz}^k & \sigma_{xz}^k & \sigma_{yz}^k & -D_z^k \end{array} \right\}.$$

Following geometrical relations can be written:

$$\boldsymbol{\mathcal{E}}_{aG}^k = \boldsymbol{D}_a \boldsymbol{V}^k; \tag{4.12}$$

$$\boldsymbol{\mathcal{E}}_{bG}^k = \boldsymbol{D}_b \boldsymbol{V}^k; \tag{4.13}$$

$$\boldsymbol{\mathcal{S}}_{bG}^k = \boldsymbol{D}_{b'} \boldsymbol{V}^k. \tag{4.14}$$

where the differential matrices in explicit form read:

$$\boldsymbol{D}_a = \begin{pmatrix} \partial_x & 0 & 0 & 0 & 0 & 0 & 0 & 0 \\ 0 & \partial_y & 0 & 0 & 0 & 0 & 0 & 0 \\ \partial_y & \partial_x & 0 & 0 & 0 & 0 & 0 & 0 \\ 0 & 0 & 0 & -\partial_x & 0 & 0 & 0 & 0 \\ 0 & 0 & 0 & -\partial_y & 0 & 0 & 0 & 0 \end{pmatrix}; \quad \boldsymbol{D}_b = \begin{pmatrix} 0 & 0 & \partial_z & 0 & 0 & 0 & 0 & 0 \\ \partial_z & 0 & \partial_x & 0 & 0 & 0 & 0 & 0 \\ 0 & \partial_z & \partial_y & 0 & 0 & 0 & 0 & 0 \\ 0 & 0 & 0 & -\partial_z & 0 & 0 & 0 & 0 \end{pmatrix};$$

$$\boldsymbol{D}_{b'} = \begin{pmatrix} 0 & 0 & 0 & 0 & 1 & 0 & 0 & 0 \\ 0 & 0 & 0 & 0 & 0 & 1 & 0 & 0 \\ 0 & 0 & 0 & 0 & 0 & 0 & 1 & 0 \\ 0 & 0 & 0 & 0 & 0 & 0 & 0 & -1 \end{pmatrix}.$$

Referring to the condensed notation and specifying which quantities are obtained by constitutive equations or by geometrical relations, one gets:

$$\widetilde{\boldsymbol{\mathcal{S}}}_C^k = \widetilde{\boldsymbol{C}}^k \widetilde{\boldsymbol{\mathcal{E}}}_G^k. \tag{4.15}$$

$\widetilde{\boldsymbol{\mathcal{S}}}_C^k$ is composed by the vector of not modeled extensive variables $\boldsymbol{\mathcal{S}}_{aC}^k$ and the vector of intensive variables $\boldsymbol{\mathcal{E}}_{bC}$ (which is associated to $\boldsymbol{\mathcal{S}}_b^k$);
$\widetilde{\boldsymbol{\mathcal{E}}}_G^k$ is composed by the vector of intensive variables $\boldsymbol{\mathcal{E}}_{aG}^k$ (which is associated to $\boldsymbol{\mathcal{S}}_a^k$) and the vector of modeled extensive variables $\boldsymbol{\mathcal{S}}_{bG}^k$ (that can be thought as a geometrical vector, see Eq. (4.14))

$$\widetilde{\boldsymbol{\mathcal{S}}}_C^{kT} = \left\{ \begin{array}{cc} \boldsymbol{\mathcal{S}}_{aC}^{kT} & \boldsymbol{\mathcal{E}}_{bC}^{kT} \end{array} \right\}; \qquad \widetilde{\boldsymbol{\mathcal{E}}}_G^{kT} = \left\{ \begin{array}{cc} \boldsymbol{\mathcal{E}}_{aG}^{kT} & \boldsymbol{\mathcal{S}}_{bG}^{kT} \end{array} \right\}.$$

$\widetilde{\boldsymbol{C}}^k$ is the modified constitutive matrix applicable for the RMVT-σ_n-D_3 formulation. The derivation of $\widetilde{\boldsymbol{C}}^k$ from the physical constitutive matrix $\boldsymbol{C}^k$ is similar to the derivation of the corresponding constitutive matrix for the pure mechanical RMVT case and shall be described in the following (to be noted: in this case tilde "˜" indicates the modified constitutive reations for RMVT). The physical constitutive matrix $\boldsymbol{C}^k$ can be partitioned by dividing cells related to modeled and not modeled quantities:

$$\boldsymbol{C}^k = \left\{ \begin{array}{cc} \boldsymbol{C}_{aa}^k & \boldsymbol{C}_{ab}^k \\ \boldsymbol{C}_{ba}^k & \boldsymbol{C}_{bb}^k \end{array} \right\}, \tag{4.16}$$

In explicit form it reads:

$$\boldsymbol{C}_{aa}^k = \begin{pmatrix} C_{11}^k & C_{12}^k & C_{16}^k & 0 & 0 \\ C_{12}^k & C_{22}^k & C_{26}^k & 0 & 0 \\ C_{16}^k & C_{26}^k & C_{66}^k & 0 & 0 \\ 0 & 0 & 0 & -\varepsilon_{11}^k & -\varepsilon_{12}^k \\ 0 & 0 & 0 & -\varepsilon_{12}^k & -\varepsilon_{22}^k \end{pmatrix}; \quad \boldsymbol{C}_{ab}^k = \begin{pmatrix} C_{13}^k & 0 & 0 & -e_{31}^k \\ C_{23}^k & 0 & 0 & -e_{32}^k \\ C_{36}^k & 0 & 0 & -e_{36}^k \\ 0 & -e_{15}^k & -e_{14}^k & 0 \\ 0 & -e_{25}^k & -e_{24}^k & 0 \end{pmatrix};$$

$$\boldsymbol{C}^k_{ba} = \begin{pmatrix} C^k_{13} & C^k_{23} & C^k_{36} & 0 & 0 \\ 0 & 0 & 0 & -e^k_{15} & -e^k_{25} \\ 0 & 0 & 0 & -e^k_{14} & -e^k_{24} \\ -e^k_{31} & -e^k_{32} & -e^k_{36} & 0 & 0 \end{pmatrix}; \quad \boldsymbol{C}^k_{bb} = \begin{pmatrix} C^k_{33} & 0 & 0 & -e^k_{33} \\ 0 & C^k_{55} & C^k_{45} & 0 \\ 0 & C^k_{45} & C^k_{44} & 0 \\ -e^k_{33} & 0 & 0 & -\varepsilon^k_{33} \end{pmatrix}.$$

where $\boldsymbol{C}^k_{ab} = \boldsymbol{C}^{kT}_{ba}$. Physical constitutive relations can be arranged according to the above partitioning:

$$\boldsymbol{\mathcal{S}}^k_{aC} = \boldsymbol{C}^k_{aa}\boldsymbol{\mathcal{E}}^k_{aG} + \boldsymbol{C}^k_{ab}\boldsymbol{\mathcal{E}}^k_{bG}, \quad \boldsymbol{\mathcal{S}}^k_{bC} = \boldsymbol{C}^k_{ba}\boldsymbol{\mathcal{E}}^k_{aG} + \boldsymbol{C}^k_{bb}\boldsymbol{\mathcal{E}}^k_{bG}. \tag{4.17}$$

From Eqs. (4.17) one has:

$$\boldsymbol{\mathcal{S}}^k_{aC} = \widetilde{\boldsymbol{C}}^k_{aa}\boldsymbol{\mathcal{E}}^k_{aG} + \widetilde{\boldsymbol{C}}^k_{ab}\boldsymbol{\mathcal{S}}^k_{bG}, \quad \boldsymbol{\mathcal{E}}^k_{bC} = \widetilde{\boldsymbol{C}}^k_{ba}\boldsymbol{\mathcal{E}}^k_{aG} + \widetilde{\boldsymbol{C}}^k_{bb}\boldsymbol{\mathcal{S}}^k_{bG}, \tag{4.18}$$

with:

$$\widetilde{\boldsymbol{C}}^k_{aa} = \boldsymbol{C}^k_{aa} - \boldsymbol{C}^k_{ab}(\boldsymbol{C}^k_{bb})^{-1}\boldsymbol{C}^k_{ba}; \quad \widetilde{\boldsymbol{C}}^k_{ab} = \boldsymbol{C}^k_{ab}(\boldsymbol{C}^k_{bb})^{-1};$$

$$\widetilde{\boldsymbol{C}}^k_{ba} = -(\boldsymbol{C}^k_{bb})^{-1}\boldsymbol{C}^k_{ba}; \quad \widetilde{\boldsymbol{C}}^k_{bb} = (\boldsymbol{C}^k_{bb})^{-1}.$$

Thus Matrix $\widetilde{\boldsymbol{C}}^k$ of Eq. (4.15) can be written as follows:

$$\widetilde{\boldsymbol{C}}^k = \begin{Bmatrix} \widetilde{\boldsymbol{C}}^k_{aa} & \widetilde{\boldsymbol{C}}^k_{ab} \\ \widetilde{\boldsymbol{C}}^k_{ba} & \widetilde{\boldsymbol{C}}^k_{bb} \end{Bmatrix}. \tag{4.19}$$

Matrix $\widetilde{\boldsymbol{C}}^k$ represents the constitutive relations suitable for the RMVT-σ_n-D_z in the form of Eq. (4.10). In Section 4.4.3 the explicit form of $\widetilde{\boldsymbol{C}}^k$ is given.
The advantage of using the condensed notation is that the above showed procedure to calculate constitutive relations is applicable also when different or more extensive variables are modeled through the thickness plate z-direction. It represents a general and automatic way to calculate the constitutive coefficients for many different cases of variational statements, as explained in [11].

4.3 Through-the-thickness assumptions of primary variables in the condensed notation

As described in Chapter 2, in the framework of the Unified Formulation the primary unknowns are assumed by using a generalized expansion. Applying the condensed notation, they can be written as follows

$$\boldsymbol{V}^{\,k}(x,y,z) = F_b(z)\boldsymbol{V}^{\,k}_{\,b}(x,y) + F_r(z)\boldsymbol{V}^{\,k}_{\,r}(x,y) + F_t(z)\boldsymbol{V}^{\,k}_{\,t}(x,y) = F_\tau\,\boldsymbol{V}^{\,k}_{\,\tau}, \quad \text{with} \quad \tau = t,b,r \quad \text{and} \quad r = 2,3,\ldots,N \tag{4.20}$$

The variables $\boldsymbol{V}_{\,t}$ and $\boldsymbol{V}_{\,b}$ are the actual primary unknowns at the top and the bottom surfaces of the layer k, the inter-laminar continuity can be easily imposed:

$$\boldsymbol{V}^{\,k}_{\,t} = \boldsymbol{V}^{\,(k+1)}_{\,b}, \quad \text{with} \quad k = 1,\ldots,N_l - 1. \tag{4.21}$$

4.4 Fundamental Nuclei and FE matrices of RMVT-σ_n-D_z

In this section, the RMVT-σ_n-D_z variational statement is derived. The application of the corresponding PVD-statement can be found in work [11].

4.4.1 Finite element discretization

In case of FEM implementation, unknowns can be expressed in terms of their nodal values using shape functions N_i:

$$\boldsymbol{V}^k_\tau(x,y) = N_i(x,y)\boldsymbol{R}^k_{\tau i} \quad i = 1,2,...,N_n, \tag{4.22}$$

while for the virtual variations:

$$\delta\boldsymbol{V}^k_s(x,y) = N_j(x,y)\delta\boldsymbol{R}^k_{sj} \quad j = 1,2,...,N_n, \tag{4.23}$$

where N_n denotes the number of nodes concerning the considered finite element. $\boldsymbol{R}^k_{\tau i}$ is the vector containing nodal values of unknowns:

$$\boldsymbol{R}^{kT}_{\tau i} = \left\{ \begin{array}{ccccccccc} R^k_{u_1\tau i} & R^k_{u_2\tau i} & R^k_{u_3\tau i} & R^k_{\phi\tau i} & R^k_{\sigma_{33}\tau i} & R^k_{\sigma_{13}\tau i} & R^k_{\sigma_{23}\tau i} & R^k_{D_3\tau i} \end{array} \right\}. \tag{4.24}$$

The final expression of the unknowns is:

$$\boldsymbol{V}^k(x,y,z) = F_\tau N_i \boldsymbol{R}^k_{\tau i}. \tag{4.25}$$

4.4.2 Derivation of Fundamental Nuclei and FE matrices

The proceeding is the same as for the mechanical case described in Sec. 2.3 and 2.4: Upon substitution of the geometrical relations (see Eqs. (4.12), (4.13), (4.14)), the constitutive relations (see Eq. (4.18)) and the FE discrtetization (Eqs. (4.22) and (4.23)), the variational statement in Eq. (4.10) leads to a set of equilibrium equations which can be formally put in the following compact form:

$$\delta\boldsymbol{R}^k_{sj}: \quad \boldsymbol{K}^{k\tau sij}\,\boldsymbol{R}^k_{\tau i} \;=\; \boldsymbol{P}^k_{sj}, \tag{4.26}$$

where $\boldsymbol{P}^k$ is the vector of nodal loads. The number of obtained equations coincides with the number of introduced variables: τ and s vary from 0 to N, i and j vary from 1 to N_n and k ranges from 1 to N_l.
Matrix $\boldsymbol{K}^{k\tau sij}$ is the fundamental nucleus. In this case it is a 8×8 array and, more in general, it provides the information to build the stiffness matrix (see the Appendix 4.4.3 for the explicit form of $\boldsymbol{K}^{k\tau sij}$).
Whatever is the considered variational statement, starting from the fundamental nucleus, for a given discretization, the stiffness matrix $\boldsymbol{K}$ can be calculated by numerical integration and the assembly procedure. It should be emphasized that the stiffness matrix $\boldsymbol{K}$ contains information pertaining to all the considered fields and not just to the mechanical field. If a static analysis is required, the system to solve is the following:

$$\boldsymbol{K}\boldsymbol{R} = \boldsymbol{P}. \tag{4.27}$$

where:
$\boldsymbol{P}$ is the vector of nodal loads;
$\boldsymbol{R}$ is the vector of nodal unknowns.

4.4.3 Explicit forms of RMVT-σ_n-D_z Fundamental Nuclei

The stiffness fundamental nucleus $\boldsymbol{K}^{k\tau sij}$ related to the RMVT-σ_n-D_z application is listed below. Constitutive information are included too. In the following, the layer-superscript k is always implied to simplify equations.
The stiffness fundamental nucleus is:

$$\boldsymbol{K}^{\tau sij} = \begin{bmatrix} K_{11} & K_{12} & K_{13} & K_{14} & K_{15} & K_{16} & K_{17} & K_{18} \\ K_{21} & K_{22} & K_{23} & K_{24} & K_{25} & K_{26} & K_{27} & K_{28} \\ K_{31} & K_{32} & K_{33} & K_{34} & K_{35} & K_{36} & K_{37} & K_{38} \\ K_{41} & K_{42} & K_{43} & K_{44} & K_{45} & K_{46} & K_{47} & K_{48} \\ K_{51} & K_{52} & K_{53} & K_{54} & K_{55} & K_{56} & K_{57} & K_{58} \\ K_{61} & K_{62} & K_{63} & K_{64} & K_{65} & K_{66} & K_{67} & K_{68} \\ K_{71} & K_{72} & K_{73} & K_{74} & K_{75} & K_{76} & K_{77} & K_{78} \\ K_{81} & K_{82} & K_{83} & K_{84} & K_{85} & K_{86} & K_{87} & K_{88} \end{bmatrix}. \tag{A.28}$$

Its elements are:

$$K_{11} = F_s F_\tau \widetilde{\boldsymbol{C}}_{\text{aa11}} \triangleleft N_{i,x} N_{j,x} \triangleright_{\Omega_k} + F_s F_\tau \widetilde{\boldsymbol{C}}_{\text{aa31}} \triangleleft N_{i,y} N_{j,x} \triangleright_{\Omega_k} + F_s F_\tau \widetilde{\boldsymbol{C}}_{\text{aa13}} \triangleleft N_{i,x} N_{j,y} \triangleright_{\Omega_k} + \\ + F_s F_\tau \widetilde{\boldsymbol{C}}_{\text{aa33}} \triangleleft N_{i,y} N_{j,y} \triangleright_{\Omega_k}$$

$$K_{21} = F_s F_\tau \widetilde{\boldsymbol{C}}_{\text{aa31}} \triangleleft N_{i,x} N_{j,x} \triangleright_{\Omega_k} + F_s F_\tau \widetilde{\boldsymbol{C}}_{\text{aa21}} \triangleleft N_{i,y} N_{j,x} \triangleright_{\Omega_k} + F_s F_\tau \widetilde{\boldsymbol{C}}_{\text{aa33}} \triangleleft N_{i,x} N_{j,y} \triangleright_{\Omega_k} + \\ + F_s F_\tau \widetilde{\boldsymbol{C}}_{\text{aa23}} \triangleleft N_{i,y} N_{j,y} \triangleright_{\Omega_k}$$

$$K_{31} = 0$$

$$K_{41} = 0$$

$$K_{51} = -F_s F_\tau \triangleleft N_i N_{j,x} \triangleright_{\Omega_k} \widetilde{\boldsymbol{C}}_{\text{ba11}} - F_s F_\tau \triangleleft N_i N_{j,y} \triangleright_{\Omega_k} \widetilde{\boldsymbol{C}}_{\text{ba13}}$$

$$K_{61} = F_\tau F_{s,z} \triangleleft N_i N_j \triangleright_{\Omega_k}$$

$$K_{71} = 0$$

$$K_{81} = F_s F_\tau \triangleleft N_i N_{j,x} \triangleright_{\Omega_k} \widetilde{\boldsymbol{C}}_{\text{ba41}} + F_s F_\tau \triangleleft N_i N_{j,y} \triangleright_{\Omega_k} \widetilde{\boldsymbol{C}}_{\text{ba43}}$$

$$K_{12} = F_s F_\tau \widetilde{\boldsymbol{C}}_{\text{aa13}} \triangleleft N_{i,x} N_{j,x} \triangleright_{\Omega_k} + F_s F_\tau \widetilde{\boldsymbol{C}}_{\text{aa33}} \triangleleft N_{i,y} N_{j,x} \triangleright_{\Omega_k} + F_s F_\tau \widetilde{\boldsymbol{C}}_{\text{aa12}} \triangleleft N_{i,x} N_{j,y} \triangleright_{\Omega_k} + \\ + F_s F_\tau \widetilde{\boldsymbol{C}}_{\text{aa32}} \triangleleft N_{i,y} N_{j,y} \triangleright_{\Omega_k}$$

$$K_{22} = F_s F_\tau \widetilde{\boldsymbol{C}}_{\text{aa33}} \triangleleft N_{i,x} N_{j,x} \triangleright_{\Omega_k} + F_s F_\tau \widetilde{\boldsymbol{C}}_{\text{aa23}} \triangleleft N_{i,y} N_{j,x} \triangleright_{\Omega_k} + F_s F_\tau \widetilde{\boldsymbol{C}}_{\text{aa32}} \triangleleft N_{i,x} N_{j,y} \triangleright_{\Omega_k} + \\ + F_s F_\tau \widetilde{\boldsymbol{C}}_{\text{aa22}} \triangleleft N_{i,y} N_{j,y} \triangleright_{\Omega_k}$$

$$K_{32} = 0$$

$$K_{42} = 0$$

$$K_{52} = -F_s F_\tau \triangleleft N_i N_{j,x} \triangleright_{\Omega_k} \widetilde{\boldsymbol{C}}_{\text{ba13}} - F_s F_\tau \triangleleft N_i N_{j,y} \triangleright_{\Omega_k} \widetilde{\boldsymbol{C}}_{\text{ba12}}$$

$$K_{62} = 0$$

$$K_{72} = F_\tau F_{s,z} \triangleleft N_i N_j \triangleright_{\Omega_k}$$

$$K_{82} = F_s F_\tau \triangleleft N_i N_{j,x} \triangleright_{\Omega_k} \widetilde{\boldsymbol{C}}_{\text{ba43}} + F_s F_\tau \triangleleft N_i N_{j,y} \triangleright_{\Omega_k} \widetilde{\boldsymbol{C}}_{\text{ba42}}$$

$$K_{13} = 0$$

$$K_{23} = 0$$

$$K_{33} = 0$$

$$K_{43} = 0$$

$$K_{53} = F_{s,z}F_\tau \triangleleft N_i N_j \triangleright_{\Omega_k}$$

$$K_{63} = F_s F_\tau \triangleleft N_i N_{j,x} \triangleright_{\Omega_k}$$

$$K_{73} = F_s F_\tau \triangleleft N_i N_{j,y} \triangleright_{\Omega_k}$$

$$K_{83} = 0$$

$$K_{14} = 0$$

$$K_{24} = 0$$

$$K_{34} = 0$$

$$K_{44} = F_s F_\tau \widetilde{\boldsymbol{C}}_{\mathrm{aa44}} \triangleleft N_{i,x} N_{j,x} \triangleright_{\Omega_k} + F_s F_\tau \widetilde{\boldsymbol{C}}_{\mathrm{aa54}} \triangleleft N_{i,y} N_{j,x} \triangleright_{\Omega_k} + F_s F_\tau \widetilde{\boldsymbol{C}}_{\mathrm{aa45}} \triangleleft N_{i,x} N_{j,y} \triangleright_{\Omega_k} + + F_s F_\tau \widetilde{\boldsymbol{C}}_{\mathrm{aa55}} \triangleleft N_{i,y} N_{j,y} \triangleright_{\Omega_k}$$

$$K_{54} = 0$$

$$K_{64} = F_s F_\tau \triangleleft N_i N_{j,x} \triangleright_{\Omega_k} \widetilde{\boldsymbol{C}}_{\mathrm{ba24}} + F_s F_\tau \triangleleft N_i N_{j,y} \triangleright_{\Omega_k} \widetilde{\boldsymbol{C}}_{\mathrm{ba25}}$$

$$K_{74} = F_s F_\tau \triangleleft N_i N_{j,x} \triangleright_{\Omega_k} \widetilde{\boldsymbol{C}}_{\mathrm{ba34}} + F_s F_\tau \triangleleft N_i N_{j,y} \triangleright_{\Omega_k} \widetilde{\boldsymbol{C}}_{\mathrm{ba35}}$$

$$K_{84} = F_{s,z}F_\tau \triangleleft N_i N_j \triangleright_{\Omega_k}$$

$$K_{15} = F_s F_\tau \triangleleft N_j N_{i,x} \triangleright_{\Omega_k} \widetilde{\boldsymbol{C}}_{\mathrm{ab11}} + F_s F_\tau \triangleleft N_j N_{i,y} \triangleright_{\Omega_k} \widetilde{\boldsymbol{C}}_{\mathrm{ab31}}$$

$$K_{25} = F_s F_\tau \triangleleft N_j N_{i,x} \triangleright_{\Omega_k} \widetilde{\boldsymbol{C}}_{\mathrm{ab31}} + F_s F_\tau \triangleleft N_j N_{i,y} \triangleright_{\Omega_k} \widetilde{\boldsymbol{C}}_{\mathrm{ab21}}$$

$$K_{35} = F_s F_{\tau,z} \triangleleft N_i N_j \triangleright_{\Omega_k}$$

$$K_{45} = 0$$

$$K_{55} = -F_s F_\tau \triangleleft N_i N_j \triangleright_{\Omega_k} \widetilde{\boldsymbol{C}}_{\mathrm{bb11}}$$

$$K_{65} = 0$$

$$K_{75} = 0$$

$$K_{85} = F_s F_\tau \triangleleft N_i N_j \triangleright_{\Omega_k} \widetilde{\boldsymbol{C}}_{\mathrm{bb41}}$$

$$K_{16} = F_s F_{\tau,z} \triangleleft N_i N_j \triangleright_{\Omega_k}$$

$$K_{26} = 0$$

$$K_{36} = F_s F_\tau \triangleleft N_j N_{i,x} \triangleright_{\Omega_k}$$

$$K_{46} = -F_s F_\tau \triangleleft N_j N_{i,x} \triangleright_{\Omega_k} \widetilde{\boldsymbol{C}}_{\mathrm{ab42}} - F_s F_\tau \triangleleft N_j N_{i,y} \triangleright_{\Omega_k} \widetilde{\boldsymbol{C}}_{\mathrm{ab52}}$$

$$K_{56} = 0$$

$$K_{66} = -F_s F_\tau \triangleleft N_i N_j \triangleright_{\Omega_k} \widetilde{\boldsymbol{C}}_{\mathrm{bb22}}$$

$$K_{76} = -F_s F_\tau \lhd N_i N_j \rhd_{\Omega_k} \widetilde{\boldsymbol{C}}_{\mathrm{bb32}}$$

$$K_{86} = 0$$

$$K_{17} = 0$$

$$K_{27} = F_s F_{\tau,z} \lhd N_i N_j \rhd_{\Omega_k}$$

$$K_{37} = F_s F_\tau \lhd N_j N_{i,y} \rhd_{\Omega_k}$$

$$K_{47} = -F_s F_\tau \lhd N_j N_{i,x} \rhd_{\Omega_k} \widetilde{\boldsymbol{C}}_{\mathrm{ab43}} - F_s F_\tau \lhd N_j N_{i,y} \rhd_{\Omega_k} \widetilde{\boldsymbol{C}}_{\mathrm{ab53}}$$

$$K_{57} = 0$$

$$K_{67} = -F_s F_\tau \lhd N_i N_j \rhd_{\Omega_k} \widetilde{\boldsymbol{C}}_{\mathrm{bb23}}$$

$$K_{77} = -F_s F_\tau \lhd N_i N_j \rhd_{\Omega_k} \widetilde{\boldsymbol{C}}_{\mathrm{bb33}}$$

$$K_{87} = 0$$

$$K_{18} = -F_s F_\tau \lhd N_j N_{i,x} \rhd_{\Omega_k} \widetilde{\boldsymbol{C}}_{\mathrm{ab14}} - F_s F_\tau \lhd N_j N_{i,y} \rhd_{\Omega_k} \widetilde{\boldsymbol{C}}_{\mathrm{ab34}}$$

$$K_{28} = -F_s F_\tau \lhd N_j N_{i,x} \rhd_{\Omega_k} \widetilde{\boldsymbol{C}}_{\mathrm{ab34}} - F_s F_\tau \lhd N_j N_{i,y} \rhd_{\Omega_k} \widetilde{\boldsymbol{C}}_{\mathrm{ab24}}$$

$$K_{38} = 0$$

$$K_{48} = F_s F_{\tau,z} \lhd N_i N_j \rhd_{\Omega_k}$$

$$K_{58} = F_s F_\tau \lhd N_i N_j \rhd_{\Omega_k} \widetilde{\boldsymbol{C}}_{\mathrm{bb14}}$$

$$K_{68} = 0$$

$$K_{78} = 0$$

$$K_{88} = -F_s F_\tau \lhd N_i N_j \rhd_{\Omega_k} \widetilde{\boldsymbol{C}}_{\mathrm{bb44}}$$

Subscripts after comma indicates derivatives and:

$$\lhd(.....)\rhd_{\Omega_k} = \int_{\Omega_k} (.....) d\Omega.$$

The explicit form of matrices $\widetilde{\boldsymbol{C}}_{aa}$, $\widetilde{\boldsymbol{C}}_{ba}$, $\widetilde{\boldsymbol{C}}_{ab}$ and $\widetilde{\boldsymbol{C}}_{bb}$ is:

$$\widetilde{\boldsymbol{C}}_{aa}(1,1) = C_{11} + \frac{C_{33}e_{31}^2 - C_{13}\left(2e_{31}e_{33} + C_{13}\varepsilon_{33}\right)}{e_{33}^2 + C_{33}\varepsilon_{33}}$$

$$\widetilde{\boldsymbol{C}}_{aa}(1,2) = \frac{e_{33}\left(-C_{13}e_{32} + C_{12}e_{33}\right) + C_{33}\left(e_{31}e_{32} + C_{12}\varepsilon_{33}\right) - C_{23}\left(e_{31}e_{33} + C_{13}\varepsilon_{33}\right)}{e_{33}^2 + C_{33}\varepsilon_{33}}$$

$$\widetilde{\boldsymbol{C}}_{aa}(1,3) = C_{16} + \frac{\left(C_{33}e_{31} - C_{13}e_{33}\right)e_{36} - C_{36}\left(e_{31}e_{33} + C_{13}\varepsilon_{33}\right)}{e_{33}^2 + C_{33}\varepsilon_{33}}$$

$$\widetilde{\boldsymbol{C}}_{aa}(1,4) = 0$$

$$\widetilde{\boldsymbol{C}}_{aa}(1,5) = 0$$

$$\widetilde{\boldsymbol{C}}_{aa}(2,1) = \frac{e_{33}\left(-C_{13}e_{32} + C_{12}e_{33}\right) + C_{33}\left(e_{31}e_{32} + C_{12}\varepsilon_{33}\right) - C_{23}\left(e_{31}e_{33} + C_{13}\varepsilon_{33}\right)}{e_{33}^2 + C_{33}\varepsilon_{33}}$$

$$\widetilde{\boldsymbol{C}}_{aa}(2,2) = C_{22} + \frac{C_{33}e_{32}^2 - C_{23}\left(2e_{32}e_{33} + C_{23}\varepsilon_{33}\right)}{e_{33}^2 + C_{33}\varepsilon_{33}}$$

$$\widetilde{\boldsymbol{C}}_{aa}(2,3) = C_{26} + \frac{\left(C_{33}e_{32} - C_{23}e_{33}\right)e_{36} - C_{36}\left(e_{32}e_{33} + C_{23}\varepsilon_{33}\right)}{e_{33}^2 + C_{33}\varepsilon_{33}}$$

$$\widetilde{\boldsymbol{C}}_{aa}(2,4) = 0$$

$$\widetilde{\boldsymbol{C}}_{aa}(2,5) = 0$$

$$\widetilde{\boldsymbol{C}}_{aa}(3,1) = C_{16} + \frac{\left(C_{33}e_{31} - C_{13}e_{33}\right)e_{36} - C_{36}\left(e_{31}e_{33} + C_{13}\varepsilon_{33}\right)}{e_{33}^2 + C_{33}\varepsilon_{33}}$$

$$\widetilde{\boldsymbol{C}}_{aa}(3,2) = C_{26} + \frac{\left(C_{33}e_{32} - C_{23}e_{33}\right)e_{36} - C_{36}\left(e_{32}e_{33} + C_{23}\varepsilon_{33}\right)}{e_{33}^2 + C_{33}\varepsilon_{33}}$$

$$\widetilde{\boldsymbol{C}}_{aa}(3,3) = C_{66} + \frac{-2C_{36}e_{33}e_{36} + C_{33}e_{36}^2 - C_{36}^2\varepsilon_{33}}{e_{33}^2 + C_{33}\varepsilon_{33}}$$

$$\widetilde{\boldsymbol{C}}_{aa}(3,4) = 0$$

$$\widetilde{\boldsymbol{C}}_{aa}(3,5) = 0$$

$$\widetilde{\boldsymbol{C}}_{aa}(4,1) = 0$$

$$\widetilde{\boldsymbol{C}}_{aa}(4,2) = 0$$

$$\widetilde{\boldsymbol{C}}_{aa}(4,3) = 0$$

$$\widetilde{\boldsymbol{C}}_{aa}(4,4) = \frac{C_{55}e_{14}^2 - 2C_{45}e_{14}e_{15} + C_{44}e_{15}^2}{C_{45}^2 - C_{44}C_{55}} - \varepsilon_{11}$$

$$\widetilde{\boldsymbol{C}}_{aa}(4,5) = \frac{C_{55}e_{14}e_{24} + C_{44}e_{15}e_{25} - C_{45}\left(e_{15}e_{24} + e_{14}e_{25}\right)}{C_{45}^2 - C_{44}C_{55}} - \varepsilon_{12}$$

$$\widetilde{\boldsymbol{C}}_{aa}(5,1) = 0$$

$$\widetilde{\boldsymbol{C}}_{aa}(5,2) = 0$$

$$\widetilde{\boldsymbol{C}}_{aa}(5,3) = 0$$

$$\widetilde{\boldsymbol{C}}_{aa}(5,4) = \frac{C_{55}e_{14}e_{24} + C_{44}e_{15}e_{25} - C_{45}\left(e_{15}e_{24} + e_{14}e_{25}\right)}{C_{45}^2 - C_{44}C_{55}} - \varepsilon_{12}$$

$$\widetilde{\boldsymbol{C}}_{aa}(5,5) = \frac{C_{55}e_{24}^2 - 2C_{45}e_{24}e_{25} + C_{44}e_{25}^2}{C_{45}^2 - C_{44}C_{55}} - \varepsilon_{22}$$

$$\widetilde{\boldsymbol{C}}_{ab} = \begin{bmatrix} \frac{e_{31}e_{33}+C_{13}\varepsilon_{33}}{e_{33}^2+C_{33}\varepsilon_{33}} & 0 & 0 & \frac{C_{33}e_{31}-C_{13}e_{33}}{e_{33}^2+C_{33}\varepsilon_{33}} \\ \frac{e_{32}e_{33}+C_{23}\varepsilon_{33}}{e_{33}^2+C_{33}\varepsilon_{33}} & 0 & 0 & \frac{C_{33}e_{32}-C_{23}e_{33}}{e_{33}^2+C_{33}\varepsilon_{33}} \\ \frac{e_{33}e_{36}+C_{36}\varepsilon_{33}}{e_{33}^2+C_{33}\varepsilon_{33}} & 0 & 0 & \frac{-C_{36}e_{33}+C_{33}e_{36}}{e_{33}^2+C_{33}\varepsilon_{33}} \\ 0 & \frac{-C_{45}e_{14}+C_{44}e_{15}}{C_{45}^2-C_{44}C_{55}} & \frac{C_{55}e_{14}-C_{45}e_{15}}{C_{45}^2-C_{44}C_{55}} & 0 \\ 0 & \frac{-C_{45}e_{24}+C_{44}e_{25}}{C_{45}^2-C_{44}C_{55}} & \frac{C_{55}e_{24}-C_{45}e_{25}}{C_{45}^2-C_{44}C_{55}} & 0 \end{bmatrix};$$

$$\widetilde{\boldsymbol{C}}_{ba} = \begin{bmatrix} -\frac{e_{31}e_{33}+C_{13}\varepsilon_{33}}{e_{33}^2+C_{33}\varepsilon_{33}} & -\frac{e_{32}e_{33}+C_{23}\varepsilon_{33}}{e_{33}^2+C_{33}\varepsilon_{33}} & -\frac{e_{33}e_{36}+C_{36}\varepsilon_{33}}{e_{33}^2+C_{33}\varepsilon_{33}} & 0 & 0 \\ 0 & 0 & 0 & \frac{C_{45}e_{14}-C_{44}e_{15}}{C_{45}^2-C_{44}C_{55}} & \frac{C_{45}e_{24}-C_{44}e_{25}}{C_{45}^2-C_{44}C_{55}} \\ 0 & 0 & 0 & \frac{-C_{55}e_{14}+C_{45}e_{15}}{C_{45}^2-C_{44}C_{55}} & \frac{-C_{55}e_{24}+C_{45}e_{25}}{C_{45}^2-C_{44}C_{55}} \\ \frac{-C_{33}e_{31}+C_{13}e_{33}}{e_{33}^2+C_{33}\varepsilon_{33}} & \frac{-C_{33}e_{32}+C_{23}e_{33}}{e_{33}^2+C_{33}\varepsilon_{33}} & \frac{C_{36}e_{33}-C_{33}e_{36}}{e_{33}^2+C_{33}\varepsilon_{33}} & 0 & 0 \end{bmatrix}.$$

$$\widetilde{\boldsymbol{C}}_{bb} = \begin{bmatrix} \frac{1}{C_{33}+e_{33}^2/\varepsilon_{33}} & 0 & 0 & -\frac{e_{33}}{e_{33}^2+C_{33}\varepsilon_{33}} \\ 0 & \frac{1}{-C_{45}^2/C_{44}+C_{55}} & \frac{C_{45}}{C_{45}^2-C_{44}C_{55}} & 0 \\ 0 & \frac{C_{45}}{C_{45}^2-C_{44}C_{55}} & \frac{1}{C_{44}-C_{45}^2/C_{55}} & 0 \\ -\frac{e_{33}}{e_{33}^2+C_{33}\varepsilon_{33}} & 0 & 0 & -\frac{1}{e_{33}^2/C_{33}+\varepsilon_{33}} \end{bmatrix}.$$

Chapter 5

Results on Electro-Mechanical RMVT

A simply supported cross-ply [0/90] laminate composed of an elastic material with piezoelectric layers bonded to the upper and lower surfaces is considered for the following electromechanical case study. The elastic layer of the [0] fiber-angle is on the top. Following data have been used for the plate:

simply supported square plate, side length a, thickness ratio $a/h = 4$, $h = 1\,\mathrm{m}$
The elastic layers have a thickness of $0.4\,h$, while the thickness of the piezoelectric layers is $0.1\,h$.

The elastic material is modeled as a fiber-reinforced composite with following properties:
$E_{11} = 132.38$ (all in [GPa]), $E_{22} = 10.756$, $E_{33} = 10.756$, $G_{44} = 3.606$, $G_{55} = 5.654$, $G_{66} = 5.654$, $\nu_{12} = 0.24$, $\nu_{13} = 0.24$, $\nu_{23} = 0.49$, $\varepsilon_{11}/\varepsilon_0 = 3.5$, and $\varepsilon_{22}/\varepsilon_0 = \varepsilon_{33}/\varepsilon_0 = 3.0$

The material of the piezoelectric layers is PZT-4, the material properties are:
$E_{11} = E_{22} = 81.3$ (all in [GPa]), $E_{33} = 64.5$, $G_{44} = G_{55} = 25.6$, $G_{66} = 30.6$, $\nu_{12} = 0.329$, $\nu_{13} = \nu_{23} = 0.432$, $e_{31} = e_{32} = -5.20$ (all in $[C/m^2]$), $e_{33} = 15.08$, $e_{24} = e_{15} = 12.72$, and $\varepsilon_{11}/\varepsilon_0 = \varepsilon_{11}/\varepsilon_0 = 1475$, $\varepsilon_{33}/\varepsilon_0 = 1300$ ($\varepsilon_0 = 8.8541878 \times 10^{-12}\,\frac{\mathrm{A\,s}}{\mathrm{V\,m}}$)

Both the sensor case and actuator case are considered in the following (see the two configuration in Fig. 5.1, where p_z indicates a pressure $[N/m^2]$ and ϕ_t indicates the potential $[V]$ imposed on the top face and $\widehat{p}_z = \widehat{\phi}_t = 1$). The analysis will be restricted to LW cases. These are capable to furnish reliable results at each layer interface. A second order thickness expansion is considered to properly calculate the through-the-thickness electric displacement, which clearly shows a parabolic-like trend through the external layers (see Fig. 5.3).

5.1 Sensor Configuration

The applied bi-sinusoidal pressure loading p_z is considered on the top plate surface (sensor configuration). The load amplitude is equal to 1 [N/m^2]. The top and bottom laminate surfaces are fixed at zero potential. The FEM results are obtained with a regular 10×10 mesh of LD2 (or LM2) Q4 FEs to minimize computational costs keeping a good accuracy. A comparison between the 3D-exact solution, PVD, and

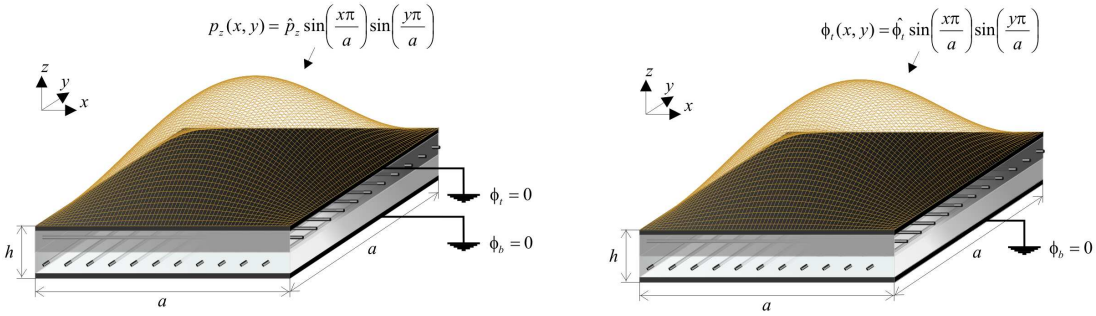

Figure 5.1: *On the left the plate is in sensor configuration (applied pressure); on the right the plate is in actuator configuration (applied potential); Courtesy by [?]*

RMVT-σ_n-D_z results is provided in Tab. 5.1 for displacement u_2 and for the electric potential ϕ: Results for both models, PVD and RMVT-σ_n-D_z are very close and they are in good agreement with the exact solution (see also Fig. 5.2). In other words, when D_z and σ_n are modeled by RMVT, the calculated primary variables of diplacement and potential do not change significantly with respect to PVD. However, if a slight difference is detected, the RMVT results are closer to the exact solution.
A comparison between the 3D-exact solution, PVD and RMVT results is provided in Tab. 5.2 for the transverse stress σ_{33} and for the in-plane stresses σ_{22} and σ_{12}: For the in-plane stresses both results are close to the exact solutions. It has been confirmed that, even for in-plane stresses, the difference between PVD, and RMVT-σ_n-D_z is negligible. On the other hand, for transverse stress σ_{33} only the RMVT-σ_n-D_z model provides continuity at the layer-interfaces. Also in the bottom layer, RMVT-σ_n-D_z results are significant closer to the 3D solution than the corresponding PVD and results. The advantage of RMVT-σ_n-D_z for modelling transverse stresses is confirmed for the actuator case in the follwing Section.
Another advantage of the presented RMVT model is evident in Tab. 5.3, where the evaluation of transverse electric displacement is referred to. The results are compared to 3D-exact and to PVD solutions. It should be underlined that the RMVT-σ_n-D_z leads to an almost 3D-exact description, while PVD results can be affected by very large errors (see also Fig. 5.3). In the RMVT-σ_n-D_z* column, the D_z is calculated by using the physical constitutive relations in the RMVT-σ_n-D_z analysis. It can be noted that the RMVT-σ_n-D_z* results are very close to the PVD ones.

	$u_2 \times 10^{12}$	$u_2 \times 10^{12}$	$u_2 \times 10^{12}$	$\phi \times 10^1$	$\phi \times 10^1$	$\phi \times 10^1$
Height	$3D$[13]	$RMVT$-σ_n-D_z	PVD	$3D$[13]	$RMVT$-σ_n-D_z	PVD
1.000	-47.549	-45.893	-45.593	0.0000	0.0000	0.0000
0.975	-41.425	-39.850	-39.527	0.0189	0.0183	0.0181
0.950	-35.424	-33.891	-33.567	0.0358	0.0340	0.0336
0.925	-29.531	-28.016	-27.715	0.0488	0.0470	0.0464
0.900	-23.732	-22.225	-21.969	0.0598	0.0575	0.0567
0.800	-10.480	-10.375	-10.058	0.0589	0.0567	0.0560
0.700	0.1413	0.1555	-0.0836	0.0589	0.0567	0.0560
0.600	9.8917	9.3673	9.5104	0.0596	0.0575	0.0567
0.500	20.392	17.260	18.205	0.0611	0.0590	0.0583
0.400	24.768	22.282	22.149	0.0634	0.0613	0.0606
0.300	29.110	27.448	26.700	0.0665	0.0645	0.0637
0.200	33.819	32.756	31.860	0.0706	0.0685	0.0677
0.100	39.309	38.208	37.628	0.0756	0.0734	0.0726
0.075	44.492	43.548	42.930	0.0602	0.0587	0.0581
0.050	49.772	48.979	48.341	0.0425	0.0415	0.0411
0.025	55.163	54.503	53.863	0.0224	0.0220	0.0218
0.000	60.678	60.118	59.494	0.0000	0.0000	0.0000

Table 5.1: *PVD and RMVT-σ_n-D_z results: comparison between LD2 and LM2 FEM solutions with the Heyliger 3D-exact solution, sensor case. Displacements are in $[m]$; electric potential is in $[V]$. $u_2 = u_2(a/2, 0)$; $\phi = \phi(a/2, b/2)$.*

	$\sigma_{33} \times 10^1$	$\sigma_{33} \times 10^1$	$\sigma_{33} \times 10^1$	σ_{22}	σ_{22}	σ_{22}
Height	$3D$[13]	$RMVT$-σ_n-D_z	PVD	$3D$[13]	$RMVT$-σ_n-D_z	PVD
1.000	10.000	10.409	9.6313	6.5643	6.2798	6.2392
0.975	9.9657	10.282	9.4336	5.8201	5.5511	5.5033
0.950	9.8682	10.164	9.3631	5.0855	4.8373	4.7857
0.925	9.7154	10.053	9.4197	4.3595	4.1385	4.0865
0.900	9.5151	9.9506	9.6034	3.6408	3.4547	3.4057
0.900	9.5151	9.9506	10.163	2.8855	3.8732	3.8364
0.800	8.5199	8.7869	8.7018	1.4499	1.9801	2.0094
0.700	7.3747	7.6086	7.4395	0.2879	0.3008	0.3332
0.600	6.1686	6.4158	6.3764	-0.7817	-1.1648	-1.1923
0.500	4.9831	5.2084	5.5124	-1.9266	-2.4166	-2.5670
0.500	4.9831	5.2084	4.9178	0.0991	0.0522	0.0527
0.400	3.8045	3.8671	3.9244	-0.0149	-0.0773	-0.0683
0.300	2.6137	2.6395	2.8259	-0.1280	-0.2168	-0.2049
0.200	1.4821	1.5255	1.6223	-0.2426	-0.3664	-0.3571
0.100	0.4868	0.5251	0.3136	-0.3616	-0.5260	-0.5248
0.100	0.4868	0.5251	0.8251	-4.2348	-4.0013	-3.9325
0.075	0.2845	0.2641	0.9872	-4.8806	-4.6334	-4.5636
0.050	0.1312	0.1006	1.0311	-5.5337	-5.2799	-5.2123
0.025	0.0340	0.0344	0.9568	-6.1951	-5.9409	-5.8785
0.000	0.0000	0.0657	0.7641	-6.8658	-6.6163	-6.5623

Table 5.2: *PVD and RMVT-σ_n-D_z results: comparison between LD2 and LM2 FEM solutions with the Heyliger 3D-exact solution, sensor case. Stresses are in $[Pa]$. $\sigma_{33} = \sigma_{33}(a/2, b/2)$; $\sigma_{22} = \sigma_{22}(a/2, b/2)$.*

	$D_z \times 10^{13}$			
Height	3D[13]	$RMVT\text{-}\sigma_n\text{-}D_z$	PVD	$RMVT\text{-}\sigma_n\text{-}D_z^*$
1.000	160.58	147.89	239.57	234.38
0.975	149.35	144.14	204.92	203.62
0.950	117.23	118.20	161.38	163.98
0.925	66.568	70.044	108.95	115.44
0.900	-0.3382	-0.311	47.621	58.008
0.900	-0.3382	-0.311	-0.2990	-0.3101
0.800	-0.1276	-0.105	-0.0977	-0.1027
0.700	0.0813	0.099	0.1037	0.1048
0.600	0.2913	0.303	0.3051	0.3123
0.500	0.5052	0.505	0.5065	0.5198
0.500	0.5052	0.505	0.4943	0.4815
0.400	0.7259	0.725	0.7236	0.7165
0.300	0.9563	0.953	0.9529	0.9515
0.200	1.1995	1.189	1.1821	1.1865
0.100	1.4587	1.433	1.4114	1.4215
0.100	1.4587	1.433	-50.162	-58.915
0.075	-58.352	-61.217	-105.53	-111.00
0.050	-103.66	-103.84	-152.63	-154.82
0.025	-132.40	-126.43	-191.45	-190.36
0.000	-142.46	-128.99	-222.00	-217.63

Table 5.3: *Comparison between FEM and Heyliger 3D-exact solutions, sensor case. LD2 and LM2 results. Electric displacement is in* $[c/m^2]$. $D_z = D_z(a/2, b/2)$. * *indicates that* D_z *is calculated by constitutive relations in the* $RMVT\text{-}\sigma_n\text{-}D_z$ *analysis.*

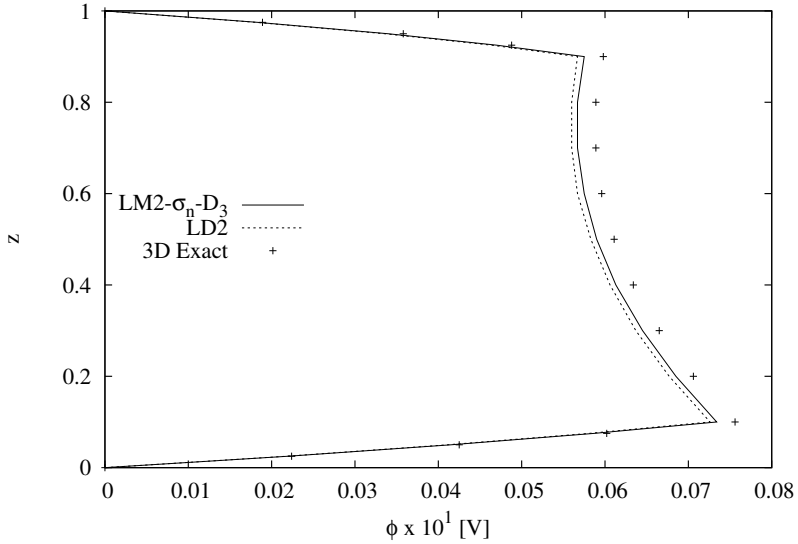

Figure 5.2: *Comparison of LD2, LM2 and 3D-exact solutions, sensor case; electric potential is in* $[V]$*;* $\phi = \phi(a/2, b/2)$

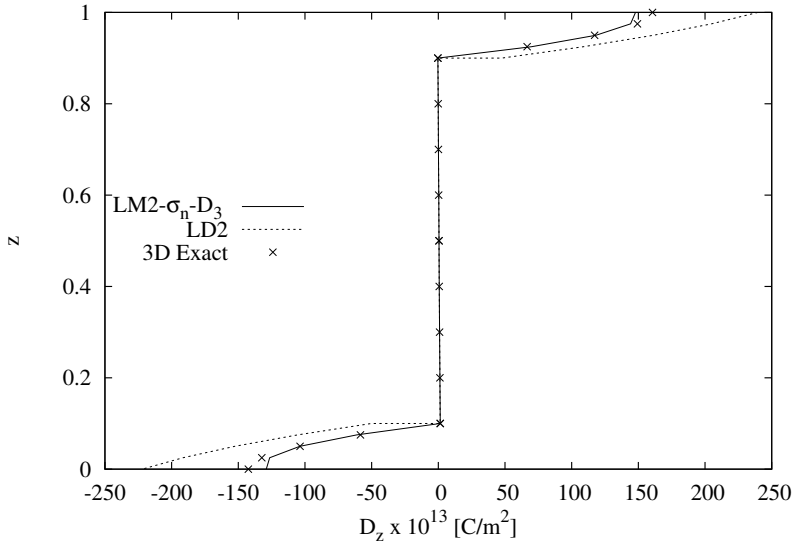

Figure 5.3: *Comparison of LD2, LM2 and 3D-exact solutions, sensor case; electric displacement is in* $[c/m^2]$*;* $D_3 = D_3(a/2, b/2)$

5.2 Actuator Configuration

The applied bi-sinusoidal potential p_z is considered in the top plate surface (actuator configuration). The load amplitude is equal to 1 [V]. The bottom laminate surfaces is fixed at zero potential. The FEM results are obtained with a regular 10×10 mesh of LD2 (or LM2) Q4 FEs. The following remarks can be made. Tab. 5.4 shows that the primary variables, u_2 and ϕ, calculated by FEM are in good agreement with the exact solution provided by Heyliger[13]. As far as Tab. 5.5 is concerned, the in-plane stresses are also calculated with good accuracy. Normal stress σ_{33} does not have reasonable values around the top and the bottom face of the plate especially for PVD analyses. By increasing the the expansion in thickness direction to third order, RMVT-D_z-σ_n leads to good results for σ_{33} even around the top and the bottom area of the plate. PVD results with third order expansion are still out of range, see Tab. 5.7 and Fig. 5.4.

	$u_2 \times 10^{12}$	$u_2 \times 10^{12}$	$u_2 \times 10^{12}$	ϕ	ϕ	ϕ
Height	$3D$	$RMVT\text{-}\sigma_n\text{-}D_z$	PVD	$3D$	$RMVT\text{-}\sigma_n\text{-}D_z$	PVD
1.000	-32.764	-33.442	-33.951	1.0000	1.0000	1.0000
0.975	-23.349	-24.014	-24.377	0.9971	0.9972	0.9972
0.950	-13.973	-14.619	-14.826	0.9950	0.9951	0.9951
0.925	-4.6174	-5.2570	-5.2983	0.9936	0.9936	0.9936
0.900	4.7356	4.0721	4.2064	0.9929	0.9929	0.9929
0.800	2.9808	2.4479	2.5445	0.8415	0.8422	0.8423
0.700	1.7346	1.2092	1.2546	0.7014	0.7011	0.7011
0.600	0.8008	0.3560	0.3368	0.5707	0.5695	0.5695
0.500	0.0295	-0.1117	-0.2091	0.4476	0.4475	0.4473
0.400	-0.4404	-0.5571	-0.5745	0.3305	0.3311	0.3310
0.300	-0.8815	-0.9741	-0.9518	0.2179	0.2177	0.2177
0.200	-1.3206	-1.3625	-1.3409	0.1081	0.1073	0.1073
0.100	-1.7839	-1.7223	-1.7419	-0.0001	-0.0001	-0.0001
0.075	-2.0470	-1.9735	-1.9963	-0.00009	-0.0001	-0.00009
0.050	-2.3140	-2.2278	-2.2554	-0.00008	-0.0001	-0.00007
0.025	-2.5856	-2.4852	-2.5191	-0.00004	-0.00004	-0.00004
0.000	-2.8625	-2.7455	-2.7875	0.00000	0.00000	0.00000

Table 5.4: *PVD and RMVT-σ_n-D_z results: comparison between LD2 and LM2 FEM solutions with the 3D Heyliger solution, actuator case. Displacements are in $[m]$; electric potential is in $[V]$. $u_2 = u_2(a/2, 0)$; $\phi = \phi(a/2, b/2)$.*

	$\sigma_{33} \times 10^3$	$\sigma_{33} \times 10^3$	$\sigma_{33} \times 10^3$	$\sigma_{22} \times 10^2$	$\sigma_{22} \times 10^2$	$\sigma_{22} \times 10^2$
Height	$3D$	$RMVT$-σ_n-D_z	PVD	$3D$	$RMVT$-σ_n-D_z	PVD
1.000	0.0000	-3.9972	-55.800	111.81	108.42	113.28
0.975	-0.8333	-0.3973	-43.279	63.736	62.944	66.186
0.950	-2.8471	-0.7247	-28.385	15.833	17.986	19.448
0.925	-5.3241	-4.9793	-11.118	-32.001	-26.455	-26.932
0.900	-7.5482	-13.161	8.5218	-79.865	-70.380	-72.955
0.900	-7.5482	-13.161	-15.579	-51.681	-65.888	-68.096
0.800	-12.957	-12.947	-11.567	-33.135	-40.198	-41.748
0.700	-15.245	-14.028	-11.713	-19.840	-20.629	-21.342
0.600	-15.510	-16.402	-16.014	-9.7737	-7.1803	-6.8792
0.500	-14.612	-20.070	-24.473	-1.3905	0.1477	1.6408
0.500	-14.612	-20.070	-17.335	-1.3089	-1.2422	-1.2973
0.400	-12.524	-12.273	-12.937	-0.5782	-0.2467	-3.3075
0.300	-9.2558	-7.3716	-9.2086	0.1348	0.6476	5.7883
0.200	-5.5018	-5.3653	-6.1487	0.8463	1.4408	1.4314
0.100	-1.8733	-6.2545	-3.7579	1.5723	2.1326	2.2270
0.100	-1.8733	-6.2545	-3.3555	14.529	13.973	14.007
0.075	-1.1074	-0.4685	-4.1098	17.801	16.911	17.041
0.050	-0.5162	1.7426	-4.3795	21.098	19.895	20.148
0.025	-0.1351	0.3790	-4.1645	24.428	22.927	23.328
0.000	0.0000	-4.5594	-3.4647	27.795	26.006	26.581

Table 5.5: *PVD and RMVT-σ_n-D_z results: comparison between LD2 and LM2 FEM solutions with the 3D Heyliger solution, actuator case. Stresses are in $[Pa]$. $\sigma_{33} = \sigma_{33}(a/2, b/2)$; $\sigma_{22} = \sigma_{22}(a/2, b/2)$;*

	$D_z \times 10^{13}$		
Height	$RMVT\text{-}\sigma_n\text{-}D_z$	PVD	$RMVT\text{-}\sigma_n\text{-}D_z^*$
1.000	-243.62	-243.82	-243.85
0.975	-183.67	-183.88	-183.88
0.950	-123.78	-123.95	-123.94
0.925	-63.930	-64.043	-64.007
0.900	-4.1326	-4.1504	-4.0924
0.900	-4.1326	-4.1274	-4.1294
0.800	-3.8750	-3.8751	-3.8757
0.700	-3.6209	-3.6228	-3.6220
0.600	-3.3703	-3.3705	-3.3682
0.500	-3.1233	-3.1182	-3.1145
0.500	-3.1233	-3.1275	-3.1313
0.400	-3.0501	-3.0492	-3.0515
0.300	-2.9735	-2.9709	-2.9718
0.200	-2.8934	-2.8925	-2.8920
0.100	-2.8099	-2.8142	-2.8123
0.100	-2.8099	-2.8425	-2.8823
0.075	-2.8400	-2.8144	-2.8393
0.050	-2.8387	-2.7898	-2.7997
0.025	-2.8059	-2.7685	-2.7635
0.000	-2.7418	-2.7507	-2.7307

Table 5.6: *Comparison between FEM results, actuator case. LD2 and LM2 results. Electric displacement is in* $[c/m^2]$. $D_z = D_z(a/2, b/2)$. * *indicates that* D_z *is calculated by constitutive relations in the* $RMVT\text{-}\sigma_n\text{-}D_z$ *analysis.*

	$\sigma_{33} \times 10^3$	$\sigma_{33} \times 10^3$	$\sigma_{33} \times 10^3$
Height	$3D$	$RMVT$-σ_n-D_z (LM3)	$RMVT$-σ_n-D_z (LM2)
1.000	0.0000	0.4571	-3.9972
0.975	-0.8333	-1.0703	-0.3973
0.950	-2.8471	-2.9855	-0.7247
0.925	-5.3241	-5.4381	-4.9793
0.900	-7.5482	-8.5777	-13.161
0.900	-7.5482	-8.5777	-13.161
0.800	-12.957	-13.923	-12.947
0.700	-15.245	-16.470	-14.028
0.600	-15.510	-16.706	-16.402
0.500	-14.612	-15.120	-20.070
0.500	-14.612	-15.120	-20.070
0.400	-12.524	-13.404	-12.273
0.300	-9.2558	-9.6210	-7.3716
0.200	-5.5018	-5.3821	-5.3653
0.100	-1.8733	-2.2994	-6.2545
0.100	-1.8733	-2.2994	-6.2545
0.075	-1.1074	-0.8874	-0.4685
0.050	-0.5162	-0.5092	1.7426
0.025	-0.1351	-0.3347	0.3790
0.000	0.0000	0.4661	-4.5594

Table 5.7: *$RMVT$-σ_n-D_z results: comparison between LM2 (10×10) and LM3 (8×8) FEM solutions with the 3D Heyliger solution. actuator case. Stresses are in $[Pa]$. $\sigma_{33} = \sigma_{33}(a/2.b/2)$;*

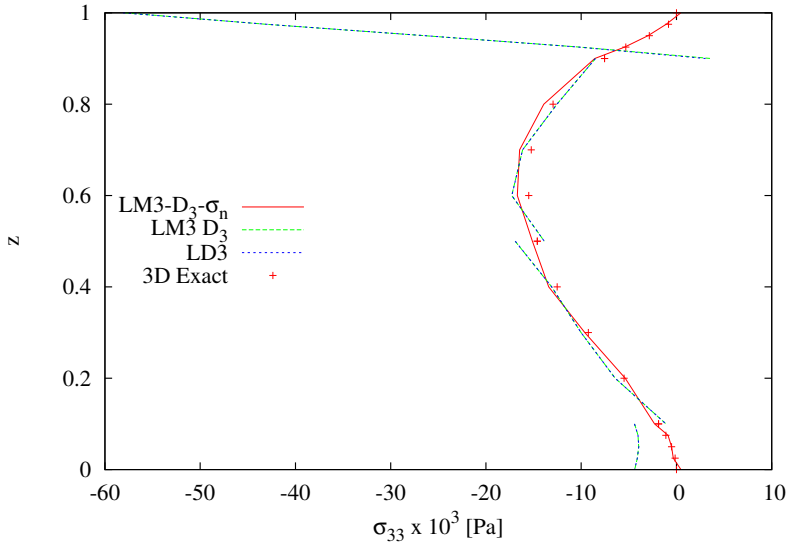

Figure 5.4: *Comparison between FEM results and 3D-exact solution, actuator case; the transverse normal stress σ_{33} is in [Pa]; $\sigma_{33} = \sigma_{33}(a/2, b/2)$*

Bibliography

[1] D Michael McFarland A.V. Srinivasan. Smart structures: Analysis and design. 2001.

[2] Bharat Bhushan. *Springer Handbook of Nanotechnology*. Springer, 2007.

[3] D. Ballhause. Assessment of multilayered theories for piezoelectric plates using a unified formulation. *Master Thesis, Universität Stuttgart, Institut für Statik und Dynamik der Luft- und Raumfahrtkonstruktionen*, 2003.

[4] J.N. Reddy. *Mechanics of laminated composite plates: Theory and analysis*. CRC Press Inc, 1996.

[5] E. Reissner. On a certain variational theorem and a proposed application. *International Journal for Numerical Methods in Engineering*, 20:1366–1368, 1984.

[6] J. N. Reddy. *An introduction to the finite element method, 2nd edition*. McGraw-Hill Inc., 1993.

[7] D.J. Gorman. Free vibration analysis of rectangular plates. *Journal of Sound and Vibration*, 85:603–604, 1982.

[8] G.J. Turvey, N. Mulcahy, and M.B. Widden. Experimental and computed natural frequencies of square pultruded GRP plates: effects of anisotropy, hole size ratio and edge support conditions. *Composite Structures*, 50:391–403, 2000.

[9] E. Carrera. An assessment of mixed and classical theories on global and local responses of multilayered orthotropic plates. *Composite Structures*, 50:183–198, 2000.

[10] N.J. Pagano. Exact solutions for composite laminates in cylindrical bending. *J. Composite Materials*, 3:398–411, 1969.

[11] S. Brischetto E. Carrera and P. Nali. Variational statements and computational models for multifield problems and multilayered structures. *Special Issue of MAMS*, 15(3):182–198, 2008.

[12] E. Carrera and M. Boscolo. Classical and mixed finite elements for static and dynamics analysis of piezoelectric plates. *International Journal Numerical Methods in Engineering*, 70:253–291, 2007.

[13] P. Heyliger. Static behavior of laminated elastic-piezoelectric plates. *AIAA Journal*, 32(12): 2481–2484, 1994.